A NUMERICAL STUDY OF NONLINEAR STATIC AND DYNAMIC BEHAVIOR OF A SQUARE THIN PLATE-MEMBRANE STRUCTURE FOR APPLICATION TO A MEMS MICRO-GENERATOR

By

OWEN I. CRABTREE

A thesis submitted in partial fulfillment of
the requirements for the degree of

MASTERS OF SCIENCE IN MECHANICAL ENGINEERING

WASHINGTON STATE UNIVERSITY
School of Mechanical and Materials Engineering

DECEMBER 2004

To the faculty of Washington State University

The members and committee appointed to examine the thesis of OWEN I. CRABTREE find it satisfactory

_____
Chair

_____

_____

_____

ACKNOWLEDGEMENT

I would like to thank all the people that made this possible. My parents contributed their moral and financial support and helped me through all my academic endeavors. And of course my friends who endured with me through all of this.

I would also like to thank my adviser, Cecilia Richards, who allowed me to work on the P3 MEMS project since my undergraduate years up to my graduate career. I would also like to thank the members of my committee, Dr. Robert Richards, Dr. David Bahr, and Dr. Sinisa Mesaoriv.

I would like to especially thank Dr. Sinisa Mesarovic for providing me with insights and guidance on my modeling endeavors. Thanks is also given to Dr. Ismail Demir for helping me with the initial development and direction of my project. Also I would like to thank the entire P3 MEMS team for their help in either experimentation or merely being there to discuss ideas.

A NUMERICAL STUDY OF NONLINEAR STATIC AND DYNAMIC BEHAVIOR OF A SQUARE THIN PLATE-MEMBRANE STRUCTURE FOR APPLICATION TO A MEMS MICRO-GENERATOR

Abstract

By Owen I. Crabtree, M.S.
Washington State University
December 2004

Chair: Cecilia D. Richards

The behavior of geometrically nonlinear, laminated, piezoelectric, square plate-membrane was predicted using a finite difference technique along with a step-by-step matrix analysis technique to predict the static and dynamic behavior. These methods were implemented using the FORTRAN 90 programming language, and then the developed program was used to optimize the plate-membrane for use in a micro-engine.

Optimum performance is such that the membrane will exhibit low frequencies of operation to accommodate heat transfer in the micro-engine and that the majority of the energy into the system will be extracted through charge on a piezoelectric layer. In order to achieve this the model was exercised and it was found that minimization of residual stress and minimization of the other lamina thicknesses, besides the piezoelectric, can assist in both these goals. For typical silicon thicknesses (1-2 μm) it was found that the optimum PZT thickness based on a strain energy ratio is in the range of 2 to 3 μm. Also it was evident that an increase in side length will cause a decrease in frequency of

vibration, and a decrease in deflection will reduce nonlinear effects therefore also reducing the frequency of vibration. The nonlinear behavior was also studied and harmonics were found and analyzed.

Table of Contents

Index of Figures

Index of Tables

Chapter 1: Introduction

1.1 Motivation

Geometric nonlinearity of membranes and plates is of general interest to the scientific and engineering communities. A multitude of applications for these structures is apparent. For instance, the basilar membrane in the ear will exhibit this nonlinear behavior [1]. The aircraft industry also has much interest in this, some of the early mathematical solutions were motivated by this industry [2]. In the civil engineering world this is of interest and this was illustrated in regards to the the behavior of window glass plating [3].

Nonlinear behavior in the MEMS world is also quite evident; membrane thermopnuematic actuators can show an impressive amount of nonlinearity as demonstrated in [4]. Power generation is also being attempted on the MEMS scale, an electromagnetic micro-generator, shown in [5], also displays these characteristics. The current application which is being worked on at Washington State University by the P3 MEMS micro-engine group is also an application of a MEMS membrane to power generation. The eventual goal of this project is to provide a micro-engine that uses a structure similar to Figure 1.1 as the generator.

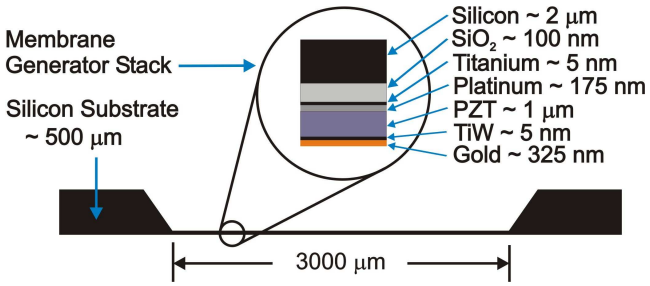

Figure 1.1: P3 membrane generator schematic

It is apparent from the figure that the aspect ratio of the membrane structure is approximately 1000. This means the behavior that the structure will undergo will be more membrane-like than plate-like. In experiments with the structure it was shown that deflections are on the order of multitudes of the thickness [6], implying a geometrically nonlinear behavior. Subsequently a solution technique that can solve for this behavior accurately is desired.

1.2 Literature Review

Plate and membrane behavior in the dynamic and static domains has been examined since the end of the 18th century where it began with the experimental work of Chladni [7]. Since then it has developed into a burgeoning and expansive field with a wide variety of theoretical and empirical techniques. The first mathematical solutions were attempted by Euler (1766) and his student, Bernouli (1789), who analyzed the free vibration problem of the membrane theory of plates [8 p. 7]. The first correct governing equation for the free vibration of plates was developed by Lagrange in 1813 [8 p. 8]. The plate problem has progressed through history until now where it is commonly analyzed using the finite element method [9] and other computationally intensive methods. Which

are capable of analyzing many geometries and parameters that can occur. The emphasis in this review is the theoretical work that has been done in order to represent and solve the plate/membrane problem.

Plates undergoing transverse deflection can be classified into regimes that describe the nature of their behavior and thus characteristics of the mathematical problem. These regimes are small deflection (linear), moderately large deflection (non-linear), and very large deflection (highly non-linear). This behavior can generally be classified by observation of the amount of deflection in comparison to plate dimensions. Small deflection theory can typically be used for deflections less than twenty percent of the thickness; moderately large deflection theory is applied when the deflection is a multiple of the plate thickness but much less than the plate side length; very large deflection theory is applied when the deflection of the plate is similar in magnitude to the plate side length. Depending on the plate classification the solution to these problems can be relatively simple or highly complex, and typically impossible without the implementation of approximating techniques. Coverage of the linear deflection problem and the moderately nonlinear problem will occur in this review, very large deflection is currently not pertinent to this work and subsequently will not be covered.

An important distinction in the following discussion is between the plate and the membrane. The membrane is a very thin structure for which flexural rigidity is of such a small magnitude in comparison to the in-plane membrane forces that the terms dependent upon the flexural rigidity can be assumed negligible. Therefore the lateral load carrying capacity of a membrane is purely due to the in-plane forces [8 p. 144], unlike a plate which can carry loads by both bending forces and in-plane forces. This distinction

between a plate or a membrane will be emphasized by the choice of vocabulary in the proceeding discussion.

1.2.1 Formulation of the Linear Deflection Theory

Small deflection vibrations have been widely studied due to the general applicability and the relative ease of obtaining solutions. Therefore a large amount of literature is available concerning these linear vibrations. Leissa compiled an excellent monograph detailing the available formulations and solution techniques for various plate shapes and parameters at the time of writing [10]. One of the classical reference for plate problems, Timoshenko's Theory of Plates and Shells, also provides an expansive amount of literature on plates and their relatives [11]. Szilard also provides an excellent overview of the linear plate problem with an emphasis on finite difference techniques [8].

The classical linear free vibration theory for an isotropic plate is governed by the differential equation, equation (1.1) [8 p. 413].

$$D\nabla^4 w + \bar{m}\frac{\partial^2 w}{\partial^2 t} = 0 \tag{1.1}$$

Which compares to the linearly vibrating membrane [8 p. 420].

$$\nabla^2 w - \frac{\bar{m}}{\sigma h}\frac{\partial^2 w}{\partial t^2} = 0 \tag{1.2}$$

w is the transverse deflection, t is time, $\bar{m}$ is mass per unit area, h denotes structure thickness, σ is a constant in-plane membrane stress, $\nabla^4 = \nabla^2 \nabla^2$ and ∇^2 is the two-dimensional Laplace operator defined in equation (1.3).

$$\nabla^2 = \frac{\partial^2}{\partial x^2} + \frac{\partial^2}{\partial y^2} \tag{1.3}$$

The flexural rigidity, D, is defined in equation (1.4) for a single lamina where E is the modulus of elasticity and v is Poisson's ratio.

$$D = \frac{E h^3}{12\left(1 - \nu^2\right)} \tag{1.4}$$

1.2.2 Solutions to the Linear Deflection Theory

Solutions to the differential equations of plates and membranes is a vast topic with many variations, although there is a consistent stream of the more popular methods. These can be broken down into two solution groups the first being exact analytical solutions and the second being approximate solutions. A limited number of exact solutions exist and these are for fairly specific conditions.

There are 21 independent boundary conditions that can be applied to a rectangular plate. Because of the lack of resistance to bending of membranes the clamped and simply

supported boundary conditions are identical, therefore only 6 independent boundary conditions exist for membranes. Leissa details these boundary conditions for rectangular plates, pointing out that the only exact solutions known are for the six cases of plates with opposite edges that are simply supported [12]. These solutions were obtained by Voigt [13] in 1893 using the aptly called Voigt solution technique. Navier also developed an "exact" method to solve these equations which utilizes a double Fourier series [11 p. 108]. This solution is only "exact" if the boundary conditions are of the Navier type, i.e. simply supported [8]. Solution of a membrane clamped on all edges can also be obtained using a separation of variables technique as detailed by Inman [14 p. 471]. Exact solutions have also been found for circular plates and membranes [11 p. 55], but these being of little use in this work will subsequently not be covered.

The most common and readily available solutions are those of the approximating techniques. These range from the familiar Rayleigh-Ritz technique [15] to the hierarchical finite element technique [16]. In the case of Warburton's and Leissa's analysis they use the Rayleigh-Ritz technique in conjunction with beam functions to obtain approximate solutions for the remaining 15 boundary conditions [12 p. 269]. This technique is actually widely used and can be found in a large assortment of the literature, referenced in Leissa's monograph [10]. The wide use of the finite difference technique to obtain solutions to problems of mathematical physics is also evident in plate and membrane literature. Szilard details this technique for multiple plate applications in his book, going as far to develop this technique to plates with irregular boundaries [8 p. 175] and also plates with orthotropic properties [8 p. 381]. Kharab used this technique in a spreadsheet program and solves the two dimensional wave equation for a membrane [17].

The finite element technique is currently a popular technique in numerical solutions. An incomplete survey performed by Cook [9 p. 319] includes references to 144 articles that included 88 different types of plate finite elements. One of the more recent finite element solution techniques for the linear plate problem is the hierarchical finite element [18, 19]. Han and Petyt have published work on this technique for plates in free vibration [18] and plates under forced vibration [19], in Houmat's paper he analyzes the vibrational behavior of a membrane instead of a plate [16]. Both sets of authors show that this technique can be advantageous in that it reduces the number of degrees of freedom that must be used to yield an accurate result, when compared with the linear finite element method.

1.2.3 Formulations of the Nonlinear Deflection Theory

Many formulations and solution techniques for the linearly vibrating plate have been derived and implemented. These techniques have been rigorously tested and tried, showing their validity in the linear plate/membrane regime. Yet, deflections on the order of approximately a tenth the thickness of a plate can cause stiffening of the structure that this theory can not predict. These forces, which are a result of the deflected shape requiring stretching or shortening of the midsurface, act to support part of the load. The linear theory breaks down and gives solutions that incorrectly estimate the displacements and vibrational characteristics considerably.

The credit of discovering the nonlinear theory that accounts for both bending and stretching of the plate is given to G. Kirchhoff (1824-1887). The analysis in his 1876

book *Lectures on Mathematical Physics* (in German) [20] is considered the first piece of literature which notices that the nonlinear terms can no longer be considered negligible [8 p. 8]. The final form of the nonlinear differential equations governing the moderately large deflection behavior of a statically deflected plate was published by von Karman in 1910 [21]. Herrmann then expounded upon von Karman's work, integrating dynamic effects into the theory [22]. The final set of von Karman like equations for an isotropic plate are shown in equations (1.5) and (1.6).

The Equilibrium Equation

$$D\nabla^4 w+\bar{m}\frac{\partial^2 w}{\partial t^2}=h\left(\frac{\partial^2 w}{\partial x^2}\frac{\partial^2 F}{\partial y^2}+\frac{\partial^2 w}{\partial y^2}\frac{\partial^2 F}{\partial x^2}-2\frac{\partial^2 w}{\partial x\partial y}\frac{\partial^2 F}{\partial x\partial y}\right) \tag{1.5}$$

The Compatibility Equation

$$\frac{\partial^4 F}{\partial x^4}+2\frac{\partial^4 F}{\partial x^2\partial y^2}+\frac{\partial^4 F}{\partial y^4}=E\left[\left(\frac{\partial^2 w}{\partial x\partial y}\right)^2-\frac{\partial^2 w}{\partial x^2}\frac{\partial^2 w}{\partial y^2}\right] \tag{1.6}$$

Equations (1.5) and (1.6) are derived using an equilibrium approach of an elastic plate representative element in Cartesian coordinates. These equations are usually referenced as the *w*-*F* formulation. The use of the Airy stress function, *F*, requires the assumption that in-plane inertia is negligible [23], which limits the applicability of this

theory. The plate can also be represented using three equations in terms of three displacements in the x, y, and z directions [24], called the *w-u-v* formulation. These equations are capable of representing the vibrating plate with inclusion of the in-plane inertia terms [23].

$$u_{,xx}+\frac{1-\nu}{2}u_{,yy}+\frac{1+\nu}{2}v_{,xy}=-w_{,x}\left(w_{,xx}+\frac{1-\nu}{2}w_{,yy}\right)-\frac{1+\nu}{2}w_{,y}w_{xy} \tag{1.7}$$

$$v_{,yy}+\frac{1-\nu}{2}v_{,xx}+\frac{1+\nu}{2}u_{,xy}=-w_{,y}\left(w_{,yy}+\frac{1-\nu}{2}w_{,xx}\right)-\frac{1+\nu}{2}w_{,x}w_{xy} \tag{1.8}$$

$$\begin{aligned} D\nabla^4 w+\rho w_{,tt}=q+\frac{Eh}{1-\nu^2}\Bigg[&\left(u_{,x}+\frac{1}{2}w_{,x}^2\right)\left(w_{,xx}+\nu w_{,yy}\right)+ \\ &\left(v_{,y}+\frac{1}{2}w_{,y}^2\right)\left(w_{,yy}+\nu w_{,xx}\right)+\left(1-\nu\right)w_{,xy}\left(u_{,y}+v_{,x}+w_{,x}w_{,y}\right)\Bigg] \end{aligned} \tag{1.9}$$

Another popular approach to the representation of plate behavior is the variational technique [25 p. 163, 26 p. 295]. Both Washizu and Reismann illustrate this technique which uses the principle of virtual work as the point of departure. Washizu then utilizes the principle of stationary potential energy to obtain equations (1.5) and (1.6) [25 p. 165].

1.2.4 Solutions to the Nonlinear Deflection Theory

Solutions for the above sets of nonlinear equations have been examined extensively in the literature. These solutions are substantially more complicated in the

geometrically nonlinear case then those discussed for the linear. Yet, some of the same solution techniques are applied in the nonlinear case that were applied in the linear (with modification).

Exact solutions to the nonlinear plate are obviously difficult to obtain. Although, an "exact" solution for a uniformly loaded circular plate with a clamped edge was developed by Way [27]. Manipulating the governing equations slightly, Way then applies a power series solution, and obtains an "exact" solution to the static deflection of a nonlinearly behaving circular plate. As far as this author has found, no exact solutions exist for the dynamic behavior of a nonlinearly deflecting rectangular plates or membranes.

The other solutions for this plate problem belong in the approximate solution category. Generally these solutions either use approximating functions, assume certain terms negligible, or use some finite discretization method. Chia published a superb compilation of information on nonlinear plates and many of the methods to approach the different plate problems in his book, Nonlinear Analysis of Plates [24].

Initially, examining the work done on the solution to static deflection of plates a large volume of techniques were found. One of the very prominent techniques found in literature is attributed to H. M. Berger and consequently referred to as the Berger formulation [28]. Writing the standard energy expression at the mid-plane of the plate, Berger assumed that the second strain invariant is negligible; based on the work done by Way [27]. This then results with the decoupling and linearization of the governing equations. Although the caveat with this assumption is that there is no direct physical

interpretation of the validity of the assumption used. Berger compares his results to that obtained by Levy [29] and Wang [2, 25] and finds agreement.

In future works many other authors use the Berger technique on a multitude of plate problems. In Leissa's monograph [10] other techniques are illustrated which extend the Berger technique to include vibrational behavior of these nonlinear plates. Application of this method to the nonlinear vibration of both plates and membranes was done by Mazumdar, with the goal of modeling vibrations of the human tympanic membrane [30]. Sathyamoorthy then extended this even further to the vibration of orthotropic clamped rectangular plates with immovable edge conditions [31]. Part of this approach is to assume a solution based on the spatial modes and some function in time [7 p. 5]. This then reduces to the well known Duffing oscillator problem. Detailed solution methods are available in [32].

Another very popular technique is the double series, typically a Fourier series, although in some cases a one term (single-mode) solution is used for the transverse deflection [33, 34]. Levy implemented the Fourier series for a simply supported rectangular plate under combined edge compression and lateral loading [29]. Deflection and pressure were defined as a Fourier series and a representation for the Airy stress function based on this was found. Levy exercised this technique and one of his findings

was that for $\frac{p a^4}{E h^4} = 400$ the membrane and bending stresses are of the same magnitude.

Where p is applied pressure, a is plate side length, E is Young's modulus, and h is plate thickness. Seide used Levy's technique as a template and applied it to the problem of

rectangular membranes with edges that are fixed normal to the edge but free to move parallel to the edge [35]. A similar technique for static deflection of membranes with the *w-u-v* formulation was developed by Timoshenko and then expanded by Maier-Schneider [36]. It combines quadratic terms with a sine function profile of the membranes. This technique is quite useful to obtain quick and fairly accurate results for load-deflection solutions.

Extending the Fourier series technique into the dynamic world is an obvious step, using a generalized Fourier series. Often the elements consist of beam functions [24, p.40]. Teng uses this technique for plates undergoing blast loading with different degrees of elastic restraint along the edges [37]. In a recent paper, Teng et al [38] used a Fourier series to obtain a governing equation for nonlinear plates that is exactly the well known Duffing equation. Lighthill's extension of the perturbation method was then used and transient solutions for rectangular plates under blast loading was obtained. Verification against experimental data confirmed the validity of this technique.

Lee analyzed the two different formulations of this problem, the *w-F and w-u-v* formulations, a generalized Fourier series and the Galerkin procedure were used for both formulations [23]. Lee found that in the case of the *w-u-v* formulation the number of terms needed, 252, precluded the application of this technique. Lee did find, however in using this procedure that the Duffing equation drops out of the mathematics.

A perturbation solution has also been investigated by Chu and Herrmann [39] where the dynamic *w-F* formulation was used which was derived in a previous work of Herrmann [22]. A double sine series was used for the deflection term and a double cosine series was used for the stress function term, but only the first mode shape was

accounted for. Nayfeh used a perturbation method of multiple scales to solve the differential equations for a symmetrically excited circular plate, and documents the solution steps in [40], finally noting that the internal resonance for plates involves three modes [40 p. 514].

Yasuda [41] also used a perturbation method of multiple scales to obtain oscillation characteristics of a square membrane near a primary resonance with one nodal line and showed that this method matched experiment, proving the validity of the technique in this case. Although to simplify the analysis, mode shapes composed of a multiple of two sine functions were used and only the (1,2) and (2,1) mode were accounted for. In 1981 Niyogi applied this same technique to the non-linear dynamic response of orthotropic plates and found good agreement with other available numerical results of the time. The perturbation method is only capable of treating problems with weak nonlinearity, and quickly becomes difficult to work with when calculating higher-order approximations [42], therefore other techniques must be explored in order to obtain results for stronger nonlinearity.

Hamilton's principle has also been applied to this problem. Benamar used this technique in his PhD dissertation to examine the changes in mode shapes and frequencies of vibration in nonlinear clamped plates and beams [7]. A dependence on mode shapes and frequencies were found, curvatures near the clamped edge increased as deflection increased. Also spatial distortion was analyzed and it was found that there is interaction at large deflections between the first and higher order odd symmetric modes. This spatial distortion characteristic was also explored in [7] using the finite element technique and the same conclusion was reached. This technique was also applied to symmetrically

laminated rectangular composite plates [43], and on rectangular plates with a combination of simply supported and clamped boundary conditions [44]. Benamar also performed experimental work to verify and compare his experiments and found agreement [7].

In the 1970's and early 1980's nonlinear plate elements were being developed using the FEM technique. Pica developed an element for static situations using a Mindlin formulation where it was found that the developed elements provided good results for straight boundary's but had difficulty with curved ones [45]. In 1984 Lau [46] illustrated a simple triangular incremental modified Discrete Kirchoff Theory plate element for dynamic behavior. Interesting results were found for differing boundary conditions. In the case where in-plane displacements are assumed zero over the entire membrane higher mode interaction is evident, but in the case where this assumption is not enforced the higher mode interaction is not evident [42]. The hierarchical finite element technique (HFEM), which uses high-order polynomial displacement functions, allows the entire plate to be modeled with one element. This technique is illustrated for both isotropic [33] and laminated plates [34]. As previously mentioned the HFEM technique can reduce the number of degrees of freedom needed to obtain a solution.

The method to be applied in this thesis is the finite difference technique. It has been applied in the linear case previously [26 p. 224] and has also been applied in the nonlinear case. A solution was detailed by Wang [2] for the static case with various boundary conditions. It has also been applied to square plates under hydrostatic loading for conditions of a flat plate in liquid containers or partitions [47]. Vallabhan used this method in an application to window glass plating [3], and he included vibration by using

the Newmark β technique [48]. Comparisons were made to other papers and agreement between the solutions was found.

1.3 Research Objectives

The primary objective of this work is too increase the understanding of the behavior of the membrane generator used to produce electrical work in the micro-engine. In order to do this a model is developed that can accurately predict what will occur. In particular, the focus of this work is the dynamic electromechanical behavior.

Model development begins with proper choice of applicable equations. That is, a set of governing equations must be found along with applicable boundary conditions. Then lamination and piezoelectricty are integrated into the model. Solution of these equations is pursued, proper choice of a solution technique that will result in accurate and relatively quick results is desired. A simplified approach is assumed, instead of modeling everything that occurs in Figure 1.1, what occurs in Figure 1.2 will be modeled. That is, sloping boundary conditions are not accounted for, and the number of layers are reduced. The developed model will be capable of modeling geometrically nonlinear behavior of a laminated, piezoelectric thin plate/membrane device.

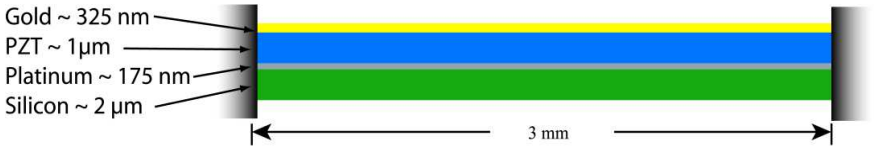

Figure 1.2: Actual modeled membrane structure

Finally, the model is used to further the understanding of the P3 MEMS micro-generator by examination of what occurs for changes in various parameters in regards to static and vibrational behavior. Specifically the examined parameters are: lamina thicknesses, pre-stress, side length, electrode coverage, loading amplitude, and excitation frequency.

Chapter 2: Theoretical Formulation

Determination of what equations and conditions are governing and affecting the behavior of the generator membrane is important to the modeling endeavor. From literature it is determined that the *w-F* formulation of the equations are applicable. Clamped boundaries are assumed and the conditions are shown below along with the reasoning behind them. A simplified lamination theory is applied along with a simplified piezoelectric theory.

2.1 Governing Equations

The membrane under examination is a geometrically nonlinear deflecting structure. This is due to the magnitude of deflection causing an in-plane stress that contributes to the stiffness of the membrane/plate. Subsequently in the derivation of the governing equations the nonlinear terms in the large-deflection strain-displacement expression must be considered (Figure 2.1).

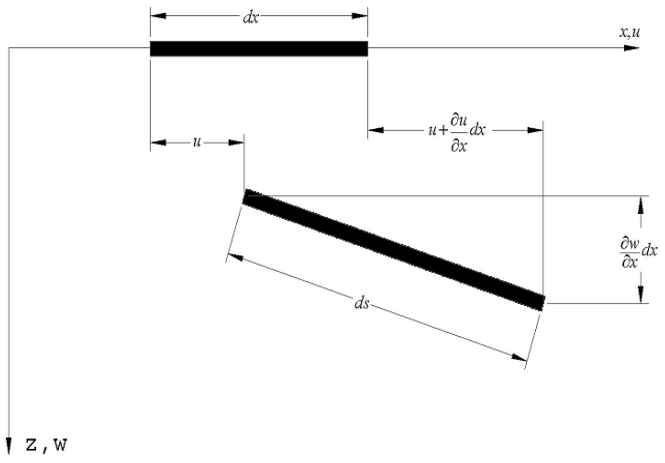

Figure 2.1: Strain, ε_x, due to large deflections.

The nonlinear strain term is

$$\epsilon_x^{NL} = \frac{ds - dx}{dx} \approx \frac{1}{2}\left(\frac{\partial w}{\partial x}\right)^2 \tag{2.1}$$

This nonlinear strain term then is introduced in the typical strain equations.

$$\begin{aligned} \epsilon_x &= \epsilon_x^L + \epsilon_x^{NL} = \tfrac{1}{E\,h}\left(n_x - \nu\, n_y\right) \\ \epsilon_y &= \epsilon_y^L + \epsilon_y^{NL} = \tfrac{1}{E\,h}\left(n_y - \nu\, n_x\right) \\ \gamma &= \gamma^L + \gamma^{NL} = \frac{\partial u}{\partial y} + \frac{\partial v}{\partial x} + \frac{\partial w}{\partial x}\frac{\partial w}{\partial y} = \frac{2\left(1+\nu\right)}{E\,h} n_{xy} \end{aligned} \tag{2.2}$$

Where n_x, n_y, and n_{xy}, are membrane forces defined as functions of the Airy stress function [49].

$$n_x = h\frac{\partial^2 F}{\partial y^2}, \quad n_y = h\frac{\partial^2 F}{\partial x^2}, \quad \text{and} \quad n_{xy} = -h\frac{\partial^2 F}{\partial x\,\partial y} \tag{2.3}$$

Using the nonlinear terms for ε_x, ε_y, γ_{xy}, and the Airy stress function the compatibility condition for moderately nonlinear behavior is obtained [8 p. 341]. The

nonlinearity is evident in the right hand side of equation (2.4), in the squared term and the directionally coupled term.

$$\nabla^4 F = E\left[\left(\frac{\partial^2 w}{\partial x \partial y}\right)^2 - \frac{\partial^2 w}{\partial x^2}\frac{\partial^2 w}{\partial y^2}\right] \tag{2.4}$$

The original static governing equation was derived by von Karman [21] in 1910 as stated in Chapter 1. Chia also shows a derivation of these equations for dynamic response of an anisotropic laminated plate [24 p. 33]. These equations account for in-plane stretching and the coupling to transverse deflection. In this application the equations are shown for an isotropic undamped vibrating plate, i.e. equation (2.5) has both bending and stretching terms. For a detailed derivation of equation (2.5) refer to Chapter 1 of reference [24].

$$\begin{aligned} &D\nabla^4 w - p(x,y,t) + \rho\frac{\partial^2 w}{\partial t^2} = \\ &h\left[\frac{\partial^2 w}{\partial x^2}\left(\frac{\partial^2 F}{\partial y^2} + \sigma_0\right) + \frac{\partial^2 w}{\partial y^2}\left(\frac{\partial^2 F}{\partial x^2} + \sigma_0\right) - 2\frac{\partial^2 w}{\partial x \partial y}\left(\frac{\partial^2 F}{\partial x \partial y}\right)\right] \end{aligned} \tag{2.5}$$

2.2 Boundary Conditions

Application of the proper boundary conditions (BCs) in order to obtain an applicable solution is of paramount importance. A cross-section of a representative generator membrane with silicon substrate is shown in Figure 2.2.

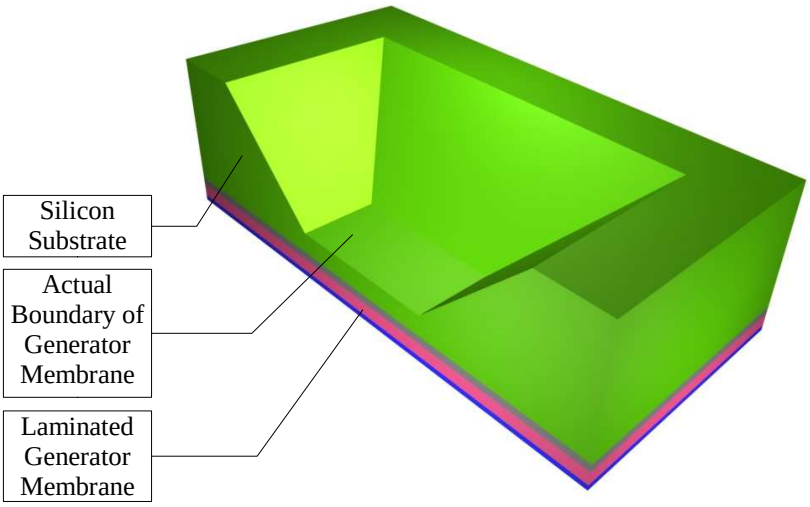

Figure 2.2: 3D view of generator cross section

From the physical situation the actual BC appears to be some form of an elastically restrained BC [24 p. 38]. The constant slope of the substrate near the boundary is indicative of an increase stiffness the further away from the generator membrane boundary. This would imply a BC that contains the terms for a clamped boundary condition with an elastically restrained against rotation modification [24 p. 167]. Where this condition can be represented by equation (2.6). The subscript *n* denotes that the value is normal to the boundary being considered.

$$M_n = \pm \xi w_{,n} \tag{2.6}$$

The bending moment, M_n, is related to the slope, $w_{,n}$, by a proportionality constant, ξ, that can vary between 0 and ∞, corresponding with a simply supported BC and a clamped BC, respectively. It is known that the angle of the incline with the horizontal plane is 54.74°, it is assumed that this is sufficient to conclude a clamped BC. Allowing elimination of the substrate from the model, and only modeling the generator membrane as shown in Figure 2.3.

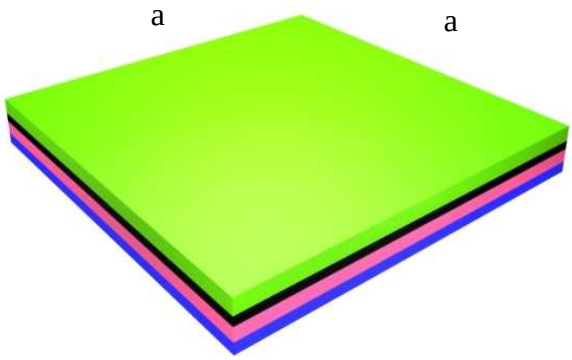

Figure 2.3: Model schematic

The pertinent equations to enforce the clamped conditions are:

Zero transverse deflection at edges

$$w_{x=0,a} = 0 \qquad \text{and} \qquad w_{y=0,a} = 0 \tag{2.7}$$

Zero slope on edges, or $\xi=\infty$

$$w_{,x}|_{x=0,a}=0 \qquad \text{and} \qquad w_{,y}|_{y=0,a}=0 \tag{2.8}$$

Zero x or y strain on respective edges

$$\begin{aligned}\epsilon_x|_{y=0,a}&=\frac{1}{E}\left(\frac{\partial^2 F}{\partial y^2}-\nu\frac{\partial^2 F}{\partial x^2}\right)=0\\ \epsilon_y|_{x=0,a}&=\frac{1}{E}\left(\frac{\partial^2 F}{\partial x^2}-\nu\frac{\partial^2 F}{\partial y^2}\right)=0\end{aligned} \tag{2.9}$$

Specified edge displacements of zero

$$\begin{aligned}u&=\int_{y=const}\left[\frac{\partial^2 F}{\partial y^2}-\nu\frac{\partial^2 F}{\partial x^2}-\frac{1}{2}\left(\frac{\partial w}{\partial x}\right)^2\right]dx=0\\ v&=\int_{x=const}\left[\frac{\partial^2 F}{\partial x^2}-\nu\frac{\partial^2 F}{\partial y^2}-\frac{1}{2}\left(\frac{\partial w}{\partial y}\right)^2\right]dy=0\end{aligned} \tag{2.10}$$

2.3 Lamination

In the fabrication of the generator membrane multiple layers are deposited for a variety of reasons: to improve adhesion between layers, to provide electrodes to harvest the charge, and to provide a piezoelectric layer. In order to model these layers they must be incorporated into the above equations in some form.

The primary assumption is that the plate-membrane is in a state of plane strain [50 p. 64].

$$\sigma_{33}=\tau_{31}=\tau_{32}=0 \qquad \text{which implies} \qquad \tau_{13}=\tau_{23}=0 \tag{2.11}$$

Equation (2.11) allows us to use the 2-D generalized Hooke's law [50 p. 152], where the layer number is denoted by superscript (k).

$$\begin{aligned}\sigma_{11}^{(k)}&=\frac{E^{(k)}}{1-\left(\nu^{(k)}\right)^2}\left(\epsilon_{11}+\nu^{(k)}\epsilon_{22}\right)\\ \sigma_{22}^{(k)}&=\frac{E^{(k)}}{1-\left(\nu^{(k)}\right)^2}\left(\epsilon_{22}+\nu^{(k)}\epsilon_{11}\right)\end{aligned} \tag{2.12}$$

From equation (2.12) a composite modulus can be obtained by first taking a weighted average of the stresses in each layer based on the thickness, displayed in equation (2.13) where superscript * stands for an effective value.

$$\sigma_{ii}^{*}=\frac{\sigma_{ii}^{(1)}h^{(1)}+\sigma_{ii}^{(2)}h^{(2)}+\cdots+\sigma_{ii}^{(n)}h^{(n)}}{h^{(1)}+h^{(2)}+\cdots+h^{(n)}}, \qquad i=1 \text{ or } 2 \tag{2.13}$$

Expansion of equation (2.13), by insertion of (2.12) results in equation (2.14) for i = x.

$$\sigma_{11}^{*}=\frac{\epsilon_{11}E^{*(1)}h^{(1)}+\epsilon_{11}E^{*(2)}h^{(2)}+\cdots+\epsilon_{11}E^{*(n)}h^{(n)}}{h^{(1)}+h^{(2)}+h^{(3)}+\cdots+h^{(n)}}+\frac{\epsilon_{22}\nu^{(1)}E^{*(1)}h^{(1)}+\epsilon_{22}\nu^{(2)}E^{*(2)}h^{(2)}+\cdots+\epsilon_{22}\nu^{(n)}E^{*(n)}h^{(n)}}{h^{(1)}+h^{(2)}+h^{(3)}+\cdots+h^{(n)}} \tag{2.14}$$

Where

$$E^{*(k)}=\frac{E^{(k)}}{1-\left(\nu^{(k)}\right)^{2}} \tag{2.15}$$

By factoring out ϵ_{11} in the first quotient of equation (2.14) and assuming $\epsilon_{22} = 0$, an effective modulus is obtained.

$$E^{*}=\frac{1}{h}\left[\sum_{k=1}^{n}E^{*(k)}h^{(k)}\right] \tag{2.16}$$

This effective modulus can then be used in the governing equations (2.4) and (2.5). An effective Poison ratio can be obtained by using the uniaxial effective modulus and solving for the composite Poison ratio using equation 2.17.

$$E^{*}=\frac{E}{1-\nu^{*2}} \tag{2.17}$$

Where the uniaxial effective modulus is

$$E = \frac{1}{h}\left[\sum_{k=1}^{n} h^{(k)} E^{(k)}\right] \tag{2.18}$$

It is apparent that the effective Poison's ratio is

$$\nu^{*} = \sqrt{1 - \frac{E}{E^{*}}} \tag{2.19}$$

For the density, a simple weighted average is used to obtain the effective property.

$$\rho^{*} = \frac{\rho^{(1)} h^{(1)} + \rho^{(2)} h^{(2)} + \cdots + \rho^{(n)} h^{(n)}}{h^{(1)} + h^{(2)} + \cdots + h^{(n)}} \tag{2.20}$$

The flexural rigidity term, equation (1.4), is for a single layer plate. This value, *D*, is then modified to account for lamination. Generically, a plate in pure bending will have the relation

$$M = DK \tag{2.21}$$

Where *M* is a moment, *D* is the flexural rigidity, and K is the curvature. *D* is solved for in terms of *M* and K. Assuming pure bending the following relations are used to solve for *D* where $\tilde{z}$ is the neutral axis and *h* is the total plate thickness.

$$0 = \int_0^h \sigma(z)\, dz \tag{2.22}$$

$$M = \int_0^h \sigma(z)(z - \tilde{z})\, dz \tag{2.23}$$

$$\epsilon = -K(z - \tilde{z}) \qquad \sigma^{(k)} = E^{*(k)}\epsilon(z) \tag{2.24}$$

Using equations (2.22) and (2.24) a value for $\tilde{z}$ can be found. The individual maximum value of a layer position from a reference, $z_0 = 0$, is z_i.

$$0 = \int_{z_0}^{z_1} E^{*(1)}(z - \tilde{z})\, dz + \int_{z_1}^{z_2} E^{*(2)}(z - \tilde{z})\, dz + \cdots \tag{2.25}$$

Through use of equation (2.23) and (2.24) the value M/ K can be solved for as shown in equation (2.26).

$$D = \frac{M}{K} = \int_{z_0}^{z_1} -E^{*(1)}(z - \tilde{z})^2\, dz + \int_{z_1}^{z_2} -E^{*(2)}(z - \tilde{z})^2\, dz + \cdots \tag{2.26}$$

In the remainder of this document it will be assumed that all material properties are considered effective properties without the superscript *.

2.4 Piezoelectricity

The lead zirconate titanate (PZT) layer is a piezoelectric material, meaning that with an applied stress a charge will be developed, or vice versa. The primary goal of this device is to extract a charge from the generator membrane and propagate electrical power. Subsequently, the direct piezoelectric effect must be integrated into the model. Obviously, if energy is put into a system it is used within the system for different tasks. The case in the generator membrane is.

$$E_{\text{in}} = E_{\text{deflection}} + E_{\text{dissipated}} + E_{\text{piezo effect}} \tag{2.27}$$

In the static derivation, dissipative forces were not included, therefore $E_{\text{dissipated}}$ can be neglected. Then to simplify this analysis a low electromechanical coupling is assumed, this is indicative of $E_{\text{piezo effect}} \approx 0$. Therefore, all of the energy put into the system goes into deflecting the membrane. This allows a charge profile to be obtained from the stress-strain field. Utilizing the direct piezoelectric effect the equation for the polarization charge per unit area is shown in equation 2.28 51, where d_{ijk} is the piezoelectric coefficient.

$$P_i = d_{ijk}\,\sigma_{jk} \tag{2.28}$$

Simplification of equation (2.28) can be done by realization of the properties of a membrane. The only pertinent stress in σ_{jk} is σ_{11} and σ_{22}, and due to crystal symmetry the shear coefficients of d_{ijk} are zero. Also, the electrodes are in the 3 direction thus, the polarization is only important in this direction. Equation (2.28) then simplifies to

$$P_3 = d_{311}\left(\sigma_{11} + \sigma_{22}\right) \tag{2.29}$$

Equation (2.12) gives us a charge per unit area, therefore integration over the electrode area is done, shown in equation (2.13). Giving the total charge accumulated under the electrode area.

$$\int_{Area-electrode} P_3\, dA = \int_{Area-electrode} d_{311}\left(\sigma_{11} + \sigma_{22}\right) dA \tag{2.30}$$

Chapter 3: Solution Technique

3.1 Nondimensionalization

Nomenclature from this point of departure differs than that used previously in that nondimensional quantities must be represented. Nondimensional variables are signified by an over bar over the variable. Nondimensionalization of the primary expressions is done by the following relations:

$$\begin{aligned}
&\bar{F}=\frac{F}{h^2 E} && \bar{w}=\frac{w}{h} && \bar{x}=\frac{x}{a}\\
&\bar{y}=\frac{y}{b} && \bar{\sigma}_0=\frac{\sigma_0}{E}\left(\frac{a}{h}\right)^2 && \bar{\epsilon}=\epsilon\left(\frac{a}{h}\right)^2\\
&\bar{p}=\frac{p a^2}{E h^2} && \bar{\nabla}=a^2\nabla && \eta=\frac{E h^3}{D}\\
&\bar{t}=\bar{\omega} t && \bar{\omega}=\frac{\rho h}{E} && \alpha=\left(\frac{h}{a}\right)^2
\end{aligned} \tag{3.1}$$

For simplicity a = b because the actual physical devices this model is developed for are square in shape. Using the definitions of equations (3.1) and combining them with equations (2.4) and (2.5). The nondimensional governing equations are obtained.

$$\bar{\nabla}^4\bar{F}=\left(\frac{\partial^2\bar{w}}{\partial\bar{x}\,\partial\bar{y}}\right)^2-\frac{\partial^2\bar{w}}{\partial\bar{x}^2}\frac{\partial^2\bar{w}}{\partial\bar{y}^2} \tag{3.2}$$

$$\bar{\nabla}^4 \bar{w} - \frac{\eta}{\alpha} p_z + \frac{\eta}{\alpha^2} \frac{\partial^2 \bar{w}}{\partial \bar{t}^2} = \eta \left[\frac{\partial^2 \bar{w}}{\partial \bar{x}^2} \left(\frac{\partial^2 \bar{F}}{\partial \bar{y}^2} + \bar{\sigma}_0 \right) + \frac{\partial^2 \bar{w}}{\partial \bar{y}^2} \left(\frac{\partial^2 \bar{F}}{\partial \bar{x}^2} + \bar{\sigma}_0 \right) - 2 \frac{\partial^2 \bar{w}}{\partial \bar{x} \partial \bar{y}} \left(\frac{\partial^2 \bar{F}}{\partial \bar{x} \partial \bar{y}} \right) \right] \tag{3.3}$$

The nondimensional boundary conditions are:

Zero transverse deflection at edges.

$$\bar{w}|_{\bar{x}=0,1} = 0 \qquad \text{and} \qquad \bar{w}|_{\bar{y}=0,1} = 0 \tag{3.4}$$

Zero slope on respective edges.

$$\bar{w}_{,\bar{x}}|_{\bar{x}=0,1} = 0 \qquad \text{and} \qquad \bar{w}_{,\bar{y}}|_{\bar{y}=0,1} = 0 \tag{3.5}$$

Zero strain on respective edges

$$\bar{\epsilon}_{\bar{x}}|_{\bar{y}=0,1} = \frac{\partial^2 \bar{F}}{\partial \bar{y}^2} - \nu \frac{\partial^2 \bar{F}}{\partial \bar{x}^2} = 0$$
$$\bar{\epsilon}_{\bar{y}}|_{\bar{x}=0,1} = \frac{\partial^2 \bar{F}}{\partial \bar{x}^2} - \nu \frac{\partial^2 \bar{F}}{\partial \bar{y}^2} = 0 \tag{3.6}$$

Specified edge displacements of zero

$$\bar{u} = \int_{\bar{y}=const} \left[\frac{\partial^2 \bar{F}}{\partial \bar{y}^2} - \nu \frac{\partial^2 \bar{F}}{\partial \bar{x}^2} - \frac{1}{2} \left(\frac{\partial \bar{w}}{\partial \bar{x}} \right)^2 \right] d\bar{x} = 0$$
$$\bar{v} = \int_{\bar{x}=const} \left[\frac{\partial^2 \bar{F}}{\partial \bar{x}^2} - \nu \frac{\partial^2 \bar{F}}{\partial \bar{y}^2} - \frac{1}{2} \left(\frac{\partial \bar{w}}{\partial \bar{y}} \right)^2 \right] d\bar{y} = 0 \qquad (3.7)$$

3.2 Finite Difference Approximation

With the nondimensional equations of section 3.1 a solution of the finite difference type is approached. Using the centered finite differences shown in Table 3.1 the nondimensional finite difference equations that will be used in the solution technique are obtained.

Derivative	***Central Finite Difference Equation for Arbitrary Variable, f***
$\frac{\partial f_{i,j}}{\partial x}$	$\frac{1}{2(\Delta x)}\left(f_{i+1,j}-f_{i-1,j}\right)$
$\frac{\partial^2 f_{i,j}}{\partial x^2}$	$\frac{1}{(\Delta x)^2}\left(f_{i+1,j}-2f_{i,j}+f_{i-1,j}\right)$
$\frac{\partial^3 f_{i,j}}{\partial x^3}$	$\frac{1}{2(\Delta x)^3}\left(f_{i+2,j}-2f_{i+1,j}+2f_{i-1,j}-f_{i-2,j}\right)$
$\frac{\partial^4 f_{i,j}}{\partial x^4}$	$\frac{1}{(\Delta x)^4}\left(f_{i+2,j}-4f_{i+1,j}+6f_{i,j}-4f_{i-1,j}+f_{i-2,j}\right)$
$\frac{\partial^2 f_{i,j}}{\partial x \partial y}$	$\frac{1}{4(\Delta x \Delta y)}\left(f_{i+1,j+1}-f_{i+1,j-1}-f_{i-1,j+1}+f_{i-1,j-1}\right)$
$\frac{\partial^4 f_{i,j}}{\partial x^2 \partial y^2}$	$\frac{1}{(\Delta x)^2(\Delta y)^2}\left[4f_{i,j}-2\left(f_{i+1,j}+f_{i-1,j}+f_{i,j+1}+f_{i,j-1}\right)+f_{i+1,j+1}+f_{i+1,j-1}+f_{i-1,j+1}+f_{i-1,j-1}\right]$

Table 3.1: Central finite difference approximations

Converting the analytical expressions of the GDE's and the BC's to finite difference expressions at the generic mesh point (i,j) and simplifying, the following discretized nondimensional compatibility equation is obtained.

$$\begin{aligned}
&20\bar{F}_{i,j}-8\left(\bar{F}_{i+1,j}+\bar{F}_{i-1,j}+\bar{F}_{i,j+1}+\bar{F}_{i,j-1}\right)\\
&\quad+2\left(\bar{F}_{i+1,j+1}+\bar{F}_{i+1,j-1}+\bar{F}_{i-1,j+1}+\bar{F}_{i-1,j-1}\right)\\
&\quad+\bar{F}_{i,j-2}+\bar{F}_{i+2,j}+\bar{F}_{i-2,j}+\bar{F}_{i,j+2}\\
&=\frac{1}{16}\left(\bar{w}_{i+1,j+1}-\bar{w}_{i+1,j-1}-\bar{w}_{i-1,j+1}+\bar{w}_{i-1,j-1}\right)^2\\
&\quad-\left(\bar{w}_{i+1,j}-2\bar{w}_{i,j}+\bar{w}_{i-1,j}\right)\left(\bar{w}_{i,j+1}-2\bar{w}_{i,j}+\bar{w}_{i,j-1}\right)
\end{aligned} \tag{3.8}$$

The discretized nondimensional equilibrium equation is.

$$
\begin{aligned}
&20\,\bar{w}_{i,j}-8\left(\bar{w}_{i+1,j}+\bar{w}_{i-1,j}+\bar{w}_{i,j+1}+\bar{w}_{i,j-1}\right)\\
&\quad+2\left(\bar{w}_{i+1,j+1}+\bar{w}_{i+1,j-1}+\bar{w}_{i-1,j+1}+\bar{w}_{i-1,j-1}\right)\\
&\quad+\bar{w}_{i,j-2}+\bar{w}_{i+2,j}+\bar{w}_{i-2,j}+\bar{w}_{i,j+2}\\
&=\left(\Delta\bar{x}\right)^4\frac{\eta}{\alpha}\,\bar{p}_z-\left(\Delta\bar{x}\right)^4\frac{\eta}{\alpha^2}\frac{\partial^2\bar{w}}{\partial\bar{t}^2}\\
&\quad+\eta\left[\left(\left(\Delta\bar{x}\right)^2\bar{\sigma}_0+\bar{F}_{i,j+1}-2\,\bar{F}_{i,j}+\bar{F}_{i,j-1}\right)\left(\bar{w}_{i+1,j}-2\,\bar{w}_{i,j}+\bar{w}_{i-1,j}\right)\right.\\
&\quad+\left(\left(\Delta\bar{x}\right)^2\bar{\sigma}_0+\bar{F}_{i+1,j}-2\,\bar{F}_{i,j}+\bar{F}_{i-1,j}\right)\left(\bar{w}_{i,j+1}-2\,\bar{w}_{i,j}+\bar{w}_{i,j-1}\right)\\
&\quad-\frac{1}{8}\left(\bar{F}_{i+1,j+1}-\bar{F}_{i+1,j-1}-\bar{F}_{i-1,j+1}+\bar{F}_{i-1,j-1}\right)\\
&\qquad\left.\left(\bar{w}_{i+1,j+1}-\bar{w}_{i+1,j}-\bar{w}_{i,j+1}+\bar{w}_{i,j}\right)\right]
\end{aligned}
\tag{3.9}
$$

The discretized nondimensional boundary conditions are:

Zero transverse deflection at edges.

$$\bar{w}_{i,j}\big|_{i=0,1}=0 \qquad \text{and} \qquad \bar{w}_{i,j}\big|_{j=0,1}=0 \tag{3.10}$$

Zero slope on respective edges.

$$\left(\bar{w}_{i+1,j}-\bar{w}_{i-1,j}\right)\big|_{i=0,1}=0 \qquad \text{and} \qquad \left(\bar{w}_{i,j+1}-\bar{w}_{i,j-1}\right)\big|_{j=0,1}=0 \tag{3.11}$$

Zero strain on edges.

$$\bar{\epsilon}_{\bar{x}}\big|_{j=0,1} = 2(\nu-1)\bar{F}_{i,j} + \bar{F}_{i,j+1} + \bar{F}_{i,j-1} - \nu\bar{F}_{i+1,j} - \nu\bar{F}_{i-1,j} = 0$$
$$\bar{\epsilon}_{\bar{y}}\big|_{i=0,1} = 2(\nu-1)\bar{F}_{i,j} + \bar{F}_{i+1,j} + \bar{F}_{i-1,j} - \nu\bar{F}_{i,j+1} - \nu\bar{F}_{i,j-1} = 0 \qquad (3.12)$$

Rearranging the elements of equation (3.7) so that F and $\bar{w}$ terms are on different sides of the equal signs, the boundary conditions specifying edge displacements of zero are obtained.

$$\int_{\bar{y}=const}\left[\frac{\partial^2\bar{F}}{\partial\bar{y}^2} - \nu\frac{\partial^2\bar{F}}{\partial\bar{x}^2}\right]d\bar{x} = \int_{\bar{y}=const}\left[\frac{1}{2}\left(\frac{\partial\bar{w}}{\partial\bar{x}}\right)^2\right]d\bar{x}$$
$$\int_{\bar{x}=const}\left[\frac{\partial^2\bar{F}}{\partial\bar{x}^2} - \nu\frac{\partial^2\bar{F}}{\partial\bar{y}^2}\right]d\bar{y} = \int_{\bar{x}=const}\left[\frac{1}{2}\left(\frac{\partial\bar{w}}{\partial\bar{y}}\right)^2\right]d\bar{y} \qquad (3.13)$$

Equation (3.13) is used to constrain the movement of the edges within the plane of the flat plate. Therefore it is integrated across half of the plate to allow different constraints to each edge, this will be reflected in the numerical expansion and integration of the equations. The finite difference expansion is:

$$\int_{\bar{y}=const}\left[2(\nu-1)\bar{F}_{i,j} + \bar{F}_{i,j+1} + \bar{F}_{i,j-1} - \nu\bar{F}_{i+1,j} - \nu\bar{F}_{i-1,j}\right]d\bar{x}$$
$$= \int_{\bar{y}=const}\left[\frac{1}{8}\left(\bar{w}_{i+1,j} - \bar{w}_{i-1,j}\right)^2\right]d\bar{x} \qquad (3.14)$$

$$\int_{\bar{x}=const} \left[2(\nu-1)\bar{F}_{i,j}+\bar{F}_{i+1,j}+\bar{F}_{i-1,j}-\nu\bar{F}_{i,j+1}-\nu\bar{F}_{i,j-1}\right] d\bar{y}$$
$$= \int_{\bar{x}=const} \left[\frac{1}{8}\left(\bar{w}_{i,j+1}-\bar{w}_{i,j-1}\right)^2\right] d\bar{y} \qquad (3.15)$$

Numerical integration of equations (3.14) and (3.15) is performed using the trapezoidal rule [52], and the numerical expansion is shown equations (3.16)-(3.19). Refer to Figure 3.1 for interpretation of numerical indices.

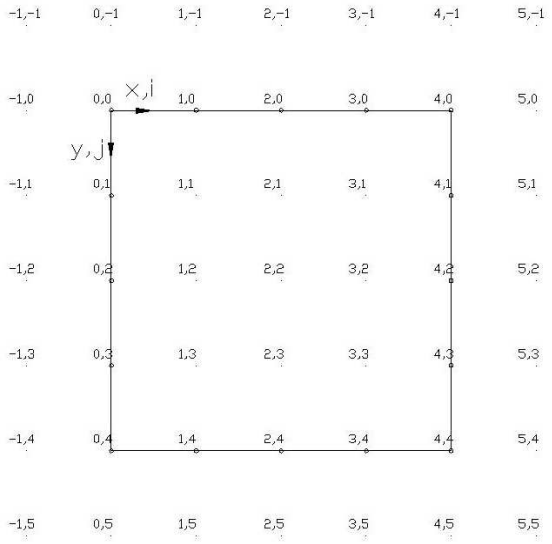

Figure 3.1: Example Finite Difference Mesh for n=5

$\bar{u}$ = 0 BC, constrained at west $\bar{y}$-edge, i = 0.

$$
\begin{aligned}
&\left[2\left(\nu-1\right)\bar{F}_{0,j}+\bar{F}_{0,j+1}+\bar{F}_{0,j-1}-\nu\,\bar{F}_{0+1,j}-\nu\,\bar{F}_{0-1,j}\right]+\\
&2\sum_{i=1}^{\frac{n-1}{2}}\left[2\left(\nu-1\right)\bar{F}_{i,j}+\bar{F}_{i,j+1}+\bar{F}_{i,j-1}-\nu\,\bar{F}_{i+1,j}-\nu\,\bar{F}_{i-1,j}\right]+\\
&\left[2\left(\nu-1\right)\bar{F}_{\frac{n-1}{2},j}+\bar{F}_{\frac{n-1}{2},j+1}+\bar{F}_{\frac{n-1}{2},j-1}-\nu\,\bar{F}_{\frac{n-1}{2}+1,j}-\nu\,\bar{F}_{\frac{n-1}{2}-1,j}\right]\\
&=\frac{1}{8}\left[\left(\bar{w}_{0+1,j}-\bar{w}_{0-1,j}\right)^2+2\sum_{i=1}^{\frac{n-1}{2}}\left(\bar{w}_{i+1,j}-\bar{w}_{i-1,j}\right)^2+\left(\bar{w}_{\frac{n-1}{2}+1,j}-\bar{w}_{\frac{n-1}{2}-1,j}\right)^2\right]d\,\bar{x}
\end{aligned}
\tag{3.16}
$$

$\bar{u}$ = 0 BC, constraining at east $\bar{y}$-edge, i = n-1.

$$
\begin{aligned}
&\left[2\left(\nu-1\right)\bar{F}_{\frac{n-1}{2},j}+\bar{F}_{\frac{n-1}{2},j+1}+\bar{F}_{\frac{n-1}{2},j-1}-\nu\,\bar{F}_{\frac{n-1}{2}+1,j}-\nu\,\bar{F}_{\frac{n-1}{2}-1,j}\right]+\\
&2\sum_{i=\frac{n-1}{2}+1}^{n-1}\left[2\left(\nu-1\right)\bar{F}_{i,j}+\bar{F}_{i,j+1}+\bar{F}_{i,j-1}-\nu\,\bar{F}_{i+1,j}-\nu\,\bar{F}_{i-1,j}\right]+\\
&\left[2\left(\nu-1\right)\bar{F}_{n-1,j}+\bar{F}_{n-1,j+1}+\bar{F}_{n-1,j-1}-\nu\,\bar{F}_{n-1+1,j}-\nu\,\bar{F}_{n-1-1,j}\right]\\
&=\frac{1}{8}\left[\left(\bar{w}_{\frac{n-1}{2}+1,j}-\bar{w}_{\frac{n-1}{2}-1,j}\right)^2+2\sum_{i=\frac{n-1}{2}+1}^{n-1}\left(\bar{w}_{i+1,j}-\bar{w}_{i-1,j}\right)^2+\left(\bar{w}_{n-1+1,j}-\bar{w}_{n-1-1,j}\right)^2\right]d\,\bar{x}
\end{aligned}
\tag{3.17}
$$

$\bar{v}$ = 0 BC, constraining at north $\bar{x}$-edge, j = 0.

$$\begin{aligned}
&\left[2(\nu-1)\bar{F}_{i,0}+\bar{F}_{i+1,0}+\bar{F}_{i-1,0}-\nu\bar{F}_{i,0+1}-\nu\bar{F}_{i,0-1}\right]+\\
&2\sum_{j=1}^{\frac{n-1}{2}-1}\left[2(\nu-1)\bar{F}_{i,j}+\bar{F}_{i+1,j}+\bar{F}_{i-1,j}-\nu\bar{F}_{i,j+1}-\nu\bar{F}_{i,j-1}\right]+\\
&\left[2(\nu-1)\bar{F}_{i,\frac{n-1}{2}}+\bar{F}_{i+1,\frac{n-1}{2}}+\bar{F}_{i-1,\frac{n-1}{2}}-\nu\bar{F}_{i,\frac{n-1}{2}+1}-\nu\bar{F}_{i,\frac{n-1}{2}-1}\right]\\
&=\frac{1}{8}\left[\left(\bar{w}_{i,0+1}-\bar{w}_{i,0-1}\right)^2+2\sum_{j=1}^{\frac{n-1}{2}-1}\left(\bar{w}_{i,j+1}-\bar{w}_{i,j-1}\right)^2+\left(\bar{w}_{i,\frac{n-1}{2}+1}-\bar{w}_{i,\frac{n-1}{2}-1}\right)^2\right]
\end{aligned} \tag{3.18}$$

$\bar{v}$ = 0 BC, constraining at south $\bar{x}$-edge, j = n-1.

$$\begin{aligned}
&\left[2(\nu-1)\bar{F}_{i,\frac{n-1}{2}}+\bar{F}_{i+1,\frac{n-1}{2}}+\bar{F}_{i-1,\frac{n-1}{2}}-\nu\bar{F}_{i,\frac{n-1}{2}+1}-\nu\bar{F}_{i,\frac{n-1}{2}-1}\right]+\\
&2\sum_{j=\frac{n-1}{2}+1}^{n-1}\left[2(\nu-1)\bar{F}_{i,j}+\bar{F}_{i+1,j}+\bar{F}_{i-1,j}-\nu\bar{F}_{i,j+1}-\nu\bar{F}_{i,j-1}\right]+\\
&\left[2(\nu-1)\bar{F}_{i,n-1}+\bar{F}_{i+1,n-1}+\bar{F}_{i-1,n-1}-\nu\bar{F}_{i,n-1+1}-\nu\bar{F}_{i,n-1-1}\right]\\
&=\frac{1}{8}\left[\left(\bar{w}_{i,\frac{n-1}{2}+1}-\bar{w}_{i,\frac{n-1}{2}-1}\right)^2+2\sum_{j=\frac{n-1}{2}+1}^{n-1}\left(\bar{w}_{i,j+1}-\bar{w}_{i,j-1}\right)^2+\left(\bar{w}_{i,n-1+1}-\bar{w}_{i,n-1-1}\right)^2\right]
\end{aligned} \tag{3.19}$$

Now, with equations (3.8), (3.9), (3.10), (3.11), (3.12), (3.16), (3.17), (3.18) and (3.19) a numerical solution can be obtained, detailed in sections 3.3 and 3.4.

3.3 Iterative Solution Technique for Static Analysis

In the following discussion variables will be bold to emphasize that matrices and vectors are being manipulated to obtain a solution. Two matrices are formed to solve for

the values of $\bar{\boldsymbol{F}}$ and $\bar{\boldsymbol{w}}$. These matrices consist of the nondimensional finite differenced governing equation and related boundary conditions. For the equilibrium equation the matrix $\boldsymbol{K}$ consists of equations (3.9), (3.10), and (3.11). The compatibility matrix $\boldsymbol{H}$ then consists of equations (3.8), (3.12), (3.16), (3.17), (3.18), and (3.19). Therefore in the iterative scheme detailed below the relations will be:

Equilibrium relation

$$\boldsymbol{K}\,\bar{\boldsymbol{w}} = \boldsymbol{P} \tag{3.20}$$

Compatibility relation

$$\boldsymbol{H}\,\bar{\boldsymbol{F}} = \boldsymbol{G} \tag{3.21}$$

The solution technique used to solve the static governing equations is the same shown by Chia [24]. It is an iterative solution technique of the two governing equations, that holds one of the variables ($\bar{\boldsymbol{F}}$ or $\bar{\boldsymbol{w}}$) constant and solves for the other, then uses the obtained values in the corresponding equations to obtain a solution for the other unknown variable. This is shown in equations (3.20) and (3.21) in that $\bar{\boldsymbol{F}}$ and $\bar{\boldsymbol{w}}$ have been uncoupled. In the text below the iteration number is denoted by the bracketed superscript number.

1. Assume stress function value of 0 over the entire membrane for the first iteration.

$\bar{\boldsymbol{F}}^{[0]}=0$

2. Using this assumed stress function solve for the deflection using the equilibrium relation (3.20). A solution of $\bar{\boldsymbol{w}}$ is obtained for the first iteration step, $\bar{\boldsymbol{w}}^{[0]}$.
3. Using $\bar{\boldsymbol{w}}^{[0]}$ in the compatibility relation (3.21), a new stress function, $\bar{\boldsymbol{F}}^{[1]}$, is solved for.
4. $\bar{\boldsymbol{F}}^{[1]}$ is then used in the same fashion as $\bar{\boldsymbol{F}}^{[0]}$ was used in step 2 to obtain a new solution for $\bar{\boldsymbol{w}}$, i.e. $\bar{\boldsymbol{w}}^{[1]}$.
5. To encourage faster convergence an acceleration factor, γ, is used.

$$\bar{\boldsymbol{w}}^{\left[n+\frac{3}{2}\right]}=\gamma\,\bar{\boldsymbol{w}}^{[n]}+\left(1-\gamma\right)\bar{\boldsymbol{w}}^{[n+1]} \tag{3.22}$$

   γ = ½ is documented as resulting in the most efficient convergence [24 p. 89], and this value is used in the implementation.
6. This process is then continued until a value is converged upon.
7. After the solution is deemed converged, stress values can be extracted along with piezoelectric charge. Convergence is determined by examining the magnitude of the center deflection in comparison to the change in value of each iteration. For example, if a 30 μm deflection is expected a change in iteration value of ~10 nm is considered converged.

3.4 Solution Technique for Dynamic Analysis – No Damping

Initially work was done pertaining to the undamped oscillation of a membrane. A time integration technique was used as shown below. In the following sections, 3.4 and 3.5, a lowercase $\boldsymbol{w}$ is used to denote any generic displacement. These equations are applicable in both the nondimensional and dimensional cases with no modification, and thus are generally shown here. The step-by-step Newmark β numerical integration technique is used [48], the equations are expressed in the form where k is the time-step number.

$$\boldsymbol{w}_{k+1} = \boldsymbol{w}_k + \Delta t\, \dot{\boldsymbol{w}}_k + \left(\Delta t\right)^2 \left(\tfrac{1}{2} - \beta\right) \ddot{\boldsymbol{w}}_k + \left(\Delta t\right)^2 \beta\, \ddot{\boldsymbol{w}}_{k+1} \tag{3.23}$$

$$\dot{\boldsymbol{w}}_{k+1} = \dot{\boldsymbol{w}}_k + \left(1 - \gamma\right) \Delta t\, \ddot{\boldsymbol{w}}_k + \gamma\, \Delta t\, \ddot{\boldsymbol{w}}_{k+1} \tag{3.24}$$

The formula for a general undamped oscillating system with a distributed mass is:

$$\boldsymbol{M}\, \ddot{\boldsymbol{w}}_k + \boldsymbol{K}\, w_k = \boldsymbol{P}_k \tag{3.25}$$

Solving for $\boldsymbol{M}\, \ddot{\boldsymbol{w}}_k$

$$\boldsymbol{M}\, \ddot{\boldsymbol{w}}_k = \boldsymbol{P}_k - \boldsymbol{K}\, w_k \tag{3.26}$$

Then multiplying equations (3.23) and (3.24) by $\boldsymbol{M}$, and substituting equation (3.26) the final equations are obtained.

$$\begin{aligned}\left[\boldsymbol{M}+\beta(\Delta t)\boldsymbol{K}\right]\boldsymbol{w}_{k+1} &= \boldsymbol{M}\,\boldsymbol{w}_k+\Delta t\,\boldsymbol{M}\,\dot{\boldsymbol{w}}_k \\ &\quad +(\Delta t)^2\left(\tfrac{1}{2}-\beta\right)\left(\boldsymbol{P}_k-\boldsymbol{K}\,w_k\right)+(\Delta t)^2\,\beta\,\boldsymbol{P}_{k+1}\end{aligned} \tag{3.27}$$

$$\boldsymbol{M}\,\dot{\boldsymbol{w}}_{k+1}=\boldsymbol{M}\,\dot{\boldsymbol{w}}_k+\Delta t(1-\gamma)\left(\boldsymbol{P}_k-\boldsymbol{K}\,\boldsymbol{w}_k\right)+\Delta t\,\gamma\left(\boldsymbol{P}_{k+1}-\boldsymbol{K}\,\boldsymbol{w}_{k+1}\right) \tag{3.28}$$

Where the stiffness matrix, $\boldsymbol{K}$, is the same used in equation (3.20). The mass matrix, $\boldsymbol{M}$, is a diagonal matrix containing the term $(\Delta\bar{x})^4\frac{\eta}{\alpha^2}$ which is the coefficient of the time derivative shown in equation (3.9).The $\boldsymbol{P}$ vector is the forcing function defined by the application of the load to the test subject. β and γ are coefficients exclusive to the Newmark technique, and can represent different methods of time integration. In this case the average acceleration technique is used, this is analogous to β = ¼ and γ = ½. These values are chosen due to being unconditionally stable, unconditionally convergent, and avoiding such problems as numerical damping and period elongation. A review of the different values of β and γ and their meaning in relation to the type of time integration can be found in [48].

Representing equations (3.27) and (3.28) in a compact form

$$\boldsymbol{K}^{*}\boldsymbol{w}_{k+1}=\boldsymbol{P}^{*}_{(d)} \tag{3.29}$$

$$\boldsymbol{M}\dot{\boldsymbol{w}}_{k+1}=\boldsymbol{P}^{*}_{(v)} \tag{3.30}$$

Where superscript * denotes effective values and subscript (d) relates to displacement and superscript (v) denotes velocity. Using equations (3.21), (3.29), and (3.30) an algorithm can be developed to iteratively solve for the dynamic behavior.

1. Assume initial values for displacement and velocity. Initial displacements and Airy stress field are typically found from the static analysis. An assumed zero initial velocity and acceleration are also implemented.
2. For the first time-step the values from step 1 are used for $\boldsymbol{K}^{*}$ and $\boldsymbol{P}^{*}_{(d)}$, a solution is obtained for $\boldsymbol{w}_{k+1}$.
3. From equation (3.21) a stress function value is calculated.
4. The stress function value from step 3 is then used in equation (3.29) to calculate a new value for $\boldsymbol{w}_{k+1}$.
5. Steps 3 and 4 are repeated until a solution is converged upon.
6. Then using the converged values from step 5 the velocity for the next time step is calculated using equation (3.30).
7. This process is repeated for additional time steps.

3.5 Solution Technique for Dynamic Analysis – Damping

This technique numerically integrates a problem in time using the modified Newmark technique for matrices developed by Wilson in 1962 [53]. The initial equations are derived by Newmark in [48] and will be expounded upon here. Beginning with the generic distributed oscillating system.

$$\boldsymbol{M}\,\ddot{\boldsymbol{w}}_k+\boldsymbol{C}\,\dot{\boldsymbol{w}}_k+\boldsymbol{K}\,\boldsymbol{w}_k=\boldsymbol{P}_k \tag{3.31}$$

Then introducing the Newmark equations

$$\boldsymbol{w}_{k+1}=\boldsymbol{w}_k+\Delta t\,\dot{\boldsymbol{w}}_k+\left(\Delta t\right)^2\left(\tfrac{1}{2}-\beta\right)\ddot{\boldsymbol{w}}_k+\left(\Delta t\right)^2\beta\,\ddot{\boldsymbol{w}}_{k+1} \tag{3.32}$$

$$\dot{\boldsymbol{w}}_{k+1}=\dot{\boldsymbol{w}}_k+\left(1-\gamma\right)\Delta t\,\ddot{\boldsymbol{w}}_k+\gamma\,\Delta t\,\ddot{\boldsymbol{w}}_{k+1} \tag{3.33}$$

Solving equation (3.32) for $\ddot{\boldsymbol{w}}_{k+1}$

$$\ddot{\boldsymbol{w}}_{k+1}=\frac{\boldsymbol{w}_{k+1}-\boldsymbol{w}_k}{\left(\Delta t\right)^2\beta}-\frac{1}{\left(\Delta t\right)\beta}\dot{\boldsymbol{w}}_k-\left(\tfrac{1}{2\beta}-1\right)\ddot{\boldsymbol{w}}_k \tag{3.34}$$

Then inserting equation (3.34) into equation (3.32)

$$\dot{\boldsymbol{w}}_{k+1}=\frac{\gamma}{\Delta t\cdot\beta}\left(\boldsymbol{w}_{k+1}-\boldsymbol{w}_{k}\right)+\left(1-\frac{\gamma}{\beta}\right)\dot{\boldsymbol{w}}_{k}+\Delta t\left(1-\frac{\gamma}{2\beta}\right)\ddot{\boldsymbol{w}}_{k} \tag{3.35}$$

Then representing the coefficients of equations (3.34) and (3.35) concisely

$$\begin{aligned} b_1&=\frac{1}{\left(\Delta t\right)^2\beta} \qquad b_2=-\frac{1}{\left(\Delta t\right)\beta} \qquad b_3=1-\frac{1}{2\beta} \\ b_4&=\frac{\gamma}{\Delta t\cdot\beta} \qquad b_5=1-\frac{\gamma}{\beta} \qquad b_6=\Delta t\left(1-\frac{\gamma}{2\beta}\right) \end{aligned} \tag{3.36}$$

Therefore equations (3.34) and (3.35) become

$$\ddot{\boldsymbol{w}}_{k+1}=b_1\left(\boldsymbol{w}_{k+1}-\boldsymbol{w}_{k}\right)+b_2\dot{\boldsymbol{w}}_{k}+b_3\ddot{\boldsymbol{w}}_{k} \tag{3.37}$$

$$\dot{\boldsymbol{w}}_{k+1}=b_4\left(\boldsymbol{w}_{k+1}-\boldsymbol{w}_{k}\right)+b_5\dot{\boldsymbol{w}}_{k}+b_6\ddot{\boldsymbol{w}}_{k} \tag{3.38}$$

Using equations (3.37) and (3.38) in equation (3.31) for k+1 and the simplifying

$$\begin{aligned} &\boldsymbol{M}\,b_1\boldsymbol{w}_{k+1}+\boldsymbol{C}\,b_4\boldsymbol{w}_{k+1}+\boldsymbol{K}\,\boldsymbol{w}_{k+1} \\ &=\boldsymbol{F}_{k}-\boldsymbol{M}\left[b_2\dot{\boldsymbol{w}}_{k}+b_3\ddot{\boldsymbol{w}}_{k}-b_1\boldsymbol{w}_{k}\right]-\boldsymbol{C}\left[b_5\dot{\boldsymbol{w}}_{k}+b_6\ddot{\boldsymbol{w}}_{k}-b_4\boldsymbol{w}_{k}\right] \end{aligned} \tag{3.39}$$

The $\boldsymbol{M}$ matrix is the coefficient of $\frac{\partial^2 W}{\partial t^2}$ in diagonal format.

$$\boldsymbol{M} = \begin{bmatrix} (\Delta \bar{x})^4 \frac{\eta}{\alpha^2} & 0 & 0 & 0 \\ 0 & \ddots & 0 & 0 \\ 0 & 0 & \ddots & 0 \\ 0 & 0 & 0 & (\Delta \bar{x})^4 \frac{\eta}{\alpha^2} \end{bmatrix} \tag{3.40}$$

Where the $\boldsymbol{K}$ matrix is the square stiffness matrix composed of the quantities that are partial derivatives in space of $\bar{\boldsymbol{w}}$. The $\boldsymbol{C}$ matrix is either proportional to the $\boldsymbol{M}$ or $\boldsymbol{K}$ matrix or a combination of the two. β = ¼ and γ = ½ are also used here for the same reason previously stated. A solution is then pursued using equations (3.37), (3.38), and (3.39). The solution algorithm proceeds as follows:

1. Obtain initial conditions for displacement, velocity, and acceleration.
2. For the 1st time-step use the initial conditions from step 1 to obtain a solution to equation (3.39), $\bar{\boldsymbol{w}}_{k+1}$.
3. Using the solution from step 2 obtain a solution for $\bar{\boldsymbol{F}}$ from equation (3.2).
4. Then using the solution from step 3 obtain another solution for $\bar{\boldsymbol{w}}_{k+1}$.
5. Repeat this procedure until a convergent solution for that time-step is obtained.
6. Solve for velocities and acceleration from step 5 using equations (3.37) and (3.38).
7. Using the solutions from step 5 and 6 solve for the next time step (i.e. $\bar{\boldsymbol{w}}_{k+2}$) in the same fashion done for the initial conditions.
8. Repeat as necessary.

Chapter 4: Model Validation and Numerical Study

4.1 Validation

In order to prove the assumptions and techniques used in the presented model verification is required. There are two regimes which must be validated; what occurs statically and what occurs dynamically. Prior experiments were performed by others involved in the P3 project, using either a Michelson interferometer and a bulge tester [54] or a laser vibrometer [55]. These experimental results are then compared to what the model predicts for the same problem parameters.

All of the shown data is for blanket PZT, and while effects of the electrode pigtails occur in experimentation they are ignored in the model. The values shown in Table 4.1 are typical of most devices examined in this thesis. When values deviate from Table 4.1 the new values are tabulated.

Number of Layers	4			
Side length (mm)	3			
Residual Stress (MPa)	105			
d_{31} (pC/m^2)	85			
Static Load (kPa)	10			
Material	Modulus (GPa)	Poison's Ratio	Density (kg/m^3)	Thickness (μm)
PZT	70	0.27	7500	1
Silicon	125	0.30	2550	1
Gold	80	0.44	19280	0.3
Platinum	170	0.38	21440	0.18
Composite	112	0.31	8027	2.48

Table 4.1: Typical/Representative generator membrane parameters for Chapter 4 and section 5.1

Static verification of the model is first done by comparison of the deflected shape upon the diagonal profile, as seen in Figure 4.1. Although the match is not exact, it is within acceptable tolerances, and displays that the simulated profile is sufficient.

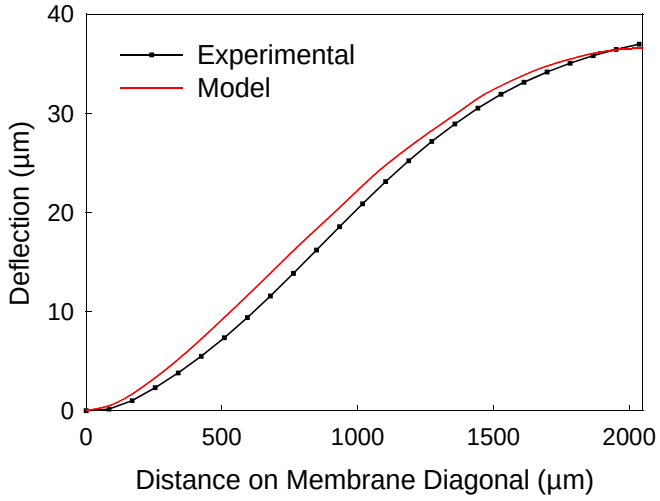

Figure 4.1: Validation of static shape profile along the membrane diagonal

Figure 4.1 Parameters	***Experimental***	***Model***
Si thickness (µm)	1.1	1.0
PZT thickness (µm)	1.0	1.0
Pressure (kPa)	21.0	21.0

Table 4.2: Parameters for runs associated with Figure 4.1

Another static verification test performed compares the center deflection for a given pressure. This test is also used in verifying the assumptions used in the applied lamination theory. Two tests were run, one was run with a single ply silicon membrane, and another was run with the typical generator membrane laminate, using parameters

shown in Table 4.1 and Table 4.3. These tests are compared to what is obtained using the developed model in Figure 4.2. In Figure 4.2 it is obvious that the two curves agree, proving that the model can fit a simple single ply membrane and also proving that the assumptions that were made in order to develop the lamination theory are correct, insofar as the regime the model will be applied too.

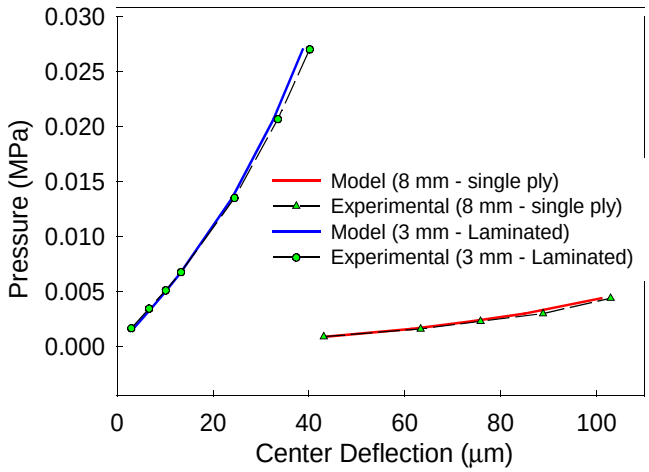

Figure 4.2: Pressure deflection curve for model validation

Figure 4.2 Parameters	***Experimental (3mm)***	***Model (3mm)***	***Experimental (8mm)***	***Model (8mm)***
Si thickness (μm)	1.1	1.1	2.0	2.0
PZT thickness (μm)	1.0	1.0	0.0	0.0
Residual Stress (MPa)	100.0	117.0	~ 40.	44.0
E^* (GPa)	NA	114.0	NA	125.0

Table 4.3: Parameters for runs associated with Figure 4.2

Comparison of the charge accumulated on the membrane experimentally and numerically is done in Figure 4.3. Charge was collected experimentally using an integrating charge circuit that collected the charge as the membrane was brought down from a maximum deflection [6]. The difference between the collected experimental charge and the charge obtained from the model is negligible. Thus, validating the piezoelectric theory used.

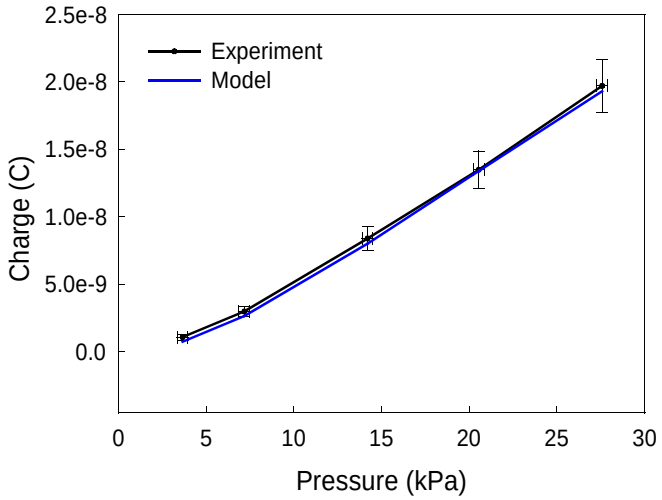

Figure 4.3: Charge comparison

Figure 4.3 Parameters	***Experimental***	***Model***
Si thickness (μm)	2.0	2.0
PZT thickness (μm)	1.0	1.0
Residual Stress (MPa)	~70.0	87.0
E^* (GPa)	NA	119.0

Table 4.4: Parameters associated with Figure 4.3

One of the primary purposes of development of this model is determination of dynamic characteristics. Subsequently it is proven that this model accurately predicts the dynamic behavior. Shown in Figure 4.4 is the comparison of predicted free vibration frequency and a resonance frequency obtained through electrical excitation [55]. The shown experimental residual stress was obtained using a pressure-deflection technique [56].These should be similar in that they both exhibit the dominant frequency in the structure at an approximate deflection of .5 μm. Although there is some discrepancy in the comparison, it is adequate to provide validation of the dynamic portion of the model. The frequency overestimation provided by the model is presumed to be due to the relatively coarse mass lumping of the finite difference method.

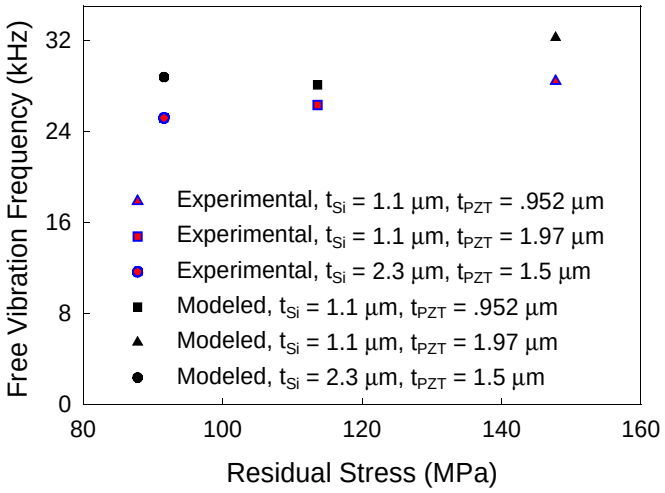

Figure 4.4: Dynamic resonance verification

It has been shown that the presented model agrees reasonably well with experimental data. Agreement with this data proves that the assumptions implemented to apply a 1) theory of lamination, 2) a theory of piezoelectricity, and 3) a solution method for dynamic and static behavior are sufficiently correct.

Errors in the proposed model will stem from the numerics implemented. Obviously, such things as using a finite difference equations for derivatives and numerical integration schemes will introduce errors. But, numerical parameters can be optimized, such as as mesh density, time steps, and numerical precision, to help minimize these spurious effects.

4.2 Numerical Study

Optimization of the numerical process is required. The goal is to decrease the CPU time needed to solve the numerical problem. Subsequently the areas of interest are the physical mesh size, shown in Figure 3.1, and the time step size. Another factor that will affect program performance is the amount of I/O, but this can be minimized and was not analyzed here.

The most common value used for the physical mesh is n = 15, less common values are n = 45 due to the increased CPU time in solving the associated matrices. The study shown in Figure 4.5 is performed for the static problem, using parameters from Table 4.1 except for silicon thickness which is 2 μm, and analyzes the effect of mesh size, *n*, on time to converge and the associated change of center deflection. From Figure 4.5 it is determined that the best choice for the static analysis, keeping accuracy in mind and desiring a run time of less than one minute, is n = 21.

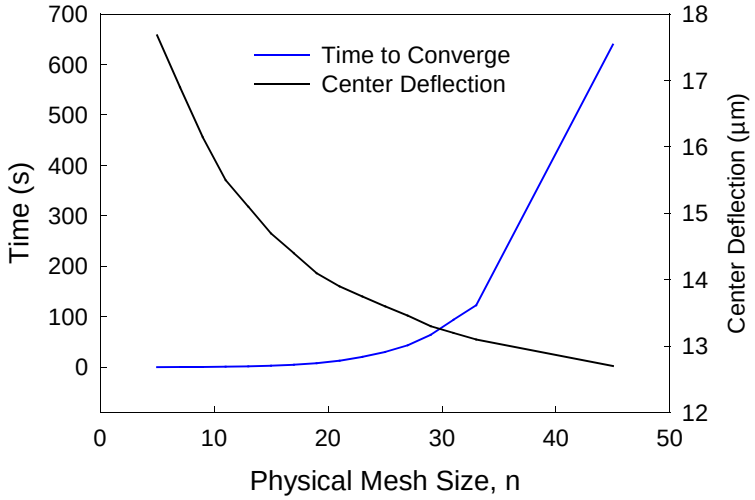

Figure 4.5: Mesh size study

The dynamic analysis requires multiples of iteration steps, i.e. number of time steps, therefore an even further decrease in *n* is done in the interest of solution time for a relatively small sacrifice in accuracy. Shown in Figure 4.6 is the effect of physical mesh on the center deflection response for free vibration. It is discernible that different mesh sizes will result in slightly different responses the further in time the analysis progresses. Though all three different mesh sizes give approximately the same amplitude and phase response, therefore a physical mesh of n = 15 is chosen to expedite the model.

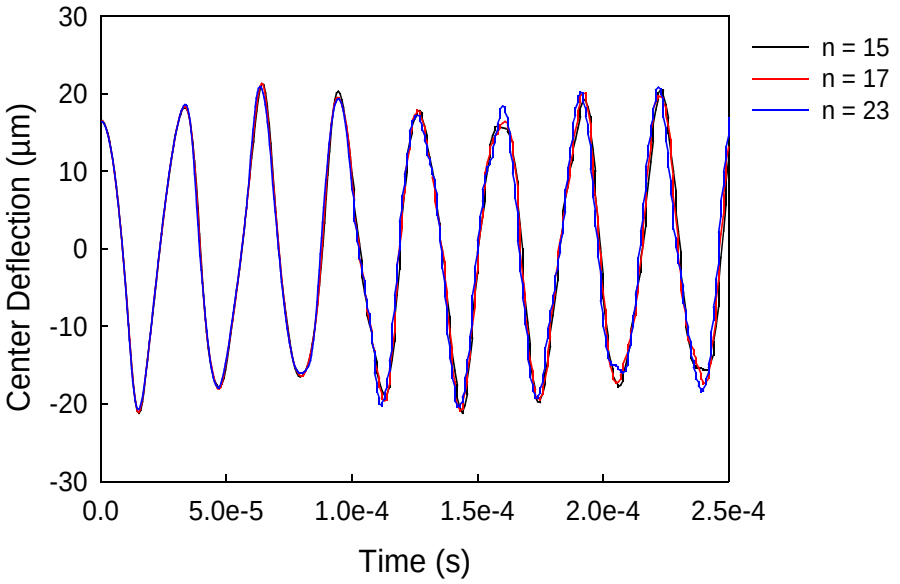

Figure 4.6: Effect on undamped free vibration of mesh size

The time step will also have an effect on the response. Figure 4.7 displays that too large of a time step, 3.38e-6 seconds, can result in numerical damping and an undesired phase shift, the other two time steps show little of these effects. The time step of 3.38e-6 is approximately 10 steps per vibration cycle, 3.38e-7 is one hundred steps per vibration cycle, and 3.45e-9 is approximately 10,000 steps per vibration cycle. The time it takes to run these models is 1 minute, 8 minutes, and 10 hours, respectively.

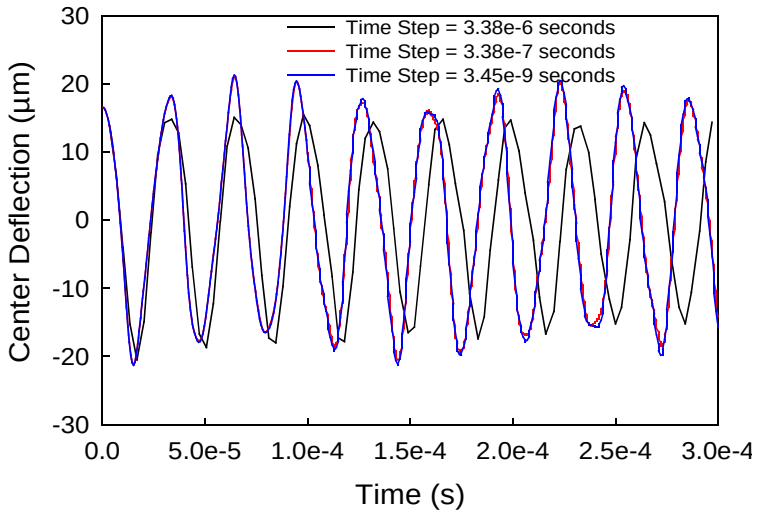

Figure 4.7: Effect of time step size on the center deflection response

Establishment of the optimum physical mesh size and the optimum time step size is shown. In the remainder of the thesis, data and figures generated with a mesh size of 15 and a time step size of 100 steps/cycle are shown. Results from these numerical parameters should be sufficiently accurate and will represent the actual behavior without significant parasitic numerical behavior.

Chapter 5: Results

5.1 Static – Profile Analysis

The static response can be better understood through examining reactionary behavior and profiles of applicable values. Visualization of the structure under its deformed configuration is a useful tool that will lend insight into optimization. The three-dimensional shape profile is shown in Figure 5.1. Refer to Table 4.1 for parameters used in this section, except for the silicon which is 2 μm.

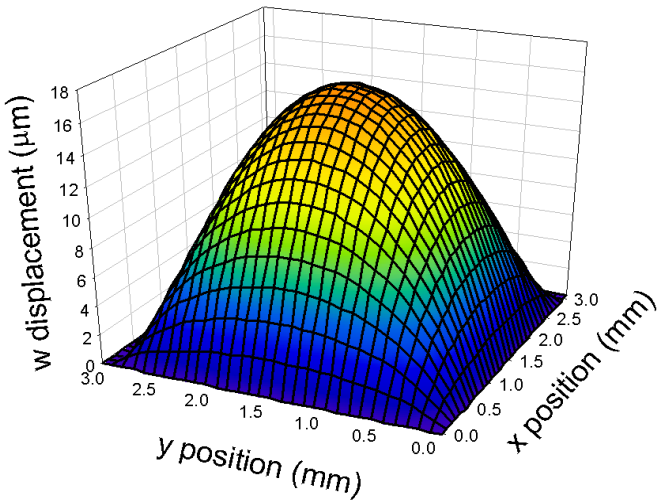

Figure 5.1: Deflected shape profile for typical membrane

Next an analysis of the stress distributions is presented. From equation (2.29) it is known that the important stresses for charge creation are σ_x and σ_y. In Figure 5.2 the stress in the x-direction is shown, the stress in the y-direction is exactly that of Figure 5.2, but shifted 90° about the z-axis.

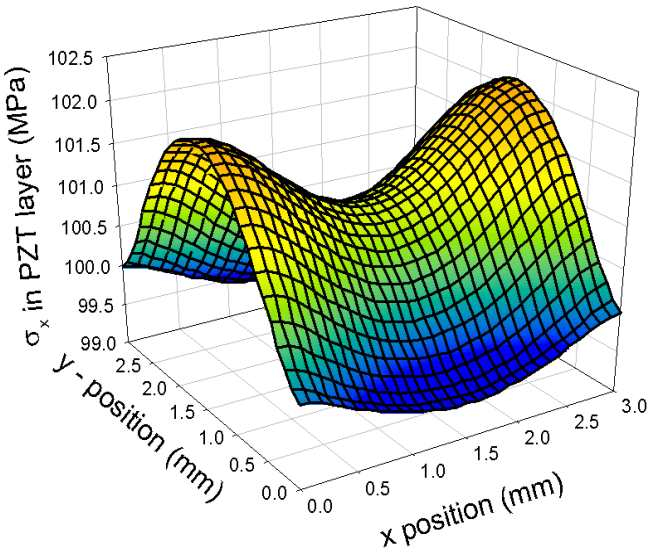

Figure 5.2: σ_x profile

From the σ_x and σ_y profiles an X-like pattern for the charge distribution is expected. In Figure 5.3 the charge profile is plotted, showing maximum charge density at the membrane center, which is expected. The interesting thing to note is that the lines of constant charge are rotated 45° in respect to the sides. Meaning that if an electrode that would harvest the maximum voltage is desired the optimum placement would be a square rotated 45° from the x or y-axis with an approximate side length of 2.12 mm.

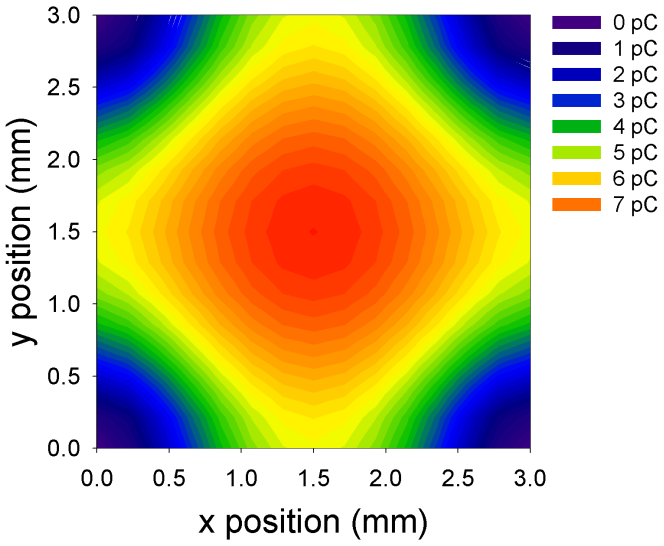

Figure 5.3: Charge profile

Principle stresses are also useful in determining where the maximum or minimum axial stresses will occur and therefore where failure might occur. The first principle stress displays the maximum tensile stress in the middle of each side of the membrane. Figure 5.4 implies that failure would occur in the middle of any of the four sides assuming there would be no imperfections in the actual structure that would accelerate failure elsewhere.

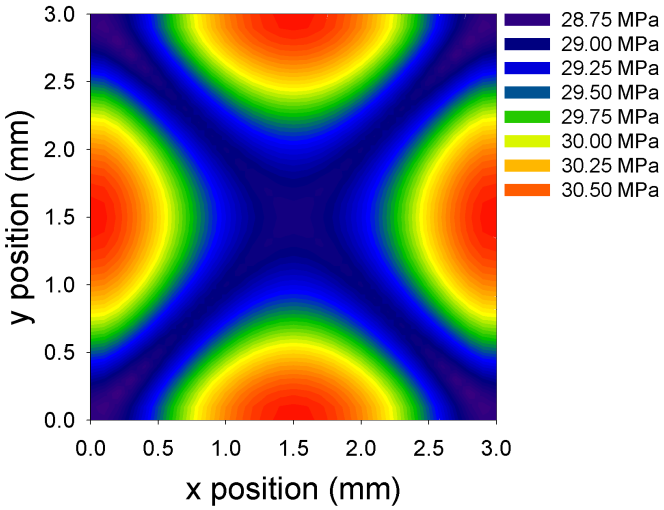

Figure 5.4: First principle stress, σ1 (Pa)

The charge distribution clearly does not match any of the principle stresses. This is due to the nature of how the charge is generated. Charge generation is dependent upon the stresses σ_x and σ_y, and not the principle stresses which are a combination of σ_x, σ_y, and τ_{xy}. The relationship between charge distribution and principle stress distribution should not be confused.

5.2 Static – Parameter Study

Characterization of the membrane generator involves understanding its static behavior. This is generally done by obtaining pressure-deflection curves on a bulge tester using a Michelson interferometer [57]. Other tests are done to also characterize the piezoelectric response [6]. The ability of this model to match the data is illustrated in Chapter 4. A parametric study is done to suggest an optimum configuration. This section uses the parameter values shown in Table 5.1. The initial examination pertains to the

effect of residual stress upon the pressure-deflection curve and the deflection-charge curve. It is also noted that the electrode size is assumed to be the same size as the membrane unless otherwise stated.

Number of Layers	4			
Side length (mm)	3			
Residual Stress (MPa)	105			
d_{31} (pC/m^2)	85			
Static Load (kPa)	1 – 20			
Material	Modulus (GPa)	Poisons Ratio	Density (kg/m^3)	Thickness (μm)
PZT	70	0.27	7500	1
Silicon	125	0.30	2550	2
Gold	80	0.44	19280	0.3
Platinum	170	0.38	21440	0.18
Composite	119	0.31	6448	3.5

Table 5.1: Typical/Representative generator membrane parameters for section 5.2

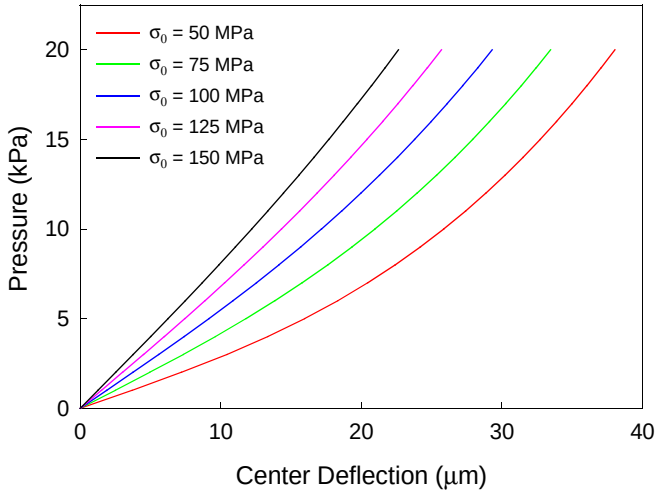

Figure 5.5: Pressure-deflection curve for a variation of σ_0

The rather obvious effect of increasing residual stress is emphasized in Figure 5.5. As σ_0 increases the structure becomes increasingly stiff, and the low pressure behavior becomes more linear due to the requirement of more generated in-plane stress to overcome σ_0.

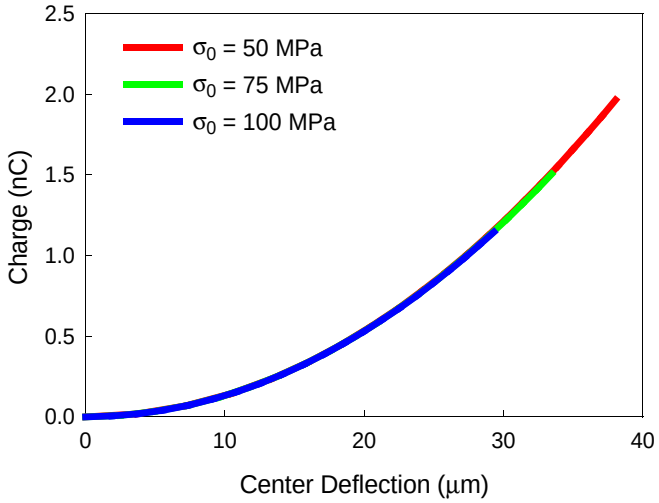

Figure 5.6: Charge-deflection for a variation of σ_0

Intuitively, residual stress will decrease the available charge purely due to the increase of effective stiffness. In Figure 5.6 the center deflection versus charge curves are obtained for a range of pressures from 1 kPa to 20 kPa, where the line endpoints are at 20 kPa. The nature of how the residual stress is applied leads to the result seen in Figure 5.6. Residual stress is assumed uniform and applied in the x and y directions, subsequently different residual stresses will not result in different shapes. The structure has the same shape at the same deflection for different residual stresses, (which requires a different applied pressure) the charge distribution must be the same and therefore the total charge

is the same. Due to this increased effective stiffness effect it is clear that reduction of residual stress in the working device is of import.

Changes in thickness of the various layers in the laminate are of interest in optimization. Shown in Figure 1.1 is the actual physical structure and in Figure 1.2 is the laminate used in the model for the sake of simplicity. The gold and platinum layer thickness cannot practically be varied because of manufacturing complications, the PZT and Si thicknesses, on the other hand, can be varied a reasonable amount in comparison. Investigation of what occurs with the variance in these layers is examined below.

Curves relating the charge generated to the center deflection are shown in Figure 5.7. The corresponding pressure-deflection curve is shown in Figure 5.8. All curves shown below have an applied pressure ranging from 1 kPa to 20 kPa, therefore each line endpoint is at 20 kPa. The other parameters are held constant in these figures and shown in Table 5.1.

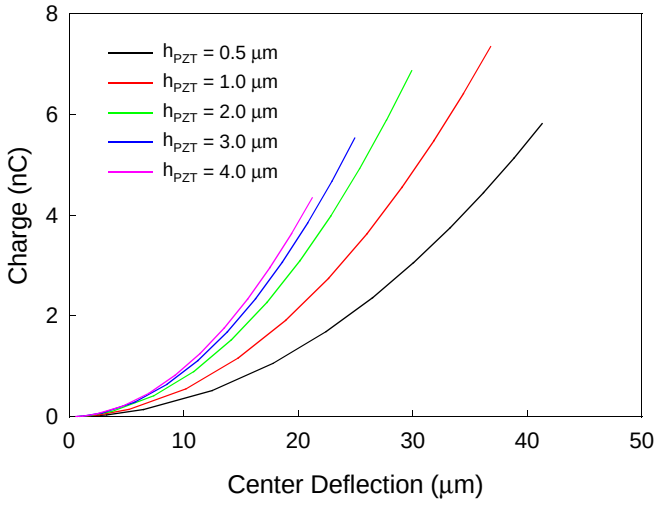

Figure 5.7: Charge-deflection curve for a membrane with h_{Si} = 1.0 μm

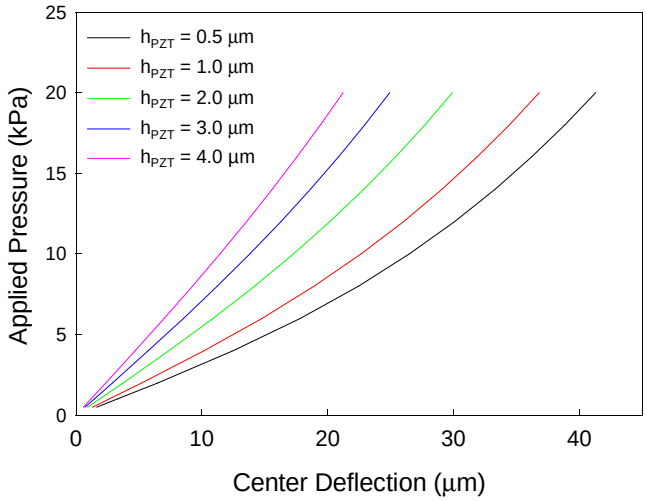

Figure 5.8: Pressure-deflection curve for a membrane with h_{Si} = 1.0 μm

As the thickness is increased it is expected that the stiffness will increase, this is proven in Figure 5.8. For thicker PZT the membrane is less compliant, yet increasing the thickness of the PZT will allow more material to be available that can generate charge. A combination of these two phenomenon result in an optimum PZT thickness. It is assumed, for simplicity, that there is no change in residual stress for changes in lamina thickness. An optimum thickness can be obtained from Figure 5.7 by observing which curve gives the maximum charge at the line endpoint (p = 20 kPa). In Figure 5.7 the optimum structure from a charge point of view contains approximately 1 μm PZT for 1 μm Si.

Although the charge extracted from the generator membrane is of importance, the energy required to obtain this charge is of importance. Analysis of this is performed by taking a ratio of the useful strain energy in the PZT and the strain energy in the entirety of the structure. What is meant by useful strain energy is the strain energy that could be

used to obtain an electric charge. From equation 2.29 the useful strain stems from σ_x and σ_y, while τ_{xy} still exists in the PZT layer it is ignored in the strain energy expression for the PZT (i.e. shear does not produce charge).

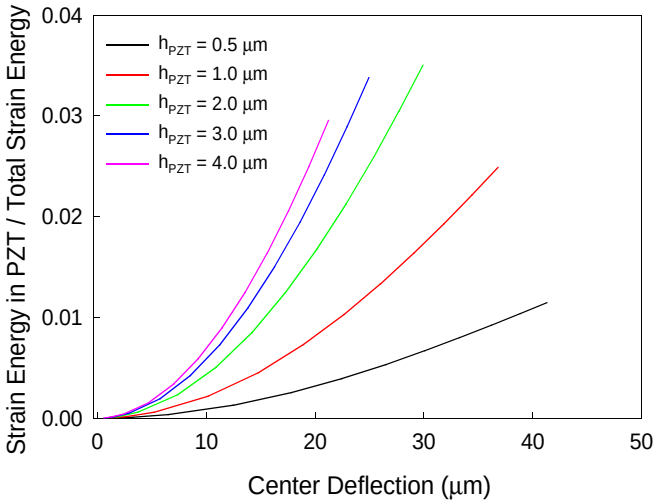

Figure 5.9: Strain energy ratio for a membrane with h_{Si} = 1.0 μm

Figure 5.9 does not agree with the optimum thickness implied by Figure 5.7, from the strain energy ratio analysis a thickness of approximately 2 μm appears to be ideal (i.e. highest dependent value for any of the thicknesses examined). Each curve is for the same pressures, i.e. 1-20 kPa, where the end points are 20 kPa. The highest strain energy ration is obtained for 2 μm PZT at 20 kPa, therefore the largest portion of strain energy in the PZT layer is for 2 μm of PZT and this is realized as the optimum. Although not as much charge is being generated by the 2 μm thick PZT, due to its increase in stiffness, a larger fraction of the total energy is contributing to charge generation.

Also of interest is what occurs at different thickness of silicon. Multiple runs where made for an applied pressure of 20 kPa and the same post processing was performed that is shown in Figures 5.7 and 5.9. Figures 5.10 and 5.11 are the result of

these runs. All data shown in Figures 5.10 and 5.11 are at 20 kPa of applied pressure and the horizontal lines correspond with constant silicon thickness and the vertical lines correspond with constant PZT thickness.

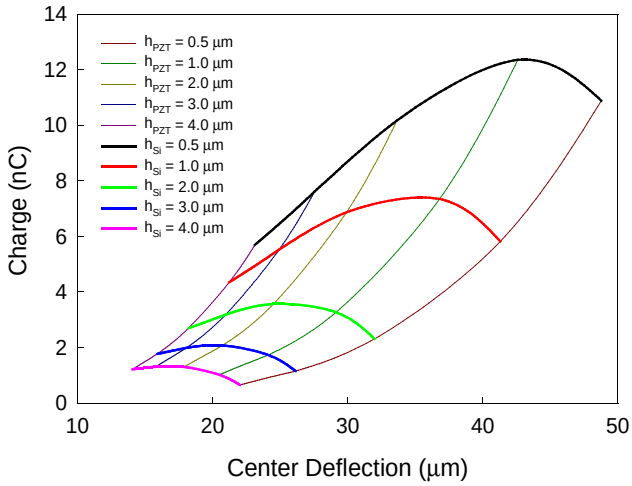

Figure 5.10: Si and PZT thickness effect on charge generated

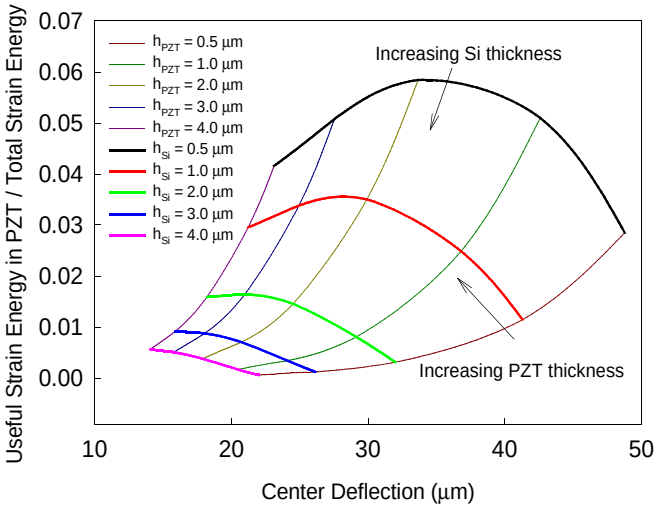

Figure 5.11: Si and PZT thickness effect on strain energy ratio

As was previously demonstrated, the optimum thickness implied by the charge curve does not correspond with that implied by the energy ratio curve; this is affirmed in Figures 5.10 and 5.11. The optimum for a specific silicon thickness is were the curve is maximum in regards to either the strain energy ratio or the charge. For maximum charge generation the PZT thickness varies from ~1 μm to ~2.5 μm and for the maximum strain energy ratio the PZT thickness varies from ~2 μm to ~4 μm. The typical working device lies between the lines with h_{si} = 1.0-2.0 μm, meaning that optimum PZT thickness for energy conversion will vary from 2 - 3 μm.

The effect of electrode size on the gathered charge is shown in Figure 5.12. From examination of the charge profile, Figure 5.3, it can be assumed that the larger the electrode the more charge will be gathered (i.e. there are no sections of negative charge). This is shown in Figure 5.12, the larger the electrode the larger the gathered charge. Experimental results show a coverage of ~50 % is ideal [55], this does not agree with the

modeled results. The reasons for this is the model only uses σ_x and σ_y to obtain charge, while in experimentation a piezoelectric moment effect occurs near the edges. Also, another reason for this discrepancy is that some of the experimental devices the PZT is etched at the boundaries creating a slightly different device which the included model cannot address. The waviness in the curve is due to the discrete nature of the model, and would not actually occur in experimentation.

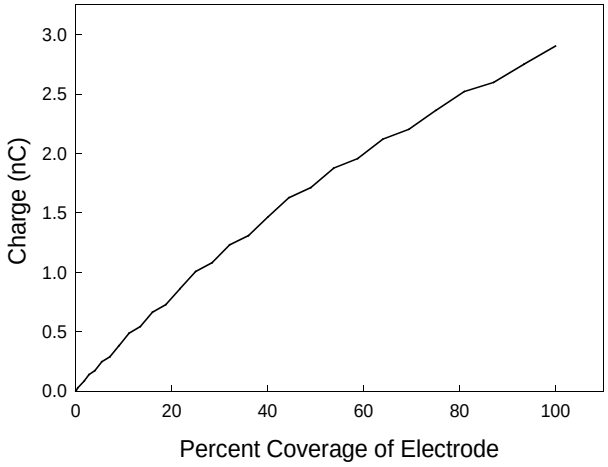

Figure 5.12: Electrode size effect on gathered charge

5.3 Dynamic – Free Undamped Vibration

A linear structure in free vibration will display its resonant frequency. This free vibration is also of interest here, yet with the interest of the contribution of various parameters. These parameters are the membrane side length, the residual stress, changes in lamina thickness, and the effect of nonlinearity. In the following figures all parameters

values, except the examined parameters and the applied pressure which is 10 kPa in the following section, are available in Table 5.1.

Examination of the effect of thickness on a single ply laminate is first examined with the interest of seeing where the behavior will change from membrane-like to plate-like. In membrane like behavior an addition of thickness will increase the overall mass, while in plate behavior an increase of thickness will not only cause an increase of mass it will also cause an increase in flexural rigidity.

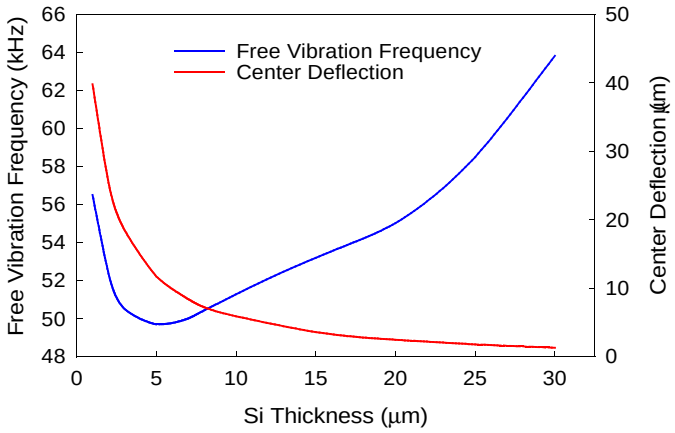

Figure 5.13: Thickness effect on free vibration of single ply structure

Number of Layers	1			
Side length (mm)	3			
Residual Stress (MPa)	105			
Static Load (kPa)	10			
Material	Modulus (GPa)	Poisons Ratio	Density (kg/m^3)	Thickness (μm)
Si	125	0.3	2500	varied

Table 5.2: Parameters associated with Figure 5.13

In Figure 5.13 the free vibration response is shown along with the center deflection for varying thickness of a silicon structure using an applied initial load of 10 kPa. At approximately 5 μm the free vibrational frequency appears to increase, this can be attributed to an increase in the contribution of plate like behavior. As can be seen from the center deflection curve, an increase in thickness stiffens the structure, causing a decrease in deflection. From 0 to 5 μm of silicon the structure exhibits membrane like behavior, from the 5 μm to 20 μm thickness range it exhibits plate like behavior, and beyond a 20 μm thickness plate behavior is even more significant.

Figure 5.14 shows the effect on free vibration for changes in PZT thickness and the silicon thickness for a residual stress of 105 MPa for all thicknesses. Although this exclusion of residual stress change is not realistic in actual devices it is assumed here for the reason of a pure thickness effect study.

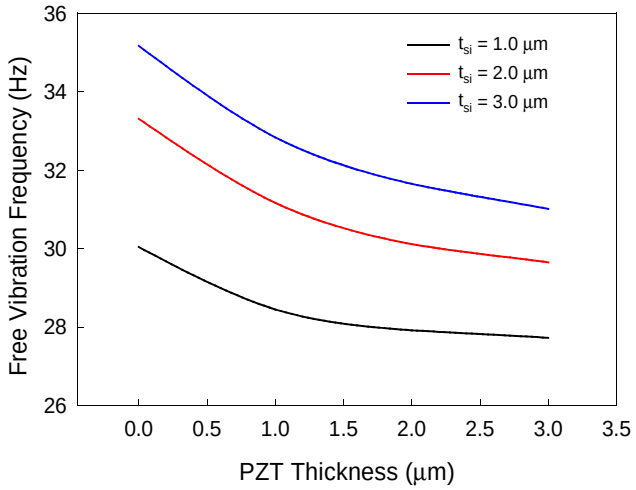

Figure 5.14: Si and PZT thickness change effects on free vibration

An increase in PZT thickness clearly causes a decrease in the free vibration frequency, while an increase in silicon thickness causes an increase in free vibration frequency. This behavior is explained by comparing the densities and moduli of PZT and silicon shown in Table 5.3.

Material	***Density (kg/m^3)***	***Modulus (GPa)***
Silicon	2550	125
PZT	7550	70

Table 5.3: PZT and Si material properties

Conceptually it is informative to examine the equation for the fundamental vibration of a single degree of freedom vibration.

$$\omega_0 = \sqrt{\frac{k}{m}} \tag{5.1}$$

From equation (5.1) it is rather obvious that an increase in stiffness, k, will cause an increase in frequency, while an increase in mass, m, will cause a decrease in frequency. Following this logic, an increase in silicon thickness causes an increase in stiffness and a decrease in mass leading to an increase in resonance. And an increase in PZT thickness causes a decrease in stiffness and an increase in mass, thus a decrease in resonance.

Another important effect, with obvious results, is the effect of residual stress on the vibrational frequency. In Figure 5.15 a comparison of a very low residual stress of 1 Pa is compared to a more realistic residual stress of 105 MPa.

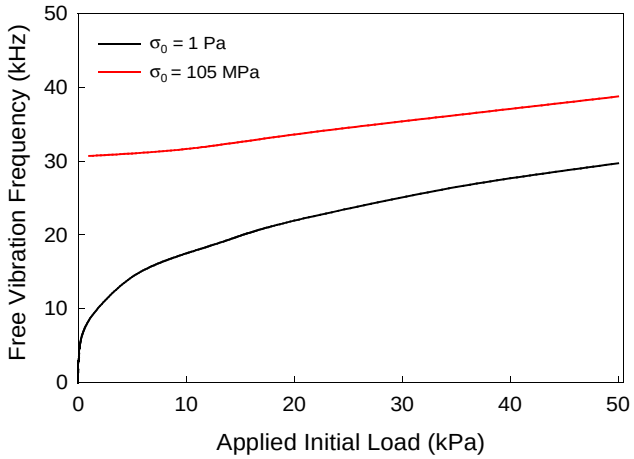

Figure 5.15: Residual stress effect on free vibration for varying initial load

From this residual stress examination it is obvious that an increase in residual stress and an increase in applied load will cause an increase in the frequency of free

vibration. A large dependence of the smaller residual stress curve on load is observed, this is due to the nonlinear effect of an increase in in-plane stress for an increase in deflection. For the 1 Pa residual stress this increase of in-plane stress is a larger portion of the total stiffness then in the 105 MPa curve, and the 1 Pa residual stress structure will therefore strongly exhibit this behavior.

Another parameter that can be studied and relatively easily changed is the side length. This side length study is also chosen as a platform to examine the linear versus nonlinear frequencies of vibration.

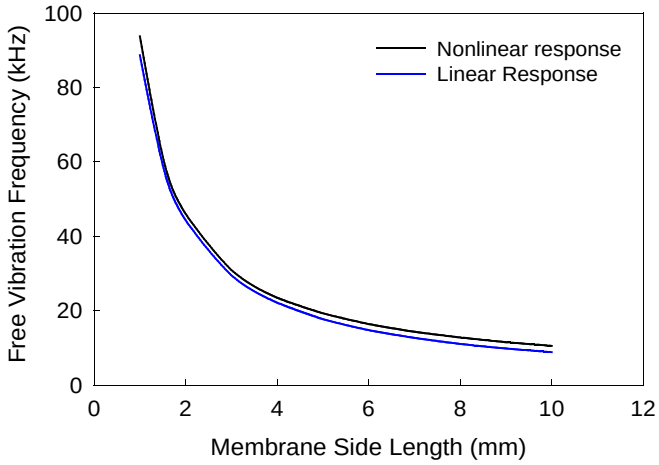

Figure 5.16: Free vibration frequency for various side lengths

From Figure 5.15 the curve with 105 MPa residual stress it is apparent that the change in frequency at low pressures is minimal when compared to the 1 Pa residual stress curve. Comparing the frequencies of nonlinear and linear vibrations in Figure 5.16 it is apparent that these two frequencies are similar. Due to the large residual stress used

in the side length analysis, the linear membrane frequency is comparable to the nonlinear. Although it is noticed that the nonlinear frequency is larger than the linear due to the comparatively small increase of total in-plane stress. Calculation of the linear frequency was done using equation (5.2) [8 p. 421].

$$\omega_0 = \pi \sqrt{\frac{\sigma_0 h}{\bar{m}} \frac{2}{a^2}} \tag{5.2}$$

Analysis of the free vibration behavior of a multitude of applicable structures implies optimum parameters depending on the chosen criteria. In the interest of decreasing vibrational frequencies decreases in the silicon thickness, the residual stress, and the amplitude of the applied load should be used and an increase in PZT thickness will also assist. It has also been shown that the linear frequency is similar to the nonlinear frequency of vibration. This is useful in that a first estimate prediction of free vibration frequency can be made with equation 5.2 without running the entire numerical model.

5.4 Dynamic – Forced Damped Vibration

In real world operation of the generator membrane it will be undergoing a periodic forced vibration. Understanding of the response is important in the application. The frequency-response behavior is analyzed and then points of interest on the curve are examined. Examination of what occurs at the membrane center will be covered in regards to displacement and velocities. Also the shapes that the membrane assumes for

certain frequencies will be shown using centerline plots. The following data in the remainder of this chapter is for a typical device, Table 5.4.

Number of Layers	4			
Side length (mm)	3			
Residual Stress (MPa)	100			
d_{31} (pC/m^2)	85			
Static Load (kPa)	10			
Material	Modulus (GPa)	Poisons Ratio	Density (kg/m^3)	Thickness (μm)
PZT	70	0.27	7500	1
Silicon	125	0.30	2550	1
Gold	80	0.44	19280	0.3
Platinum	170	0.38	21440	0.18
Composite	112	0.31	8027	2.48

Table 5.4: Typical/Representative generator membrane parameters for section 5.4

Presentation of the frequency response curve in the dimensional regime follows. Figure 5.17 displays the dimensional frequency-response curve. Frequency-response curves are useful tools in displaying the behavior of the structure at a specified frequency or amplitude. A linear oscillator will display a dominant resonant frequency [14 p. 103] on a frequency-response curve, but a non-linear oscillator will not and therefore the different behavior at different frequencies is examined.

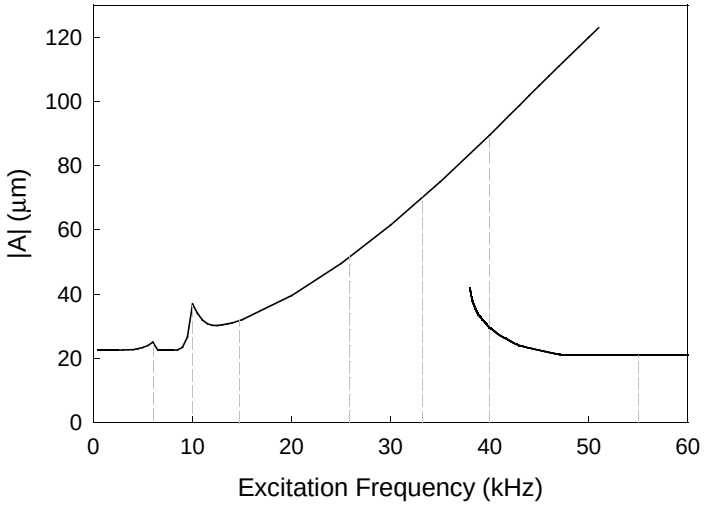

Figure 5.17: Dimensional frequency response curve

From the above shown curve specific points of interest are chosen (shown by dashed lines in Figure 5.17); the harmonics (6 and 10 kHz), a transition section (15, 26.3, and 33 kHz), a double valued portion of the curve (40 kHz), and on the bottom branch beyond the double valued portion (55 kHz). Nondimensionalization of Figure 5.17 is also of interest, in that others may easily compare their results with those shown. In Figure 5.18 this nondimensional response curve is plotted, where f_0 is obtained from equation (5.2) and converted to units of Hz.

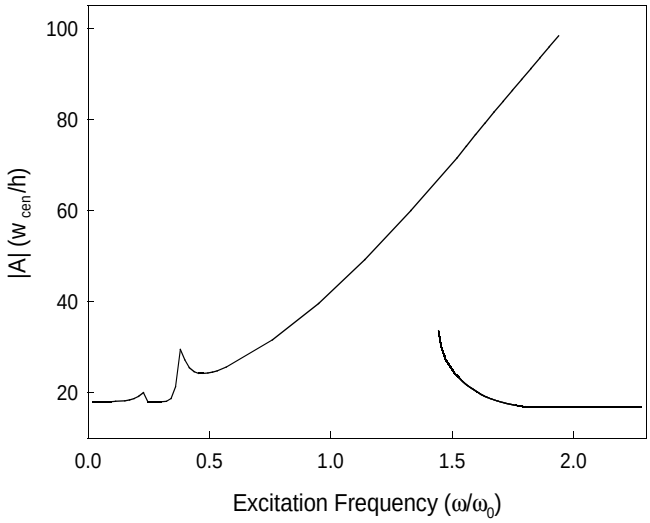

Figure 5.18: Nondimensional frequency-response curve for typical membrane

Further examination of the behavior at the before mentioned frequencies follows, commencing with study of behavior at the 5th harmonic. The response as time progresses is of direct interest, therefore in Figure 5.19 the response at the membrane center is shown for a number of cycles.

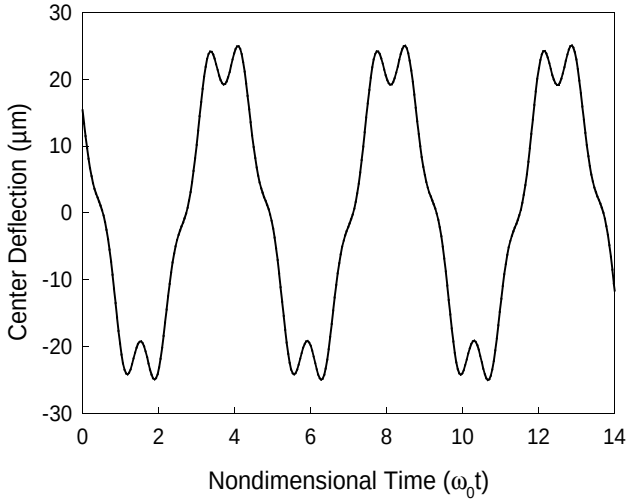

Figure 5.19: Center deflection time response for f = 6 kHz

This response clearly shows interaction of another frequency. Knowledge that this is the 5th harmonic it is expected that this other frequency is five times the forcing frequency. This can be easily proven by taking a Fast Fourier Transform (FFT) of the response which is shown in Figure 5.20.

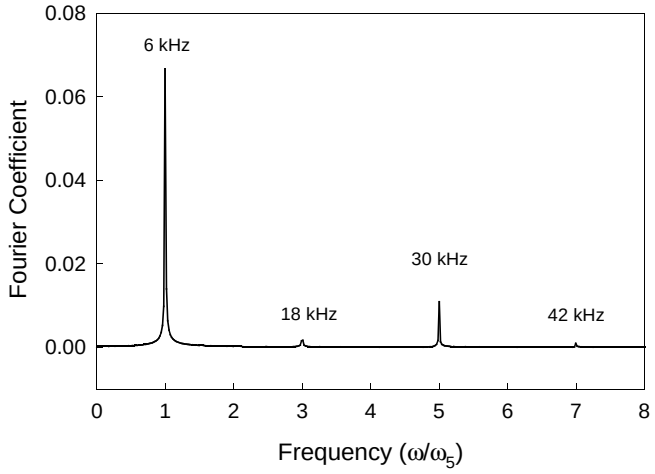

Figure 5.20: FFT of center response for f = 6 kHz

The forcing frequency of f = 6 kHz results in another response at 30 kHz which is 5f. Analysis of what occurs in the phase plane is also of interest. The phase space plots can be used to represent the behavior of many cycles upon one curve, and emphasize behavior such as changes in velocity and non-symmetric vibrations. When the phase space curves lie upon each other for many cycles the steady state behavior is assured. In the following phase space curves at least one hundred cycles are typically plotted. Shown in Figure 5.21 is the phase plane result at the center point of the membrane.

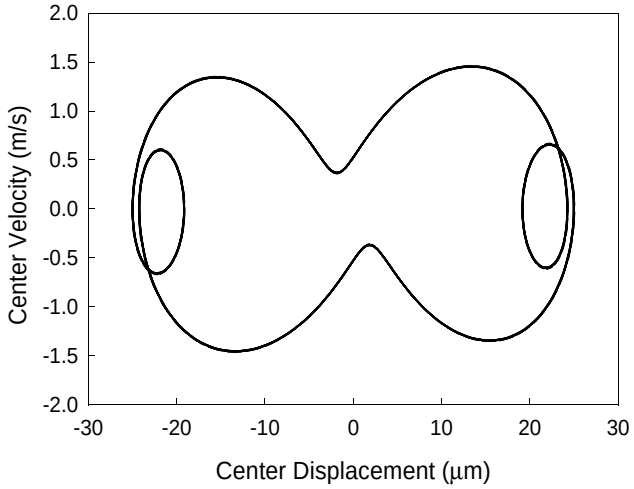

Figure 5.21: Phase plane for center response at f = 6 kHz

A similar examination is done for the 3rd harmonic with the results being displayed in Figures 5.22, 5.23, and 5.24. The response at f = 10 kHz is obviously the 3rd harmonic; a response at 10 kHz and 30 kHz is apparent in Figure 5.23. Also the appearance of the phase plot is what is expected.

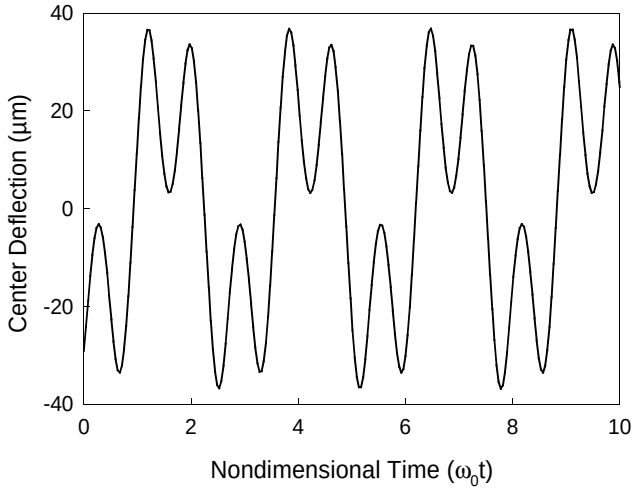

Figure 5.22: Center deflection time response for f = 10 kHz

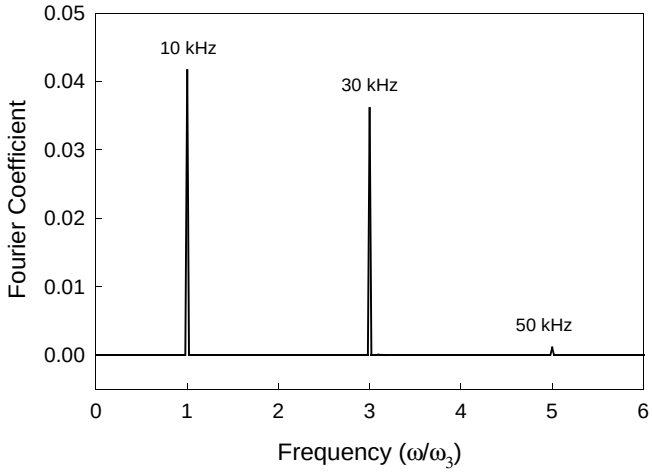

Figure 5.23: FFT of center response for f = 10 kHz

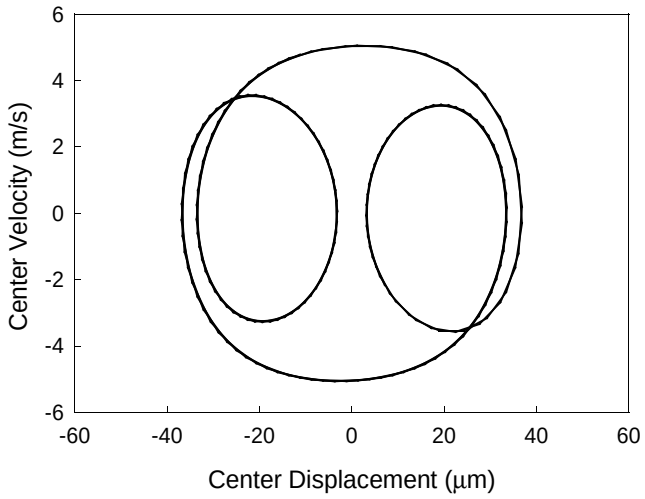

Figure 5.24: Phase plane for center response at f = 10 kHz

At the 3rd and 5th harmonics there is an expectation that the membrane shape during vibration will exhibit other shapes beyond that of the (1,1) mode. At the 5th harmonic expected shapes of the (1,1) mode and the (5,5) mode should occur and at the 3rd harmonic expected shapes of the (1,1) mode and the (3,3) should occur. Summarily, for these odd harmonics expected shapes will occur that are odd and symmetric. Taking a closer examination of Figure 5.22 in Figure 5.25, closer analysis of the response at the shown section 1 and 2 is taken by plotting of the centerline shape profiles. Section 3 was examined, but found to show the same response in section 2 and subsequently will not be shown.

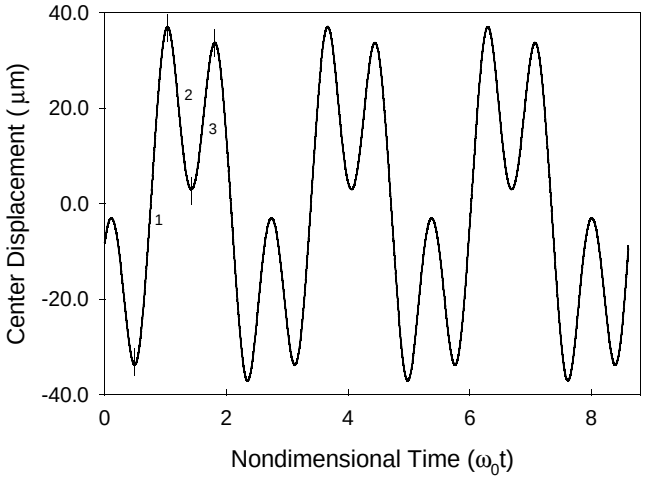

Figure 5.25: Zoomed in center response for f = 10 kHz

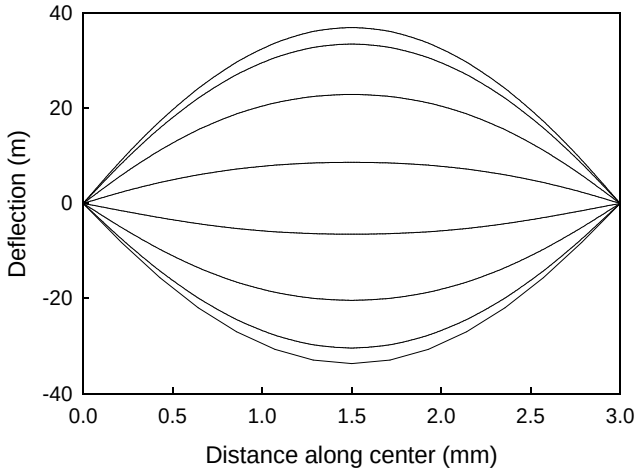

Figure 5.26: Center line profile shapes for section 1

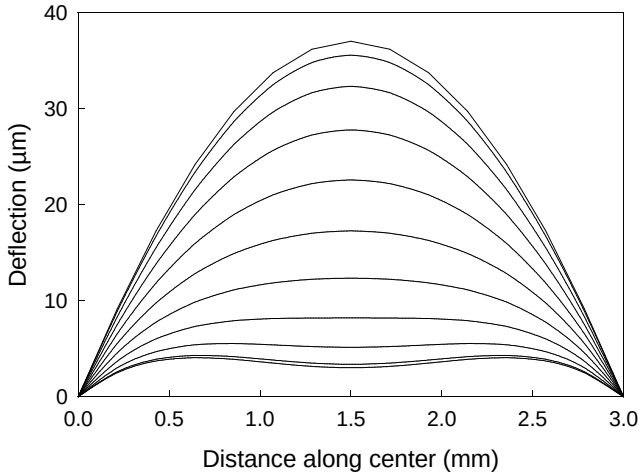

Figure 5.27: Center line profile shapes for section 2

Figure 5.26 shows no obvious other mode interaction, section 1 appears to be a solely (1,1) mode reaction. Yet, section 2 shows obvious other mode interaction. A single sine function of the form $\sin(\pi x/L)$ could be used to approximate the shapes shown in Figure 5.26, while a double sine would have to be used in Figure 5.27 of the form $\sin(\pi x/L)\sin(3\pi x/L)$. This is an important observation in that $\sin(\pi x/L)\sin(3\pi x/L)$ can be considered an approximation to the combination of modes (1,1) and (3,3).

What occurs at the single-valued rising portion of the frequency-response curve is analyzed using the frequencies of 15 kHz, 26.3 kHz (linear resonance), and 33 kHz. The center deflection versus time plots will be shown first for 15 and 33 kHz, then a figure showing all of the FFT's, and finally one figure displaying all the phase plots.

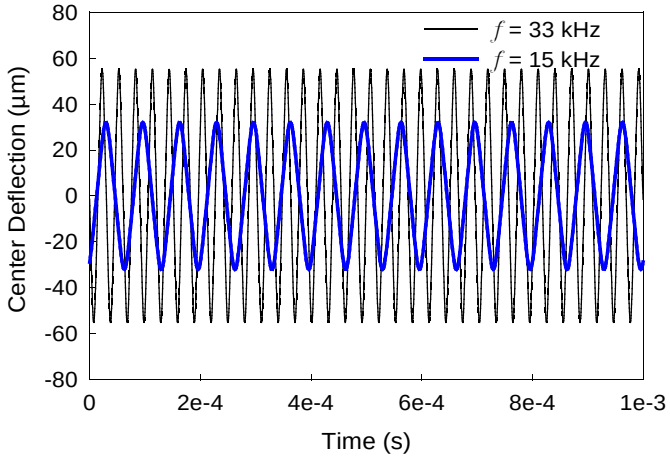

Figure 5.28: Center response for f = 15 and 33 kHz

Figure 5.28 shows that, unlike the responses at 6 and 10 kHz, there is not an obvious other frequency interaction. To assert this claim an FFT of the responses are shown in Figure 5.29.

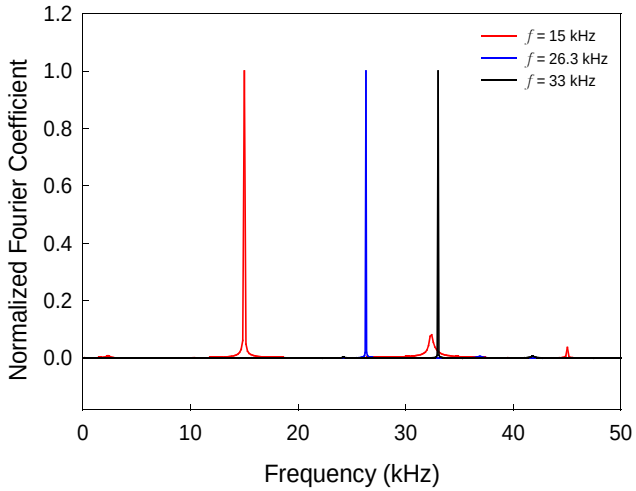

Figure 5.29: FFT for f = 15, 26.3, and 33 kHz

At the 15 kHz excitation frequency there appears to be a higher frequency of much smaller amplitude occurring. This is because an excitation frequency of 15 kHz is close to the 3rd harmonic and interactions might still occur. Examination of the phase space occurs in Figure 5.30.

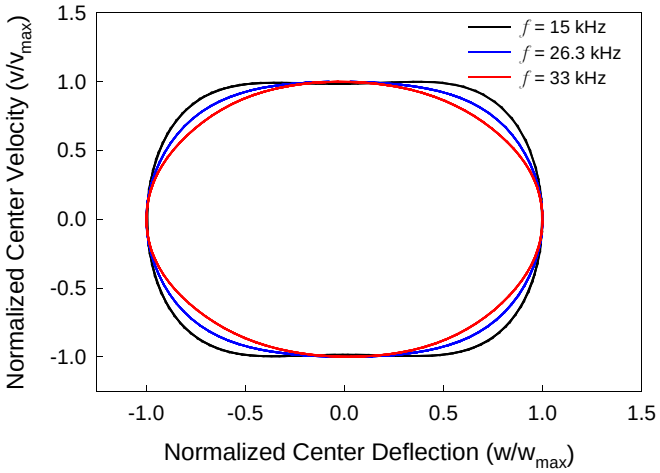

Figure 5.30: Phase plot for f = 15, 26.3, and 33 kHz

The rising single valued section on the frequency-response curve shows similar behavior in the non-dimensional phase space. Yet, the phase space curves become more elliptical for higher frequencies possibly due to a decrease in the amount of additive effects due to other frequency contributions.

Examination of the what occurs to the shape of the membrane for one cycle at 15 kHz is shown in Figure 5.31. Similar shapes were found for the other excitation frequencies (26.3 and 33 kHz), and are not shown for reasons of brevity.

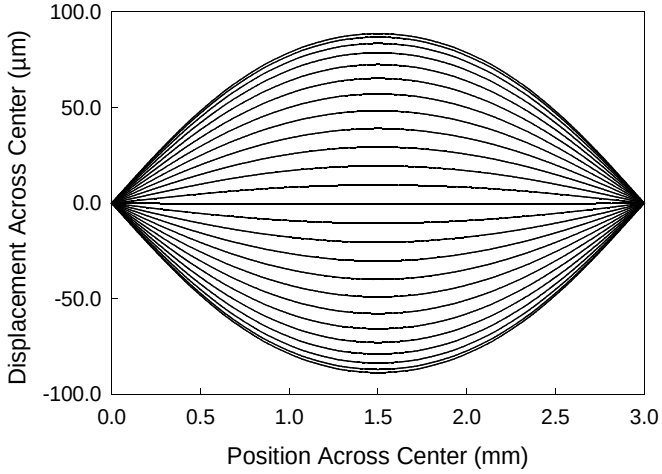

Figure 5.31: Center line shape profiles for f = 15 kHz

Next, analysis of the behavior at an arbitrary picked double valued frequency is commenced and the value chosen here is f = 40 kHz. The center response over time is not shown here, but was found to be very similar in shape to the responses shown in Figure 5.28. Examination of the phase space provides some interesting results discussed in the following and shown in Figures 5.32 and 5.33.

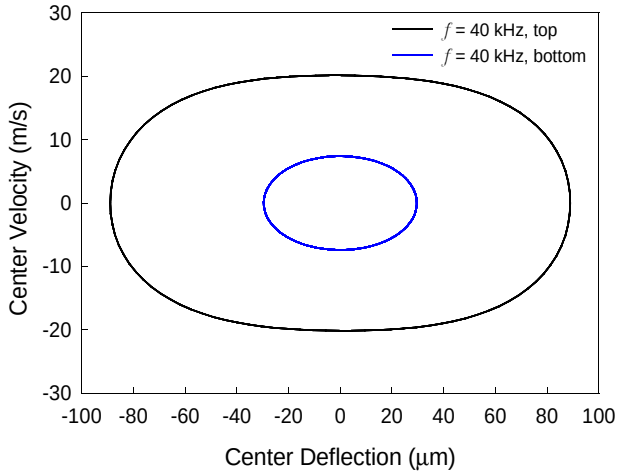

Figure 5.32: Dimensional phase space for 40 kHz, bottom and top branches

Through use of Figure 5.32 analysis and understanding of the behavior that different initial conditions will result in can be performed. For example, if the initial conditions lie within the small orbit, steady state behavior will follow the smaller orbit and conversely if the initial conditions lie outside of the larger orbit, the steady state response will tend towards the larger orbit, while if the initial conditions lie within the two orbits the response is not as predictable and for prediction of what will occur the model would need to be run. For example some initial center point conditions that would follow the low amplitude response would be $w_0 = 0$ μm, $v_0 = 4.9$ m/s, and $a_0 = 0$ m/s^2 and some initial conditions that would follow the high amplitude response would be $w_0 = 20$ μm, $v_0 = 30$ m/s, and $a_0 = 0$ m/s^2. Where w_0 is initial center displacement, v_0 is initial center velocity, and a_0 is initial center acceleration.

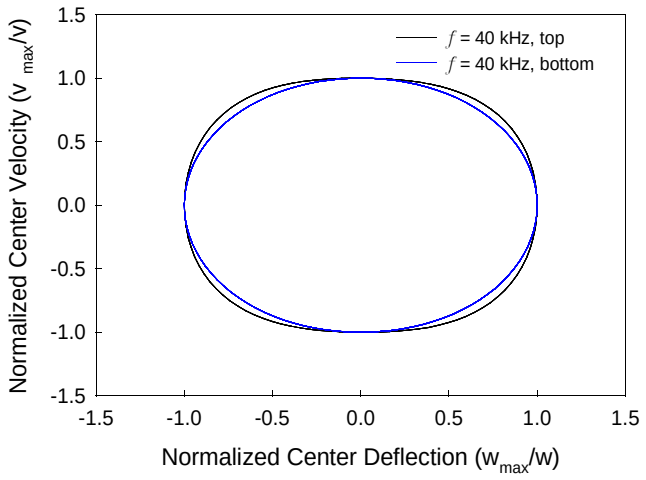

Figure 5.33: Normalized phase space for 40 kHz,bottom and top branches

The normalized phase space plot lends insight into the type of resulting behavior. It is known that more elliptic phase space curves tend to be less nonlinear. Figure 5.33 agrees with this. The bottom branch curve deflection response is much less than the top branch response, meaning that less in-plane stretching occurs for the bottom branch and subsequently it doesn't have as high a degree of nonlinearity as the top curve, which is squarer.

The FFT of the both the bottom and top branch is shown in Figure 5.34. It is obvious that both of responses on the top and bottom branches show the same dominant frequency of 40 kHz.

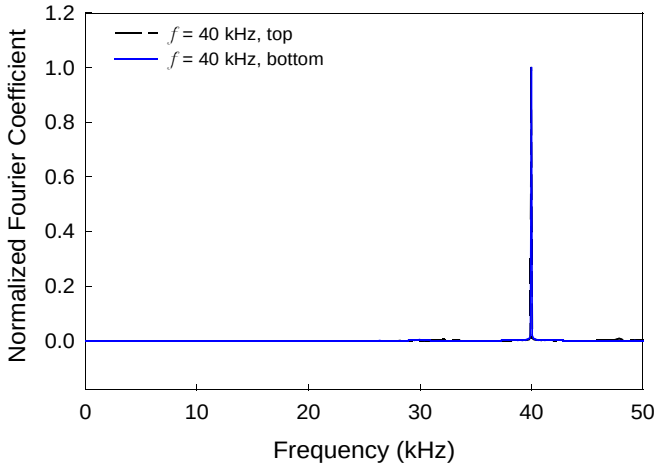

Figure 5.34: FFT at 40 kHz, bottom and top branches

The shape at 40 kHz on the top branch looks much like Figure 5.31, while the bottom branch is shown in Figure 5.35. It is apparent that the shapes for the top and the bottom branches don't match at 40 kHz. This is due to the much smaller deflection on the bottom branch, and a flattening out of the profile near the boundary.

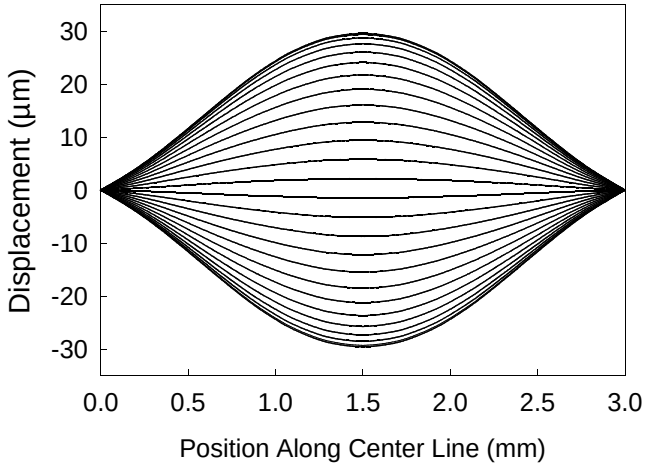

Figure 5.35: Center line profile for f = 40 kHz on the bottom branch

Results for the behavior on the bottom branch past the double valued portion is shown below. The typical plots of phase space, FFT, and center profiles are shown. The center response over time plot is not shown, but it is stated that this response is similar in shape to Figure 5.28.

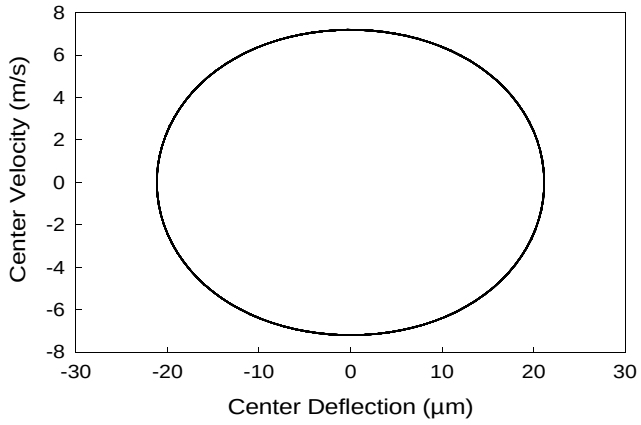

Figure 5.36: Phase space plot for f = 55 kHz

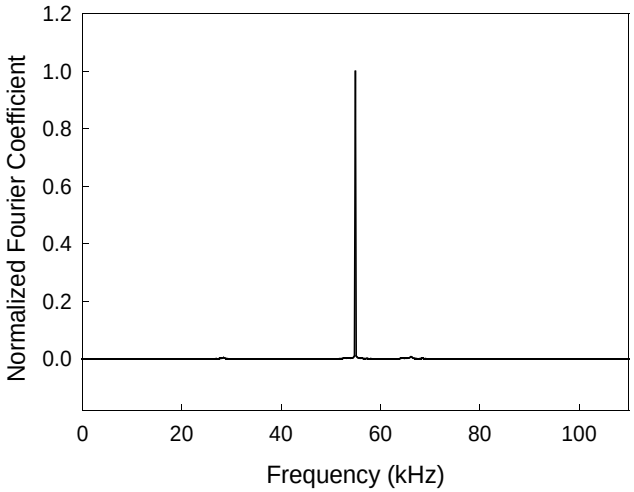

Figure 5.37: FFT for f = 55 kHz

Figures 5.36 and 5.37 show the phase space plot and the FFT for f = 55 kHz. The dominant frequency is the excitation frequency which is 55 kHz, no other notable responses occur. Also, of interest is what occurs in relation to the membrane shape, centerline profiles are shown below in Figure 5.38. Comparing the two shapes, Figures 5.35 and 5.38, it is interesting to note that the shape seems to be changing as the frequency increases on the bottom branch. There appears to be a flattening of the profile near the boundaries that becomes more dominant as f is increased.

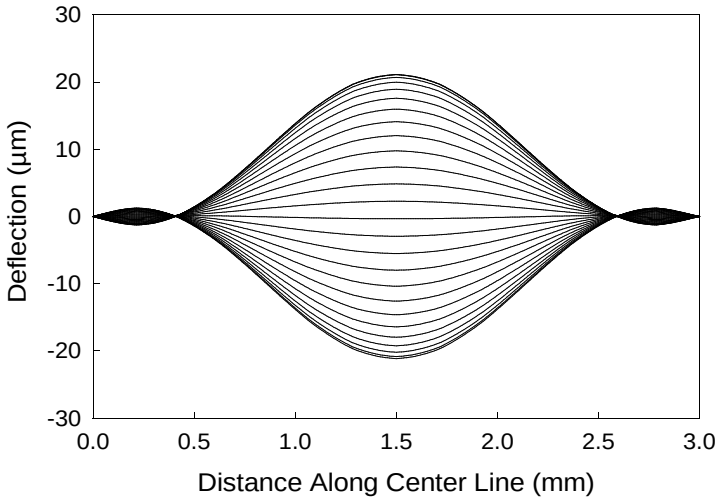

Figure 5.38: Centerline profiles for f = 55 kHz

A comparative analysis of what occurs near $w_{cen} = 0$ is shown in Figure 5.39. Shown are the centerline profiles for the previously discussed excitation frequencies. The precise reason for the difference in shapes is not know, but it is known that these shape differences are due to the inherent nonlinearity in this structure. It is interesting to note a

very low amplitude occurrence of other vibrational modes throughout any excitation frequency, though some occurrences are more obvious than others.

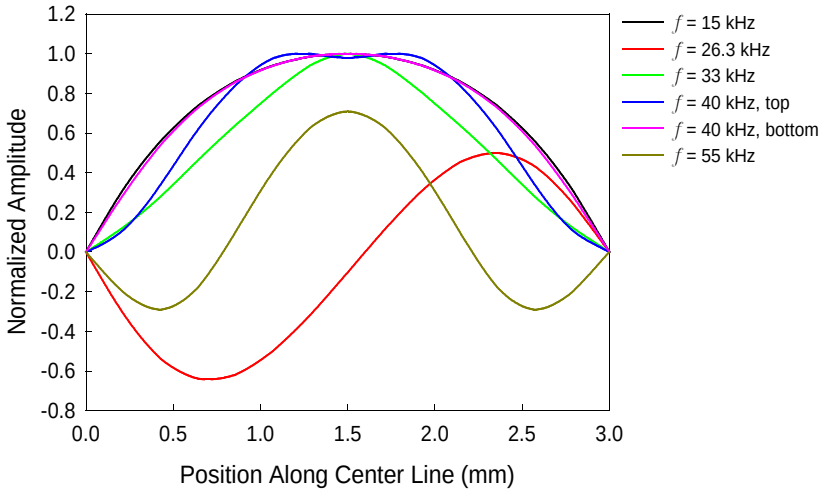

Figure 5.39: Centerline profiles for $w_{cen} \approx 0$

Specific points on the frequency-response curve were examined and results showing obvious differences in behavior at different excitation frequencies were shown. These different behaviors could be utilized in power generation or avoided. For example, a possible advantage to using a 3rd harmonic response would be that excitation can occur at a lower frequency then the overall response. Also, different shapes will affect power generation, this work shows that different shapes will occur and therefore an optimum shape will exist, and that this optimum shape will correspond with an excitation frequency.

Chapter 6: Conclusion

A finite difference model has been developed using governing equations for a nonlinear vibrating plate with fully clamped boundary conditions. Theories were then applied to allow for lamination and extraction of charge information. Solution of this problem was then pursued using a step-by-step matrix analysis procedure in conjunction with an iterative solution technique. Using a common desktop computer, these theories were then implemented using the FORTRAN 90 programming language. It was then illustrated that this model was valid for both the static and dynamic regimes by comparison to experimental data of a MEMS device.

From the solution produced by the program a variety of information was extracted. Three dimensional profiles for various stresses, deflection, and charge were obtained. From these plots it can be determined where to place electrodes to gain the largest voltage signal, where the structure might fail in operation, and what the deflected structure looks like. All of which are useful visual cues as to what is occurring in the actual device.

A parameter study was done using static analysis to understand the effect of different thicknesses of silicon and PZT and the effect of residual stress on the device. It was shown that an optimum device will have a PZT thickness of 2 – 3 μm, a minimum of silicon, and a minimum residual stress (other values available in Table 5.4). These parameters were also studied in relation to vibration. It was found that depending on what layer thickness is increased, the free vibration frequency will either increase

(increase in silicon thickness) or decrease (increase in PZT thickness). The rather obvious result of an increase in residual stress is an increase in vibrational frequency.

The nature of the nonlinear behavior was analyzed using forced vibration. From the frequency-response curve it was found that the occurrence of the 3rd and 5th harmonics is expected along with a jump phenomena that is expected of Duffing oscillators. From literature and these simulations it is determined that the thin plate-membrane that is studied within is a Duffing oscillator like and shows behavior indicative of this.

Chapter 7: Recommendations

From this finite-difference model specific recommendations for device improvement are proposed with the goal in mind to reduce vibrational frequency and increase available output energy from the PZT.

1. Minimum substrate thickness (i.e. silicon).
2. Minimum Au and Pt thickness to increase strain energy ratio.
3. 2 – 3 μm thick PZT to increase strain energy ratio.
4. Reduce residual stress to decrease vibrational frequency and increase available output energy.
5. Operate at low deflections to minimize nonlinear effects therefore reducing vibrational frequency.
6. Increase device side length to decrease vibrational frequency.
7. Operate away from harmonics to maintain a steady sinusoidal behavior for application in the P3 micro-engine.

Observing the double valued portion of the frequency-response curve and the phase plot at this portion of the plot, Figure 5.32. It is apparent that this structure has two responses of different deflections at the same excitation frequency. Utilizing this, a switch could be developed that would always operate at one frequency yet with some imposed condition that could turn it off or on. Further analysis of this, and how to control this phenomenon would be of interest and the developed model could be modified to perform this.

Examination of the relationship between the excited shape and power generation should also be investigated. That is, if a device is used in a spectrum of excitation frequencies where will it obtain the most efficient power generation and what would be the contributing factors to this.

Improvement upon the program is also of interest in order to decrease model run times and maintain accuracy. Possible avenues to do this are 1) decrease numerical need 2) improve solution technique. Decreasing of the numerical need of the program could be done by taking advantage of symmetry and only analyzing ¼ of the structure. Therefore imposing symmetry conditions upon two of the boundaries instead of fully clamped on all four. This could decrease program run time significantly and still maintain accuracy. Improvement of the solution technique could be pursued by implementing banded storage schemes instead of a full matrix scheme, then using solvers that could take advantage of this. Further investigation into both of these would be required, and would greatly increase the efficiency of the developed code.

Chapter 8: Appendix

8.1 Flowcharts for program VENM

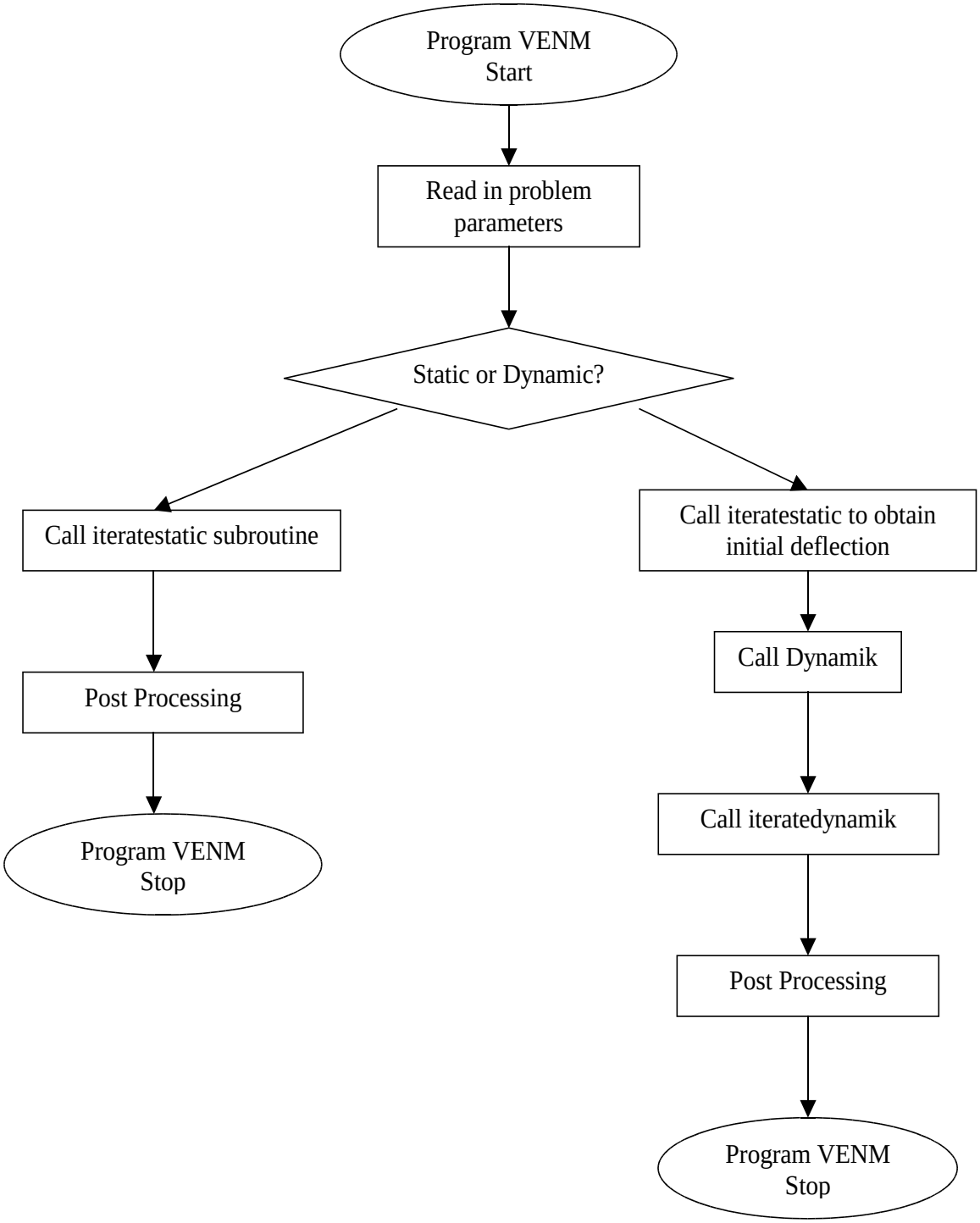

Figure 8.1: VENM main program body flowchart

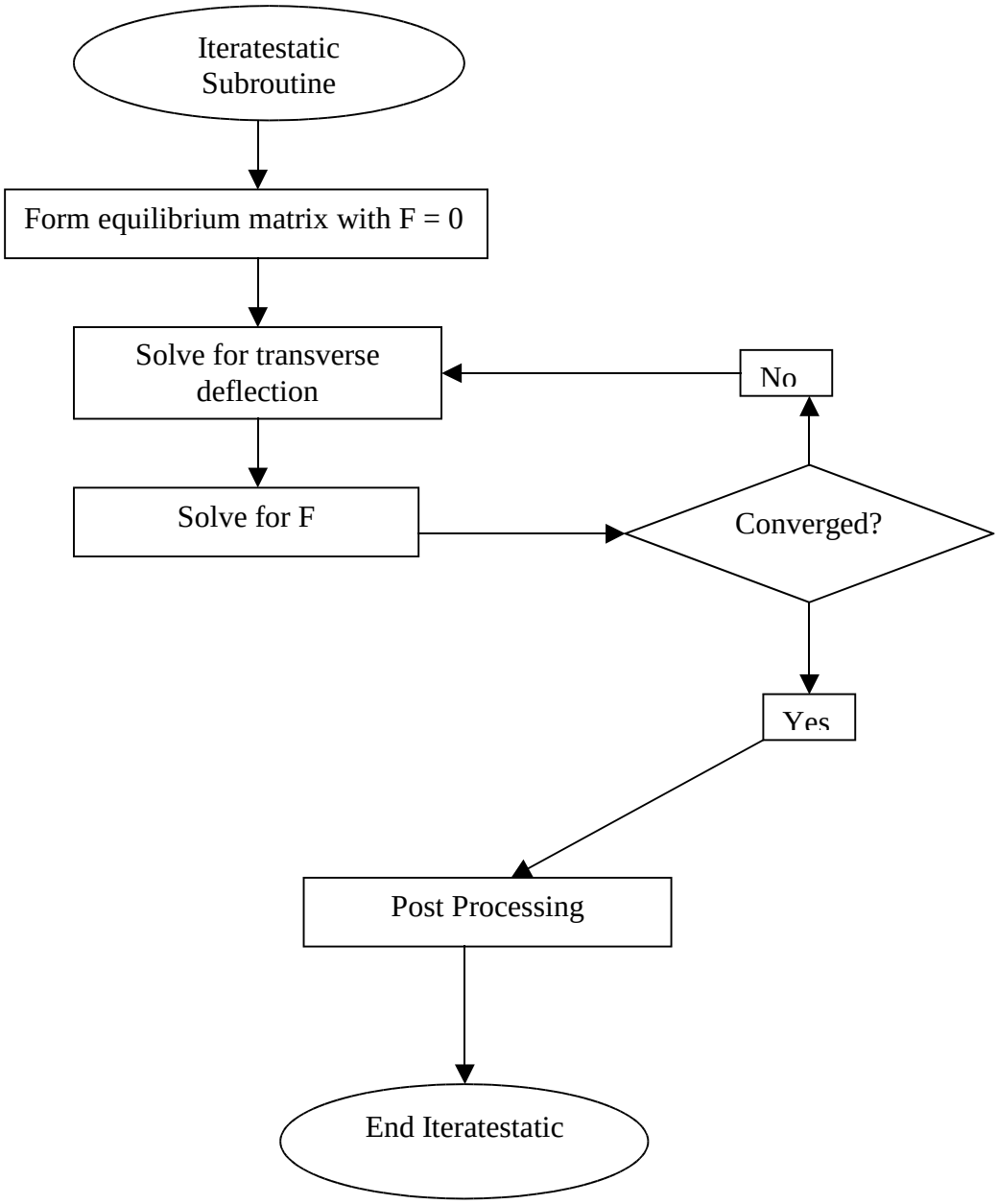

Figure 8.2: VENM subroutine Iteratestatic flowchart

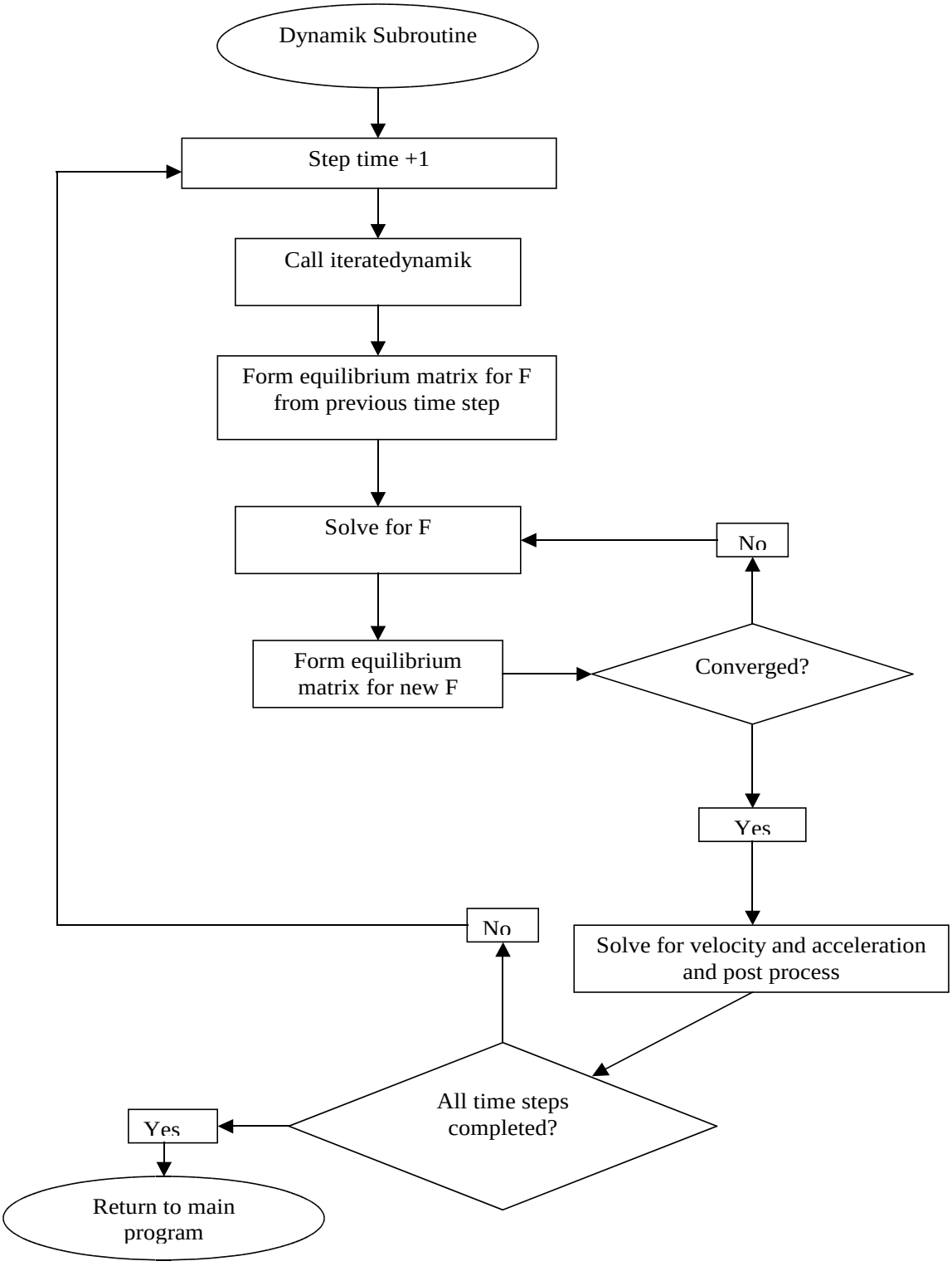

Figure 8.3: VENM subroutine Dynamik flowchart

8.2 FORTRAN Source Code for Developed Model

The following is the FORTRAN source code for the developed model.

FORTRAN Free 90 format was used along with Microsoft Developer Studio, Fortran Power Station 4.0 for debugging and compiling.

```
program VENM

use msimsl
use portlib

double precision, ALLOCATABLE :: wst(:),pst(:),Em(:),num(:),z(:), &
        hm(:),rhom(:),psa(:),strsx(:,:),strsy(:,:),strsxy(:,:),strs1(:,:)
character(9), ALLOCATABLE :: matnme(:)
double precision a,h,ps,nu,dx,E,rs,drs,rho,ftm,ts,d31,es,Capc,chrgm,cc,delta,k2, &
        E_uniaxial,nu1,D,D_singlelayer,eta,alpha
character dyndec
CHARACTER(9)TODAY
CHARACTER(8)char_time
integer cj,cen,writcntr,n,nm,md,nl

!       Debugging files
!       open(unit=2000,file='pk.txt')

!       General use files
!       open(unit=10,file='w.txt')
!       open(unit=11,file='wbend.txt')
!       open(unit=12,file='wstrt.txt')
!       open(unit=13,file='wr.txt')
!       open(unit=14,file='wk.txt')
!       open(unit=15,file='wkp.txt')
!       open(unit=20,file='ps.txt')
!       open(unit=21,file='psb.txt')
!       open(unit=31,file='pss.txt')
!       open(unit=40,file='conver.txt')
!       open(unit=50,file='wconv.txt')
!       open(unit=51,file='pssconv.txt')
!       open(unit=61,file='vk.txt')
```

```
!       open(unit=62,file='vkp.txt')
!       open(unit=71,file='p-d.txt')
        open(unit=72,file='p-q.txt')
        open(unit=81,file='parameters.txt')

!       Shape
        open(unit=105,file='shapew-d.txt')
        open(unit=100,file='shapew.txt')            !Writes w-shape to file
        open(unit=101,file='shapeps.txt')
        open(unit=110,file='profile.txt')           !center profile shape
        open(unit=112,file='profile-d.txt')         !center profile of shape - dimensional
        open(unit=115,file='shape-frc.txt')         !forced shapes
        open(unit=120,file='profile-diag.txt')      !profile across membrane diagonal
        open(unit=125,file='profile-diag-d.txt')    !profile across membrane diagonal -
                                                    !dimensional

!       Stress Output
        open(unit=200,file='strsx.txt')
        open(unit=205,file='strsy.txt')
        open(unit=210,file='strsxy.txt')
        open(unit=215,file='strs1.txt')
        open(unit=220,file='strs2.txt')

!       Electrical Output
        open(unit=400,file='charge.txt')
!       open(unit=410,file='voltage.txt')
!       open(unit=420,file='power.txt')

!       Time Output
        open(unit=300,file='cent-time.txt')   !Writes the center
        open(unit=320,file='fourier.txt')
        open(unit=330,file='wkmax.txt')       !writes max center defl at forcing freq
        open(unit=340,file='time-freq.txt')
!       open(unit=310,file='soln-time.txt')   !Writes CPU time taken.

!       Material Properties
        nm=4                          !number of materials
        allocate(Em(nm),num(nm),hm(nm),rhom(nm),matnme(nm),z(nm+1))
!       Materials
        matnme(1)="Silicon"
        matnme(2)="Platinum"
        matnme(3)="PZT"
        matnme(4)="Gold"
!       Moduli of elasticity
        Em(1)=125.D9        !Silicon
```

```
      Em(2)=170.D9          !Platinum
      Em(3)=70.D9           !PZT
      Em(4)=80.D9           !Gold
!     Poisons ratio
      num(1)=0.3            !Silicon
      num(2)=0.38           !Platinum
      num(3)=0.27           !PZT
      num(4)=0.44           !Gold
!     Density
      rhom(1)=2500.         !Silicon
      rhom(2)=21440.        !Platinum
      rhom(3)=7550.         !PZT
      rhom(4)=19280.        !Gold
!     Thickness  (m)
      hm(1)=1.D-6           !Silicon
      hm(2)=175.D-9         !Platinum
      hm(3)=1.D-6           !PZT
      hm(4)=325.D-9         !Gold

      z(1)=0.
      do i=1,nm
       h=h+hm(i)            !Total thickness
       z(i+1)=h
      enddo
!     Effective Constants
      do i=1,nm
       E_uniaxial=E_uniaxial+Em(i)*hm(i)/h
       E=E+(hm(i)/h)*(Em(i)/(1.-num(i)**2.))          !E*
       nu1=nu+(hm(i)/h)*num(i)
       nu=sqrt(1-E_uniaxial/E)
       rho=rho+(hm(i)/h)*rhom(i)
      enddo
      write(*,*)E_uniaxial,E
      write(*,*)nu,nu1

      CALL D_value(hm,Em,num,z,nm,D)

      D_singlelayer=(E*h**3.)/(12.*(1-nu**2.))

!     Geometry
      a=0.003               !Sidelength (m)
!     es=0.002              !Electrode size (m), es <= a
      es=a
!     Piezoelectric properties
      Capc=40.D-9
```

```
      d31=85.D-12          !C/m^2

!     Finite Difference Parameters
      n=15                 !Number of inclusive interior nodes
      dx=1./(n-1.)         !Nodal spacing, i.e. mesh size.
      md=(n+2)**2          !Matrix dimension
!     Time parameters
      ftm=10000.D0         !Total time of vibration study (seconds)
      ts=2.5D-7
!     ts=(dx/(E/((1.-nu**2.)*rho))) !Time step (seconds), based on wave speed.

      writcntr=1 !Problem information written to file every "writcntr" time step
!     Residual Stress
      drs=1.D8             !Residual Stress, Pa
      rs=(12.*(1.-nu**2.)*(drs/E)*(dx*a/h)**2.)   !Non-dimensional residual stress
!     Damping
      delta=0.
      cc=2000.       !equivalent to 3.33 % of critical.  cc=600 eqv to 1 % of critical
!     delta=0.*ts/3.14159   !Stiffness proportional damping

!     Vector/Matrix position quick reference values
      cj=(n-1)/2                 !Center in i
      cen=cj+2+(cj+1)*(n+2)      !Matrix row/column for center node.

!     Nondimensional Coefficients
      eta=E*h**3./D
      alpha=(h/a)**2.

!     Static/Initial Loading(s)
      nl=1                                !number of loads applied
      ALLOCATE (wst(md),pst(md),psa(nl),strsx(nm,md),strsy(nm,md),strsxy      &
                (nm,md),strs1(nm,md)) !Sets size for static solution vectors
      psa(1)=1.e-9
!     psa(1)=500.                !Multiple loads to obtain P-D curves.
!     psa(2)=1000.
!     psa(3)=2000.
!     psa(4)=4000.
!     psa(5)=6000.
!     psa(6)=8000.
!     psa(7)=10000.
!     psa(8)=12000.
!     psa(9)=14000.
!     psa(10)=16000.
!     psa(11)=18000.
!     psa(12)=20000.
```

```
!Outputs the problem parameters to a file.
        Call Date(Today)
        Call Time(char_time)
        write(81,*)"Problem Parameters"
        write(81,*)"All units are SI."
        write(81,*)"This file is comma seperated."
        write(81,*)"Date:,",today
        write(81,*)"Time:,",char_time
        write(81,*)"Mesh size:,",n
        write(81,*)"Number of layers:,",nm
        write(81,*)"Side Length:,",a
        write(81,*)"Residual Stress:,",drs
        write(81,*)"D31:,",d31
        write(81,*)"Total time of vibration:,",ftm
        write(81,*)"Time step size:,",ts
        write(81,*)
        write(81,*)"Material,Modulus,Poisons,Density,Thickness"
        do i=1,nm
         write(81,1004)matnme(i),",",Em(i),",",num(i),",",rhom(i),",",hm(i)
        enddo
        write(81,1004)"Composite/Total",",",E,",",nu,",",rho,",",h
        write(81,*)
        write(81,*)"Static Loads Applied"
        do i=1,nl
         write(81,*)psa(i)
        enddo
        CLOSE(81)

!Program main execution body - Static
        DO ic=1,nl                      !ic = load count
         ps=psa(ic)
         write(*,*)"Pressure:  ",ps
         write(*,*)"Residual Stress: ",drs
         CALL iteratestatic(n,a,h,dx,md,ps,nu,E,rs,drs,wst,pst,d31,Em,num,hm,nm,      &
                            es,Capc,chrgm,strsx,strsy,strsxy,strs1,k2,eta,alpha)
         write(*,*)"Deflection: ",wst(cen)*h
!        write(71,*)ps,wst(cen)*h                !Write P-D curve file
         write(72,1030)ps,wst(cen)*h,chrgm,k2    !writes p-d-Q data
         write(100,*)"Pressure Stamp: ",ps
         do ii=0,n
          do ij=0,n
           write(100,*)ii*a*dx,ij*a*dx,wst(ii+2+(ij+1)*(n+2))*h          !Shape
          enddo
         enddo
```

```
!         Writes stresses out to file.
!          do ii=0,n-1
!           do ij=0,n-1
!            write(200,1020)ii*a*dx,ij*a*dx,(strsx(mn,ii+2+(ij+1)*(n+2)),mn=1,nm)
!            write(205,1020)ii*a*dx,ij*a*dx,(strsy(mn,ii+2+(ij+1)*(n+2)),mn=1,nm)
!            write(210,1020)ii*a*dx,ij*a*dx,(strsxy(mn,ii+2+(ij+1)*(n+2)),mn=1,nm)
!            write(215,1020)ii*a*dx,ij*a*dx,(strs1(mn,ii+2+(ij+1)*(n+2)),mn=1,nm)
!           enddo
!          enddo

ENDDO

!Program main execution body - Dynamic
        write(*,'(/,A38)')"Continue into dynamic analysis (y/n)?"
        read(*,'(a1)')dyndec    !dynamic decision
        if (dyndec .eq. "y") then
         continue
        else
         STOP
        endif
        write(*,'(/,a38)')"Commencing dynamic analysis."
        Call Dynamik(E,nu,rho,n,a,h,dx,md,ftm,ts,rs,drs,pst,wst,d31,Em,num,hm,nm,    &
                     es,Capc,writcntr,cc,delta,eta,alpha,D)

1004    FORMAT(a16,a1,E9.3E3,a1,F3.2,a1,F6.0,a1,E8.4E1)
1020    FORMAT(2(e16.10),4(e20.10e2))
1030    FORMAT(4(e20.10e2))
END
-------------------------------------------------------------------------------------------------------
SUBROUTINE iteratestatic(n,a,h,dx,md,p,nu,E,rs,drs,ws,pss,d31,Em,num,hm,nm,es,    &
                         Capc,chrgm,strsx,strsy,strsxy,strs1,k2,eta,alpha)

        double precision w(md,md),pss(md),wr(md),ws(md),a,h,p,nu,dx,E,             &
                ps(md,md),psb(md),wspi(md),clim,concrt,lamb,rs,drs,d31,            &
                strsx(nm,md),strsy(nm,md),ct,Em(nm),num(nm),hm(nm),da,             &
                voltage,voltwork(2,2),strainx(md),strainy(md),strainxy(md),        &
        es,Capc,strsxy(nm,md),chrgm,strs1(nm,md),k2,eta,alpha
        real*8 timefin,timef
        integer ci,cj,cen,counti,nnes,nnie,n,i,j,md

        do i=1,md
         pss(i)=0.
         ws(i)=0.
         wspi(i)=0.
```

```
        enddo

        ci=(n-1)/2                      !Center in x
        cj=(n-1)/2                      !Center in i
        cen=ci+2+(cj+1)*(n+2)           !Matrix row/column for center node.

        clim=1.D-6                      !Convergence Limit
        concrt=10.                      !Convergence Criteria
        counti=0                        !Iteration counter
        lamb=0.5                        !Multiplicative factor

        timefin=Timef()

do while (concrt .gt. clim)
        counti=counti+1
        do i=1,md
         do j=1,md
          w(i,j)=0.
          ps(i,j)=0.
         enddo
         wr(i)=0.
         psb(i)=0.
         w(i,i)=1.
enddo

        CALL bending(w,md,n)                !Forms bending part of the eql. eqn
        CALL membrane(w,pss,md,nu,n,eta) !Forms membrane part of the eql. eqn.
        CALL clampedeqlBC(w,md,n)       !Apply boundary conditions
        CALL wrmat(wr,a,nu,p,dx,E,h,md,n,eta,alpha)       !Forms right side
        CALL ResidualStress(md,n,rs,w)              !Adds residual stress
        CALL DLSARG(md,w,md,wr,1,ws)        !Solves equilibrium equation

        do i=1,md
         ws(i)=lamb*wspi(i)+(1.-lamb)*ws(i)        !Convergence augmentation.
        enddo

        CALL compat(n,md,ps)        !Forms compatibility equation portion
        CALL clampstrainbc(n,md,nu,ps)     !Forms strain = 0
        CALL uvDispBC(n,nu,md,ps)          !Forms u, v = 0 portion
        CALL psbvec(psb,ws,n,md)           !Forms right side

!       do i=1,md
!        write(10,1000)(w(i,j),j=1,md)
!        write(20,1000)(ps(i,j),j=1,md)
!        write(13,*)wr(i)
```

```
!         write(21,*)psb(i)
!        enddo

         CALL DLSARG(md,ps,md,psb,1,pss)        !Both, Solves compatibility matrix.

         concrt=ABS(ws(cen)-wspi(cen))          !Convergence Tests

         do i=1,md
          wspi(i)=ws(i)
         enddo

write(*,*)ws(cen)*h

ENDDO ! END ITERATION LOOP
write(*,*)ws(cen)*h

!         do ii=(-1),n
!          do ij=(-1),n
!           write(105,*)ii*a*dx,ij*a*dx,ws(ii+2+(ij+1)*(n+2))*h              !Shape wd
!           write(101,*)ii*a*dx,ij*a*dx,pss(ii+2+(ij+1)*(n+2))*E*h**2       !Shape psi
!          enddo
!         enddo

         timefin=Timef()
         write(*,*)"Time to converge in seconds:",timefin

!        Compute x-y stress values
         CALL StrainCompute(pss,dx,a,nu,n,md,E,h,drs,Em,num,nm,strsx,strsxy,strsy,  &
                            strainx,strainxy,strainy,strs1,hm)
!        write(400,*)"Static"
         ct=0.

         CALL piezo(strsx,strsy,md,d31,dx,a,n,ct,nm,voltage,voltwork,nnes,nnie,es,       &
                    Capc,drs,chrgm)

         voltwork(2,1)=voltwork(2,2)
         voltwork(1,1)=voltwork(1,2)

!        write(*,*)"Voltage: ",voltage
!        write(410,*)ct,voltage

         CALL StrainEnergy(strsx,strsxy,strsy,strainx,strainxy,strainy,md,nm,nnes,       &
                           nnie,a,dx,n,hm,drs,k2)

!        Write membrane shape across center
```

```
        do i=-1,n
         write(110,*)i*a*dx,ws(i+2+(cj+1)*(n+2))/ws(cen)
         write(112,*)i*a*dx,ws(i+2+(cj+1)*(n+2))*h
        enddo
!       Write membrane shape across diagonal
        da=((a*dx)**2+(a*dx)**2.)**(1./2.)
        do i=0,n-1
         write(120,*)i*da,ws(i+2+(i+1)*(n+2))/ws(cen)
         write(125,*)i*da,ws(i+2+(i+1)*(n+2))*h
        enddo

1000    FORMAT(49(F6.2,1X))
END
-------------------------------------------------------------------------------------------------------
SUBROUTINE Dynamik(E,nu,rho,n,a,h,dx,md,ftm,ts,rs,drs,pss,wst,d31,Em,num,hm,   &
                           nm,es,Capc,writcntr,cc,delta,eta,alpha,D)
!       Handles the dynamic time-stepping for the vibrational problem.      *

double precision E,nu,rho,a,h,dx,ftm,ts,rs,ctp,drs,pss(md),pkp,d31,strsx(nm,md),        &
                 strsy(nm,md),Em(nm),num(nm),hm(nm),voltage,voltwork(2,2),             &
                 strsxy(nm,md),strainx(md),strainy(md),strainxy(md),es,Capc,chrgm,     &
                 strs1(nm,md),wst(md),wkm(md),wk(md),wkp(md),vk(md),vkp(md),           &
                 ak(md),akp(md),cc,delta,pkpd,f(50),nosc(50),f,pi2,tf,tf1,ctc,tsc,da,  &
                 wkmax,freq,time_current,time_prev,w_prev,w_current,k2,eta,alpha,D
        real*8 timefin,timef
        integer countk,writcntr,nf
        logical convergence


!       wkp='w' solution for k+1
!       wk='w' solution for k

        timefin=Timef()
        tf1=0.

        countk=0

        c=(rho*h*(dx*a)**4.)/(D)

        tts=int(ftm/ts)+1                   !Total time steps
        ci=(n-1)/2                          !Center in x
        cj=(n-1)/2                          !Center in y
        cen=ci+2+(cj+1)*(n+2)               !Matrix row/column for center node.

!       Initial conditions
```

```
          do i=1,md
           wk(i)=wst(i)
           vk(i)=0.
           ak(i)=0.
          enddo

! Excitation frequencies (hz)
j=1
f(j)=15000.          ;nosc(j)=50    ;j=j+1
f(j)=20000.          ;nosc(j)=50    ;j=j+1
f(j)=25000.          ;nosc(j)=75    ;j=j+1
f(j)=30000.          ;nosc(j)=75    ;j=j+1
f(j)=35000.          ;nosc(j)=75    ;j=j+1
f(j)=39000.          ;nosc(j)=100   ;j=j+1
f(j)=40000.          ;nosc(j)=400   ;j=j+1

nf=j-1               !number of frequencies.

!       Starts stepping through time after initial conditions applied

iii=1
pf=f(iii)
kk=1
tf1=0.

write(*,*)
write(*,*)"VENM program running, will be taking days of CPU time."
write(*,*)
write(*,*)"Number of frequencies",nf
write(*,*)pf

write(320,*)1.4e-6


DO k=2,tts
kk=kk+1

!       Establishes time step for forcing frequencies
 if (f(iii) .le. 15000.) then
  ts=1.4e-6
!  ts=0.01/f(iii)       !100 iterations per cycle for frequencies < 15 kHz
 else
  ts=0.01/f(iii)       !100 iterations per cycle.
 endif
```

```
 ct=tf1+(kk)*ts                !current time
 ctp=tf1+(kk+1.)*ts            !future time, k
 ctc=ctp                       !time in case of nonconvergence
 tf=nosc(iii)/pf+tf1
 tws=(nosc(iii)-5)/pf+tf1      !time to write shapes

if (ctp .ge. tf) then
  write(320,*)ts
  write(*,*)pf,wkmax
  write(330,*)pf,wkmax
  iii=iii+1
  pf=f(iii)
  tf1=ctp
  tf=0.
  kk=0
  wkmax=0.
  write(*,*)f(iii)
  write(115,*)pf
  write(320,*)pf,"-------------------------------------------"
  write(320,*)writcntr*ts
endif

pi2=2*3.14159256
pkpd=10000.*Dsin(pf*ctp*pi2-pf*tf1*pi2)   !LOAD, change coefficent to change
                                          !magnitude
pkp=12.*(1.-nu**2.)*((a*dx)**4.*pkpd)/(E*h**4.)  !N-D load

if (iii .gt. nf) then
 write(*,*)"Run is completed"
 read(*,*)
 STOP
endif

CALL iteratedynamik(n,a,h,dx,md,nu,E,rs,pss,rho,ts,pkp,wk,wkp,vk,vkp,ak,akp,cc,      &
                    delta,convergence,eta,alpha,D)
!Solves current time deflection/stress

if (convergence .eqv. .FALSE.) then           !exercise caution when using
        tsc=(ctc-ct)/2.
        ctc=ct+tsc
        pi2=2*3.14159256
        pkpd=10000.*Dsin(pf*ctc*pi2-pf*tf1*pi2)
        pkp=12.*(1.-nu**2.)*((a*dx)**4.*pkpd)/(E*h**4.)  !N-D load
        CALL iteratedynamik(n,a,h,dx,md,nu,E,rs,pss,rho,tsc,pkp,wk,wkp,vk,vkp,      &
                            ak,akp,cc,delta,convergence,eta,alpha,D)
```

```
                                    !Solves current time deflection/stress
        if (convergence .eqv. .TRUE.) then
            write(300,1030)ctc,wkp(cen)*h,vkp(cen)*h,akp(cen)*h,pkpd,pf
        endif
        write(*,*)"Time Step,",tsc," Current time,",ctc
        write(*,*)"Time #: ",k
endif

if (wkp(cen) .LT. wk(cen)) then
 if (wkm(cen) .LT. wk(cen)) then
        !maximize freq
        w_prev=w_current
        time_prev=time_current
        time_current=ctp
        w_current=wkp(cen)*h

        freq=1./(time_current-time_prev)
        write(340,1030)ctp,freq,w_current,pf

        if (abs(w_current-w_prev) .LT. 0.001*.5*(w_current+w_prev)) then
                write(*,*)"Deflections close",w_prev,w_current
        endif
 endif
endif


!       The below if statement causes the data to only be written to the file at certain
        intervals.  Therefore saving time and file space.

countk=countk+1

IF (ctp .ge. tws) then   !writes information for the last five forced cycles.
        write(115,*)ctp
        write(112,*)ctp
        write(110,*)ctp
        write(120,*)ctp
        write(125,*)ctp
        !Write membrane shape across center
        do i=-1,n
         write(110,*)i*a*dx,wkp(i+2+(cj+1)*(n+2))/wkp(cen),pf
         write(112,*)i*a*dx,wkp(i+2+(cj+1)*(n+2))*h,pf
        enddo
        !Write membrane shape across diagonal
        da=((a*dx)**2+(a*dx)**2.)**(1./2.)
        do i=0,n-1
```

```
          write(120,*)i*da,wkp(i+2+(i+1)*(n+2))/wkp(cen),pf
          write(125,*)i*da,wkp(i+2+(i+1)*(n+2))*h,pf
        enddo
        !Write maximum amplitude deflection
        if (wkp(cen) .GE. wk(cen)) then
         wkmax=wkp(cen)*h
        endif
        !Writes full dimensional shape profile
        write(100,*)ct
        do ii=0,n-1
         do ij=0,n-1
         write(100,*)ii*a*dx,ij*a*dx,wkp(ii+2+(ij+1)*(n+2))*h              !Shape
         enddo
        enddo

        !       Compute x-y stress values
         CALL StrainCompute(pss,dx,a,nu,n,md,E,h,drs,Em,num,nm,strsx,strsxy,     &
                  strsy,strainx,strainxy,strainy,strs1,hm)
        !       Call stresscompute(pss,dx,a,n,md,E,h,drs,wk,strsx,strsy)
         CALL piezo(strsx,strsy,md,d31,dx,a,n,ctp,nm,voltage,voltwork,           &
                  nnes,nnie,es,Capc,drs,chrgm)
        !       Obtain strain energy and k2
        CALL StrainEnergy(strsx,strsxy,strsy,strainx,strainxy,strainy,md,        &
                  nm,nnes,nnie,a,dx,n,hm,drs,k2)
!        For writing membrane shape across diagonal
!        write(*,*)pkpd,pf,wkp(cen)*h
!        write(*,1004)"Current Problem Time (s): ",ct
!        write(*,1006)"Center deflection (um):  ",wkp(cen)*h,pkp

ENDIF

IF (countk .eq. writcntr) THEN  !writes info at write center inc.
 timefin=Timef()
 write(320,*)wkp(cen)*h
 write(300,1030)ctp,wkp(cen)*h,vkp(cen)*h,akp(cen)*h,pkpd,pf
 countk=0
ENDIF

!       Steps the k+1 deflection solution to the kth solution.
        do i=1,md
         wkm(i)=wk(i)
         wk(i)=wkp(i)
         wkp(i)=0.
         vk(i)=vkp(i)
         vkp(i)=0.
```

```
          ak(i)=akp(i)
          akp(i)=0.
         enddo

ENDDO

!        File format specifiers.
1002   FORMAT(2(F16.10,1x))
1004   FORMAT(a27,E9.3E3)
1006   FORMAT(a26,E15.8E2,E15.8e2)
1008   FORMAT(a31,F7.4)
1020   FORMAT(2(d16.10),4(d16.10))
1030   FORMAT(6(E15.8E3,1X))
END
-----------------------------------------------------------------------------------------------------
!        Subroutine that iterates the current time step for the dynamic solution
SUBROUTINE iteratedynamik(n,a,h,dx,md,nu,E,rs,pss,rho,ts,pkp,wk,wkp,vk,vkp,      &
                                  ak,akp,cc,delta,convergence,eta,alpha,D)

        double precision w(md,md),pss(md),a,h,nu,dx,E,ps(md,md),psb(md),          &
                         clim,concrt,rs,c,D,rho,ts,pkp,wkpi(md),wk(md),wkp(md),   &
                         vk(md),vkp(md),ak(md),akp(md),b(6),beta,gam,cc,delta,eta,alpha
        integer ci,cj,cen,counti
        logical convergence

convergence=.TRUE.

!Newmark parameters
 beta=1./4.
 gam=1./2.

 !Calculate integration constants
b(1)=(1.)/(ts**2.*beta);b(2)=-(1.)/(ts*beta);b(3)=1.-(1.)/(2.*beta)
b(4)=gam/(ts*beta);b(5)=1.-gam/beta;b(6)=ts*(1.-gam/(2.*beta))

        do i=1,md
         wkpi(i)=wk(i)
        enddo

        ci=(n-1)/2                      !Center in x
        cj=(n-1)/2                      !Center in i
        cen=ci+2+(cj+1)*(n+2)           !Matrix row/column for center node.
        clim=1.E-9                      !Convergence Limit
        concrt=1.                       !Convergence Criteria
        counti=0                        !Iteration counter
```

```
        c=(rho*h*(dx*a)**4.)/(D)              !Effective mass term, m_eff.
!       c=rho*eta/alpha**2.

!       Start iteration to get convergent solution
DO WHILE (concrt .gt. clim)
        counti=counti+1                 !Iteration counter

!       Zero's out pertinent tensors, matrices, vectors.
        do i=1,md
         do j=1,md
          w(i,j)=0.
          ps(i,j)=0.
         enddo
         wkp(i)=0.
         psb(i)=0.
         w(i,i)=1.
   enddo

!       Dynamic
        CALL bending(w,md,n)        !Adds in bending portion of plate problem
        CALL membrane(w,pss,md,nu,n,eta)          !Adds in membrane portion
        CALL clampedeqlBC(w,md,n)
        CALL ResidualStress(md,n,rs,w)
        CALL wilsoneqleqn(n,md,w,pkp,c,wk,wkp,vk,ak,b,cc,delta)

!       Compatibility equation section
        CALL compat(n,md,ps)        !Forms compatibility equation portion.
        CALL clampstrainbc(n,md,nu,ps)     !Forms strain = 0 portion
        CALL uvDispBC(n,nu,md,ps)          !Forms u, v = 0 portion
        CALL psbvec(psb,wkp,n,md)          !Forms right side of compatibility matrix.
        CALL DLSARG(md,ps,md,psb,1,pss)         !Solves compatibility matrix.

!       Convergence Tests
        concrt=ABS(wkpi(cen)-wkp(cen))
!       Set previous iteration value for next iteration
        do i=1,md
         wkpi(i)=wkp(i)
        enddo

!       Safety criteria to help avoid divergent solutions
 if (counti .gt. 1000) then
        write(*,*)"Error - ",counti," Iterations for single time-step"
        write(*,*)cen,wkp(cen)
pause
```

```
          convergence=.FALSE.
!          write(105,*)ctp
!           do ii=(-1),n
!            do ij=(-1),n
!            write(105,*)ii*a*dx,ij*a*dx,wk(ii+2+(ij+1)*(n+2))*h                !Shape
!            enddo
!           enddo
!          close(100);close(105);close(300);close(320)
 endif

if (convergence .eqv. .FALSE.) then
          exit
endif

ENDDO                    !ENDs convergence iteration loop

do i=1,md
 vkp(i)=b(4)*(wkp(i)-wk(i))+b(5)*vk(i)+b(6)*ak(i)  !Calculate velocity for k+1
 akp(i)=b(1)*(wkp(i)-wk(i))+b(2)*vk(i)+b(3)*ak(i)  !Calculate acceleration for k+1
enddo

!         write(*,*)"Time to converge in seconds:",timefin

1000    FORMAT(49(F8.3,1X))
1001    FORMAT(E10.4,F10.4,a8,f10.4)

END
-------------------------------------------------------------------------------------------------------
SUBROUTINE wilsoneqleqn(n,md,Kb,Fwp,m_eff,wk,wkp,vk,ak,b,cc,delta)
 !         Where (var)b signifies bold, and is considered a matrix or vector.
 !         Kb is the stiffness matrix for the equilibrium equation, otherwise
 !                   referenced as 'w' in other subrs.
 !         Fw is the "forcing" vector for Kw, otherwise references as 'pk', needs to be
!                   nondimensional*
 !         Mb = ms
 !         dva = displacement, velocity, and acceleration
 !         cc = damping multiplicative coefficient

 double precision Kb(md,md), Cb(md,md),Mb(md,md),b(6),Kb_Eff(md,md),              &
           m_eff, Fkp_eff(md), Fwp,wk(md),wkp(md),vk(md),ak(md),cc,delta,          &
          Cbk(md,md),Cdva(md),Fwpp(md)

!zero
do i=1,md
 Cdva(i)=0.
```

```
 fwpp(i)=0.
 do j=1,md
 Kb_eff(i,j)=0.
 enddo
 Fkp_eff(i)=0.
enddo

!Damping factor
do i=1,md
 do j=1,md
  Cbk(i,j)=delta*Kb(i,j)
 enddo
 Mb(i,i)=m_eff
 Cb(i,i)=cc*m_eff
enddo

!Coefficient matrix
 do i=1,md
  do j=1,md
   Kb_Eff(i,j)=Kb(i,j) + b(1)*Mb(i,j) + b(4)*(Cbk(i,j)+Cb(i,j))  !effective stiffness matrix
  enddo
 enddo

 !Damping contribution to load
 do i=1,md
  do j=1,md
   Cdva(i)=(Cbk(i,j)+Cb(i,j))*(-b(4)*wk(j)+b(5)*vk(j)+b(6)*ak(j))+Cdva(i)
  enddo
 enddo

!Effective load vector
!Mass and damping contributions
do i=1,n-2
 do j=1,n-2
 fwpp(i+2+(j+1)*(n+2))=Fwp
 enddo
enddo

 do i=1,md
  Fkp_eff(i)=Fwpp(i) + Mb(i,i)*( b(1)*wk(i)-b(2)*vk(i)-b(3)*ak(i) ) - Cdva(i)
 enddo

 CALL DLSARG(md,Kb_Eff,md,Fkp_eff,1,wkp)

END
```

```
!-----------------------------------------------------------------------------------------------------------
!       Adds in the bending portion into the equilibrium matrix.
        SUBROUTINE bending(wbend,md,n)

        double precision wbend(md,md)
        integer i,j,r,n,md                !r=row

        r=0
        do j=1,(n-2)
         do i=1,(n-2)
         r=i+2+(j+1)*(n+2)
         wbend(r,i+2+(j+1)*(n+2))=20.
         wbend(r,i+1+2+(j+1)*(n+2))=-8.
         wbend(r,i-1+2+(j+1)*(n+2))=-8.
         wbend(r,i+2+(j+1+1)*(n+2))=-8.
         wbend(r,i+2+(j-1+1)*(n+2))=-8.
         wbend(r,i+1+2+(j+1+1)*(n+2))=2.
         wbend(r,i+1+2+(j-1+1)*(n+2))=2.
         wbend(r,i-1+2+(j+1+1)*(n+2))=2.
         wbend(r,i-1+2+(j-1+1)*(n+2))=2.
         wbend(r,i-2+2+(j+1)*(n+2))=1.
         wbend(r,i+2+2+(j+1)*(n+2))=1.
         wbend(r,i+2+(j+2+1)*(n+2))=1.
         wbend(r,i+2+(j-2+1)*(n+2))=1.
         enddo
        enddo

        END
!-----------------------------------------------------------------------------------------------------------
!       Adds in the membrane contribution to the equilibrium matrix
SUBROUTINE membrane(wstrt,pss,md,nu,n,eta)

        double precision wstrt(md,md),pss(md),psx,psy,psxy,nu,eta
        integer i,j,r,n,md

        r=0
        do j=1,(n-2)
         do i=1,(n-2)
         r=i+2+(j+1)*(n+2)

! 2nd derivative of Airy Stress in the y
!        psy=12.*(1.-nu**2.)*(pss(i+2+(j+1+1)*(n+2))-2.*pss(i+2+(j+1)*(n+2))+        &
                pss(i+2+(j-1+1)*(n+2)))
! 2nd derivative of Airy Stress in the x
!        psx=12.*(1.-nu**2.)*(pss(i+1+2+(j+1)*(n+2))-2.*pss(i+2+(j+1)*(n+2))+        &
```

```
                pss(i-1+2+(j+1)*(n+2)))
! 2nd derivative of Airy Stress in the xy
!       psxy=(12./8.)*(1.-nu**2.)*(pss(i-1+2+(j+1+1)*(n+2))-                    &
                pss(i-1+2+(j-1+1)*(n+2))+pss(i+1+2+(j-1+1)*(n+2))-              &
                pss(i+1+2+(j+1+1)*(n+2)))
! psxy=0.
! 2nd derivative of Airy Stress in the y
        psy=eta*(pss(i+2+(j+1+1)*(n+2))-2.*pss(i+2+(j+1)*(n+2))+                &
                pss(i+2+(j-1+1)*(n+2)))
! 2nd derivative of Airy Stress in the x
        psx=eta*(pss(i+1+2+(j+1)*(n+2))-2.*pss(i+2+(j+1)*(n+2))+                &
                pss(i-1+2+(j+1)*(n+2)))
! 2nd derivative of Airy Stress in the xy
        psxy=eta/8.*(pss(i-1+2+(j+1+1)*(n+2))-pss(i-1+2+(j-1+1)*(n+2))+         &
                pss(i+1+2+(j-1+1)*(n+2))-pss(i+1+2+(j+1+1)*(n+2)))
! psxy=0.
        wstrt(r,i+1+2+(j+1)*(n+2))=wstrt(r,i+1+2+(j+1)*(n+2))-psy
        wstrt(r,i+2+(j+1)*(n+2))=wstrt(r,i+2+(j+1)*(n+2))+2.*psy+2.*psx
        wstrt(r,i-1+2+(j+1)*(n+2))=wstrt(r,i-1+2+(j+1)*(n+2))-psy
        wstrt(r,i+2+(j+1+1)*(n+2))=wstrt(r,i+2+(j+1+1)*(n+2))-psx
        wstrt(r,i+2+(j-1+1)*(n+2))=wstrt(r,i+2+(j-1+1)*(n+2))-psx
        wstrt(r,i+1+2+(j+1+1)*(n+2))=wstrt(r,i+1+2+(j+1+1)*(n+2))-psxy
        wstrt(r,i+1+2+(j-1+1)*(n+2))=wstrt(r,i+1+2+(j-1+1)*(n+2))+psxy
        wstrt(r,i-1+2+(j+1+1)*(n+2))=wstrt(r,i-1+2+(j+1+1)*(n+2))+psxy
        wstrt(r,i-1+2+(j-1+1)*(n+2))=wstrt(r,i-1+2+(j-1+1)*(n+2))-psxy

        enddo
       enddo

END
-----------------------------------------------------------------------------------------------------
!       Applies zero deflection at edges and zero slope at edges condition
!               to the equilibrium matrix.  It does this by setting the
!               deflection at the wall and outside the wall (substrate nodes)
!               to zero.
SUBROUTINE clampedeqlBC(wbd,md,n)

        double precision wbd(md,md)
        integer i,m,md,n,nn


!       Zero's row corresponding to zero edge deflection
        do m=-1,n
         do i=1,md
          wbd(m+2+(-1+1)*(n+2),i)=0.
```

```
          wbd(i,m+2+(-1+1)*(n+2))=0.
          wbd(m+2+(0+1)*(n+2),i)=0.
          wbd(i,m+2+(0+1)*(n+2))=0.
          wbd(m+2+(n-1+1)*(n+2),i)=0.
          wbd(i,m+2+(n-1+1)*(n+2))=0.
          wbd(m+2+(n+1)*(n+2),i)=0.
          wbd(i,m+2+(n+1)*(n+2))=0.
          wbd(-1+2+(m+1)*(n+2),i)=0.
          wbd(i,-1+2+(m+1)*(n+2))=0.
          wbd(0+2+(m+1)*(n+2),i)=0.
          wbd(i,0+2+(m+1)*(n+2))=0.
          wbd(n-1+2+(m+1)*(n+2),i)=0.
          wbd(i,n-1+2+(m+1)*(n+2))=0.
          wbd(n+2+(m+1)*(n+2),i)=0.
          wbd(i,n+2+(m+1)*(n+2))=0.
         enddo
        enddo

!       The BC programmed below uses forward and backward difference
!       Sets edge nodes to zero deflection w(x=0,L)=w(y=0,L)=0

  do m=-1,n
        wbd(m+2+(-1+1)*(n+2),m+2+(-1+1)*(n+2))=1.
        wbd(m+2+(0+1)*(n+2),m+2+(0+1)*(n+2))=1.
        wbd(m+2+(n-1+1)*(n+2),m+2+(n-1+1)*(n+2))=1.
        wbd(m+2+(n+1)*(n+2),m+2+(n+1)*(n+2))=1.
       enddo
       do nn=1,(n-2)
        wbd(-1+2+(nn+1)*(n+2),-1+2+(nn+1)*(n+2))=1.
        wbd(0+2+(nn+1)*(n+2),0+2+(nn+1)*(n+2))=1.
        wbd(n-1+2+(nn+1)*(n+2),n-1+2+(nn+1)*(n+2))=1.
        wbd(n+2+(nn+1)*(n+2),n+2+(nn+1)*(n+2))=1.
       enddo


END
-----------------------------------------------------------------------------------------------------
!       Forms b-matrix for equilibrium matrix.  Adds the load in.
SUBROUTINE wrmat(wr,a,nu,p,dx,E,h,md,n,eta,alpha)

       double precision wr(md),nu,p,dx,E,h,a,eta,alpha
       integer i,j,n,md

       do i=1,(n-2)
        do j=1,(n-2)
```

```
!          wr(i+2+(j+1)*(n+2))=12.*(1.-nu**2.)*((a*dx)**4.*p)/(E*h**4.)
           wr(i+2+(j+1)*(n+2))=(a**2.*dx**4.)/(E*h**2.)*(eta/alpha)*p
           enddo
          enddo

END
-----------------------------------------------------------------------------------------------------------
!         This subroutine enters the compatibility equation into the
!         compatibility matrix.
SUBROUTINE compat(n,md,psc)

          double precision psc(md,md)
          integer r,i,j,n,md

          r=1
          do j=1,(n-2)
           do i=1,(n-2)
           psc(r,i+2+(j+1)*(n+2))=20.
           psc(r,i+1+2+(j+1)*(n+2))=-8.
           psc(r,i+2+(j+1+1)*(n+2))=-8.
           psc(r,i-1+2+(j+1)*(n+2))=-8.
           psc(r,i+2+(j-1+1)*(n+2))=-8.
           psc(r,i+1+2+(j+1+1)*(n+2))=2.
           psc(r,i-1+2+(j+1+1)*(n+2))=2.
           psc(r,i-1+2+(j-1+1)*(n+2))=2.
           psc(r,i+1+2+(j-1+1)*(n+2))=2.
           psc(r,i+2+2+(j+1)*(n+2))=1.
           psc(r,i+2+(j+2+1)*(n+2))=1.
           psc(r,i-2+2+(j+1)*(n+2))=1.
           psc(r,i+2+(j-2+1)*(n+2))=1.
           r=r+1
           enddo
          enddo


END
-----------------------------------------------------------------------------------------------------------
!         Sets the x-strains at the y=constant edges to zero and the
!                   y-strains at the x=constant edges to zero.  Also sets the
!                   corner airy-stress values=0.
SUBROUTINE clampstrainbc(n,md,nu,pse)

          double precision pse(md,md),nu
          integer r,n,md
```

```
          r=(n-2)**2

!         Strain x = 0 at y = 0 and y = L
          j=0
    do i=1,(n-2)
           r=r+1
     pse(r,i+2+(j+1+1)*(n+2))=1.
           pse(r,i+2+(j+1)*(n+2))=2.*(nu-1.)
           pse(r,i+2+(j-1+1)*(n+2))=1.
           pse(r,i+1+2+(j+1)*(n+2))=-nu
           pse(r,i-1+2+(j+1)*(n+2))=-nu
          enddo
          j=n-1
    do i=1,(n-2)
           r=r+1
           pse(r,i+2+(j+1+1)*(n+2))=1.
           pse(r,i+2+(j+1)*(n+2))=2.*(nu-1.)
           pse(r,i+2+(j-1+1)*(n+2))=1.
           pse(r,i+1+2+(j+1)*(n+2))=-nu
           pse(r,i-1+2+(j+1)*(n+2))=-nu
          enddo

!         Strain y = 0 at x = 0 and x = L
          i=0
          do j=1,(n-2)
           r=r+1
           pse(r,i+1+2+(j+1)*(n+2))=1.
     pse(r,i+2+(j+1)*(n+2))=2.*(nu-1.)
           pse(r,i-1+2+(j+1)*(n+2))=1.
           pse(r,i+2+(j+1+1)*(n+2))=-nu
           pse(r,i+2+(j-1+1)*(n+2))=-nu
          enddo
          i=n-1
          do j=1,(n-2)
           r=r+1
           pse(r,i+1+2+(j+1)*(n+2))=1.
           pse(r,i+2+(j+1)*(n+2))=2.*(nu-1.)
           pse(r,i-1+2+(j+1)*(n+2))=1.
           pse(r,i+2+(j+1+1)*(n+2))=-nu
           pse(r,i+2+(j-1+1)*(n+2))=-nu
          enddo

          r=r+1
          i=0
          j=0
```

```
        pse(r,i+2+(j+1)*(n+2))=1.
        r=r+1
        i=n-1
        j=0
        pse(r,i+2+(j+1)*(n+2))=1.
        r=r+1
        i=0
        j=n-1
        pse(r,i+2+(j+1)*(n+2))=1.
        r=r+1
        i=n-1
        j=n-1
        pse(r,i+2+(j+1)*(n+2))=1.

!       Set "imaginary" corner nodes equal zero so that matrix is non-singular.
        r=r+1
         pse(r,-1+2+(-1+1)*(n+2))=1.
        r=r+1
         pse(r,-1+2+(n+1)*(n+2))=1.
        r=r+1
         pse(r,n+2+(-1+1)*(n+2))=1.
        r=r+1
         pse(r,n+2+(n+1)*(n+2))=1.

END
-----------------------------------------------------------------------------------------------------
!       Applies the conditino that the u and v displacements must be zero
!       over constant lines in the membrane.
SUBROUTINE uvDispBC(n,nu,md,psd)

        double precision psd(md,md),nu
        integer cen,r,i,j,n

        r=int(((n-2)**2+4*n)+1)
        cen=int((n-1)/2)

!       v=0 at x=constant
!       Top section
        do i=0,(n-1)
         do j=0,(cen-1)
         psd(r,i+1+2+(j+1)*(n+2))=1.+psd(r,i+1+2+(j+1)*(n+2))
         psd(r,i+2+(j+1)*(n+2))=nu-2.+psd(r,i+2+(j+1)*(n+2))
         psd(r,i-1+2+(j+1)*(n+2))=1.+psd(r,i-1+2+(j+1)*(n+2))
         psd(r,i+2+(j+1+1)*(n+2))=nu-2.+psd(r,i+2+(j+1+1)*(n+2))
         psd(r,i+2+(j-1+1)*(n+2))=-nu+psd(r,i+2+(j-1+1)*(n+2))
```

```
 psd(r,i+1+2+(j+1+1)*(n+2))=1.+psd(r,i+1+2+(j+1+1)*(n+2))
 psd(r,i-1+2+(j+1+1)*(n+2))=1.+psd(r,i-1+2+(j+1+1)*(n+2))
 psd(r,i+2+(j+2+1)*(n+2))=-nu+psd(r,i+2+(j+2+1)*(n+2))
 enddo
r=r+1
enddo
!       Bottom section
do i=0,(n-1)
 do j=cen,(n-2)
 psd(r,i+1+2+(j+1)*(n+2))=1.+psd(r,i+1+2+(j+1)*(n+2))
 psd(r,i+2+(j+1)*(n+2))=nu-2.+psd(r,i+2+(j+1)*(n+2))
 psd(r,i-1+2+(j+1)*(n+2))=1.+psd(r,i-1+2+(j+1)*(n+2))
 psd(r,i+2+(j+1+1)*(n+2))=nu-2.+psd(r,i+2+(j+1+1)*(n+2))
 psd(r,i+2+(j-1+1)*(n+2))=-nu+psd(r,i+2+(j-1+1)*(n+2))
 psd(r,i+1+2+(j+1+1)*(n+2))=1.+psd(r,i+1+2+(j+1+1)*(n+2))
 psd(r,i-1+2+(j+1+1)*(n+2))=1.+psd(r,i-1+2+(j+1+1)*(n+2))
 psd(r,i+2+(j+2+1)*(n+2))=-nu+psd(r,i+2+(j+2+1)*(n+2))
 enddo
r=r+1
enddo

!       u=0 at y=constant
!       Left section.
do j=0,(n-1)
 do i=0,(cen-1)
  psd(r,i+2+(j+1+1)*(n+2))=1.+psd(r,i+2+(j+1+1)*(n+2))
  psd(r,i+2+(j+1)*(n+2))=nu-2.+psd(r,i+2+(j+1)*(n+2))
  psd(r,i+2+(j-1+1)*(n+2))=1.+psd(r,i+2+(j-1+1)*(n+2))
  psd(r,i+1+2+(j+1)*(n+2))=nu-2.+psd(r,i+1+2+(j+1)*(n+2))
  psd(r,i-1+2+(j+1)*(n+2))=-nu+psd(r,i-1+2+(j+1)*(n+2))
  psd(r,i+1+2+(j+1+1)*(n+2))=1.+psd(r,i+1+2+(j+1+1)*(n+2))
  psd(r,i+1+2+(j-1+1)*(n+2))=1.+psd(r,i+1+2+(j-1+1)*(n+2))
  psd(r,i+2+2+(j+1)*(n+2))=-nu+psd(r,i+2+2+(j+1)*(n+2))
 enddo
r=r+1
enddo
!       Right Section
do j=0,(n-1)
 do i=cen,(n-2)
  psd(r,i+2+(j+1+1)*(n+2))=1.+psd(r,i+2+(j+1+1)*(n+2))
  psd(r,i+2+(j+1)*(n+2))=nu-2.+psd(r,i+2+(j+1)*(n+2))
  psd(r,i+2+(j-1+1)*(n+2))=1.+psd(r,i+2+(j-1+1)*(n+2))
  psd(r,i+1+2+(j+1)*(n+2))=nu-2.+psd(r,i+1+2+(j+1)*(n+2))
  psd(r,i-1+2+(j+1)*(n+2))=-nu+psd(r,i-1+2+(j+1)*(n+2))
  psd(r,i+1+2+(j+1+1)*(n+2))=1.+psd(r,i+1+2+(j+1+1)*(n+2))
```

```
            psd(r,i+1+2+(j-1+1)*(n+2))=1.+psd(r,i+1+2+(j-1+1)*(n+2))
            psd(r,i+2+2+(j+1)*(n+2))=-nu+psd(r,i+2+2+(j+1)*(n+2))
           enddo
          r=r+1
          enddo

END
```

```
!       Forms the b-vector for the Psi matrix.
SUBROUTINE psbvec(psb,w,n,md)

double precision psb(md),w(md),compatr
integer r

!       Form right hand side of compatibility eqn.
r=1
do j=1,(n-2)
 do i=1,(n-2)
 psb(r)=compatr(w,md,n,i,j)
 r=r+1
 enddo
enddo

cen=(n-1)/2
r=((n-2)**2+4*n)+1

!       v=0 at x=constant
!       Top section.
do i=0,(n-1)
 do j=0,(cen-1)
  psb(r)=(1./8.)*((w(i+2+(j+1+1)*(n+2))-w(i+2+(j-1+1)*(n+2)))**2+                    &
                  (w(i+2+(j+2+1)*(n+2))-w(i+2+(j+1)*(n+2)))**2)+psb(r)
 enddo
r=r+1
enddo
!       Bottom section.
do i=0,(n-1)
 do j=cen,(n-2)
  psb(r)=(1./8.)*((w(i+2+(j+1+1)*(n+2))-w(i+2+(j-1+1)*(n+2)))**2+                    &
                  (w(i+2+(j+2+1)*(n+2))-w(i+2+(j+1)*(n+2)))**2)+psb(r)
 enddo
r=r+1
enddo

!       u=0 at y=constant
```

```
!       Left section.
do j=0,(n-1)
 do i=0,(cen-1)
  psb(r)=(1./8.)*((w(i+1+2+(j+1)*(n+2))-w(i-1+2+(j+1)*(n+2)))**2+                    &
                  (w(i+2+2+(j+1)*(n+2))-w(i+2+(j+1)*(n+2)))**2)+psb(r)
 enddo
r=r+1
enddo
!       Right section.
do j=0,(n-1)
 do i=cen,(n-2)
  psb(r)=(1./8.)*((w(i+1+2+(j+1)*(n+2))-w(i-1+2+(j+1)*(n+2)))**2+                    &
                  (w(i+2+2+(j+1)*(n+2))-w(i+2+(j+1)*(n+2)))**2)+psb(r)
 enddo
r=r+1
enddo

END
-------------------------------------------------------------------------------------------------------
double precision FUNCTION compatr(w,md,n,i,j)

        double precision w(md)

        compatr=(1./16.)*(w(i+1+2+(j+1+1)*(n+2))-w(i-1+2+(j+1+1)*(n+2))          &
                +w(i-1+2+(j-1+1)*(n+2))-w(i+1+2+(j-1+1)*(n+2)))**2               &
                -(w(i+1+2+(j+1)*(n+2))-2.*w(i+2+(j+1)*(n+2))                     &
                +w(i-1+2+(j+1)*(n+2)))*(w(i+2+(j+1+1)*(n+2))                     &
                -2.*w(i+2+(j+1)*(n+2))+w(i+2+(j-1+1)*(n+2)))

END
-------------------------------------------------------------------------------------------------------
SUBROUTINE ResidualStress(md,n,rs,wres)

        double precision rs,wres(md,md)

        do j=1,(n-2)
         do i=1,(n-2)
         r=i+2+(j+1)*(n+2)

         wres(r,i+1+2+(j+1)*(n+2))=wres(r,i+1+2+(j+1)*(n+2))-rs
         wres(r,i+2+(j+1)*(n+2))=wres(r,i+2+(j+1)*(n+2))+2.*rs+2.*rs
         wres(r,i-1+2+(j+1)*(n+2))=wres(r,i-1+2+(j+1)*(n+2))-rs
         wres(r,i+2+(j+1+1)*(n+2))=wres(r,i+2+(j+1+1)*(n+2))-rs
         wres(r,i+2+(j-1+1)*(n+2))=wres(r,i+2+(j-1+1)*(n+2))-rs
```

```
         enddo
        enddo

END
------------------------------------------------------------------------------------------------------
SUBROUTINE StrainCompute(pss,dx,a,nu,n,md,E,h,drs,Em,num,nm,strsx,strsxy,      &
                                 strsy,strainx,strainxy,strainy,strs1,hm)

        double precision dx,a,E,h,drs,Em(nm),num(nm),pss(md),strainx(md),      &
              strainy(md),nu,strsx(nm,md),strsy(nm,md),compst(md),             &
              strainxy(md),strsxy(nm,md),strs1(nm,md),hm(nm),strs2(nm,md)      &

        ci=(n-1)/2                          !Center in x
        cj=(n-1)/2                          !Center in i
        cen=ci+2+(cj+1)*(n+2)               !Matrix row/column for center node.

!       Calculate strain in the membrane
        do i=0,(n-1)
         do j=0,(n-1)
         r=i+2+(j+1)*(n+2)
         strainx(r)=(pss(i+2+(j+1+1)*(n+2))+pss(i+2+(j+1-1)*(n+2))             &
              +2.*(nu-1)*pss(i+2+(j+1)*(n+2))-nu*pss(i+1+2+(j+1)*(n+2))        &
              -nu*pss(i-1+2+(j+1)*(n+2)))*(h/(a*dx))**2.
         strainy(r)=(pss(i+1+2+(j+1)*(n+2))+pss(i-1+2+(j+1)*(n+2))             &
              +2.*(nu-1)*pss(i+2+(j+1)*(n+2))-nu*pss(i+2+(j+1+1)*(n+2))        &
              -nu*pss(i+2+(j+1-1)*(n+2)))*(h/(a*dx))**2.
         strainxy(r)=(pss(i+1+2+(j+1+1)*(n+2))-pss(i+1+2+(j-1+1)*(n+2))        &
              -pss(i-1+2+(j+1+1)*(n+2))+pss(i-1+2+(j-1+1)*(n+2)))              &
              *(1./4.)*(-2.)*(1+nu)*(h/(a*dx))**2.
         enddo
        enddo

        do mn=1,nm              !material number loop
         do i=1,md
          strsx(mn,i)=hm(mn)/h*(Em(mn)/(1.-num(mn)**2.))                       &
              *(strainx(i)-num(mn)*strainy(i))+drs
          strsy(mn,i)=hm(mn)/h*(Em(mn)/(1.-num(mn)**2.))                       &
              *(strainy(i)-num(mn)*strainx(i))+drs
          strsxy(mn,i)=hm(mn)/h*(Em(mn)/(2.+2.*num(mn)))*strainxy(i)
         enddo
        enddo

!       Principle Stress Calculations (sigma 1)
     do mn=1,nm
         do i=0,(n-1)
```

```
          do j=0,(n-1)
           strs1(mn,i+2+(j+1)*(n+2))=hm(mn)/h*0.5*(strsx(mn,i+2+(j+1)              &
                 *(n+2))+strsy(mn,i+2+(j+1)*(n+2)))                               &
                 +(0.5*(strsx(mn,i+2+(j+1)*(n+2))                                 &
                 -strsy(mn,i+2+(j+1)*(n+2)))**2.                                  &
                 +(strsxy(mn,i+2+(j+1)*(n+2)))**2.)**(1./2.)
           strs2(mn,i+2+(j+1)*(n+2))=hm(mn)/h*0.5*(strsx(mn,i+2+(j+1)              &
                 *(n+2))+strsy(mn,i+2+(j+1)*(n+2)))                               &
                 -(0.5*(strsx(mn,i+2+(j+1)*(n+2))                                 &
                 -strsy(mn,i+2+(j+1)*(n+2)))**2.                                  &
                 +(strsxy(mn,i+2+(j+1)*(n+2)))**2.)**(1./2.)
          enddo
         enddo
        enddo


!        do ii=0,n-1
!         do ij=0,n-1
!          write(220,1020)ii*a*dx,ij*a*dx,(strs2(mn,ii+2+(ij+1)*(n+2)),mn=1,nm)
!         enddo
!        enddo


!       do i=1,md
!         compst(i)=hm(mn)/h*(E/(1.-nu**2.))*(strainy(i)-nu*strainx(i))+drs
!       enddo

!       write(*,*)"Stress in Silicon: ",strsx(1,cen)
!       write(*,*)"Stress in PZT:     ",strsx(2,cen)
!       write(*,*)"Composite Stress:  ",compst(cen)

1020   FORMAT(2(e16.10),4(e20.10e2))
END
-------------------------------------------------------------------------------------------------------
SUBROUTINE piezo
(strsx,strsy,md,d31,dx,a,n,ct,nm,voltage,voltwork,nnes,nnie,es,Capc,drs,chrgm)

!       plrz:   polarization, units of charge/area
!       Ar:             Electrode area per node
!       Qc:             charge (coulombs)
!       Capc:   Capacitance
!       nnes:   number of nodes from wall to electrode
!       nnie:   number of nodes on one edge of the electrode
!       voltage: voltage accumulation over entire electrode area
```

```
      integer md,n,nnie,nnes
      double precision strsx(nm,md),strsy(nm,md),plrz(md),Qc(md),d31,dx,          &
             a,Ar,Capc,voltage,ct,voltwork(2,2),chrg(md),chrgm,es,drs

      ci=(n-1)/2                        !Center in x
      cj=(n-1)/2                        !Center in i
      cen=ci+2+(cj+1)*(n+2)             !Matrix row/column for center node.

      voltwork(1,2)=ct
      voltwork(2,2)=0.
      voltage=0.
      chrgm=0.
      Ar=(dx*a)**2.

      do i=1,md
       plrz(i)=0.
      enddo

      do i=1,md
       plrz(i)=d31*(strsx(3,i)+strsy(3,i)-2.*drs)
       Qc(i)=(Ar*plrz(i))/Capc
       chrg(i)=Ar*plrz(i)
      enddo

!     Computes total voltage in membrane for specified electrode size (es)
      nnes=int((a-es)/(2*dx*a))      !number of nodes from wall to electrode side
      nnie=int(es/(dx*a))            !number of nodes within electrode

      do i=nnes,(nnes+nnie)
       do j=nnes,(nnes+nnie)
       voltage=voltage+Qc(i+2+(j+1)*(n+2))
       chrgm=chrgm+chrg(i+2+(j+1)*(n+2))
       enddo
      enddo

      voltwork(2,2)=(Capc*voltage**2.)*.5

!     write(*,*)"Total Charge. ",chrgm

!     write(*,*)"Charge: ",chrgm
!     write(400,*)chrgm

!     Write charge profile.
      do ii=0,(n-1)
       do ij=0,(n-1)
```

```
          write(400,*)ii*a*dx,ij*a*dx,chrg(ii+2+(ij+1)*(n+2))
         enddo
        enddo

!       STOP
        write(400,*)"STOP"

END
-----------------------------------------------------------------------------------------------------
SUBROUTINE StrainEnergy(ox,oxy,oy,ex,exy,ey,md,nm,nnes,nnie,a,dx,n,hm,drs,k2)
!       se: strain energy (dim: number of materials)
!       ox: stress x, oxy: stress xy, oy: stress y
!       ex: strain x, exy: strain xy, ey: stress y
!       sep: strain energy in PZT
!       tse: total strain energy in stack

        double precision se(nm),ox(nm,md),oxy(nm,md),oy(nm,md),ex(md),          &
              exy(md),ey(md),sep,tse,hm(nm),a,dx,k2,drs

        tse=0.
        sep=0.
        do i=1,nm
         se(i)=0.
        enddo

!       Energy in PZT layer
        do i=nnes,(nnes+nnie)
         do j=nnes,(nnes+nnie)
          r=i+2+(j+1)*(n+2)
          sep=(.5*(ox(3,r)-drs)*ex(r)+.5*(oy(3,r)-drs)*ey(r))*hm(3)*(a*dx)**2.+sep
         enddo
        enddo

!       Energy in each layer.
        do m=1,nm
         do i=0,(n-1)
          do j=0,(n-1)
          r=i+2+(j+1)*(n+2)
          se(m)=(.5*ox(m,r)*ex(r)+oxy(m,r)*exy(r)                               &
              +.5*oy(m,r)*ey(r))*hm(m)*(a*dx)**2.+se(m)
          enddo
         enddo
        enddo

!       Total Energy in the Stack
```

```
        do m=1,nm
         tse=tse+se(m)
        enddo

!       write(*,*)"Total Strain Energy: ",tse
        k2=sep/tse

!       write(*,*)"Energy Ratio: ",k2

END
-----------------------------------------------------------------------------------------------------------
SUBROUTINE D_value(hm,Em,num,z,nm,D)

double precision A,B,hm(nm),Em(nm),num(nm),z(nm),E_star(nm),z_neutral,D

z_neutral=0.
D=0.

 do i=1,nm
        E_star(i)=Em(i)/(1.-num(i)**2.)
        A=A+E_star(i)*(z(i+1)-z(i))
        B=B+E_star(i)*(z(i+1)**2.-z(i)**2)/2.
 enddo
 z_neutral=B/A

 do i=1,nm
        D=D+E_star(i)*((z(i+1)**3.-z(i)**3.)/3.-z_neutral*(z(i+1)**2.                    &
                -z(i)**2.)+ z_neutral**2.*(z(i+1)-z(i)))
 enddo


 write(*,*)"Nuetral Axis at: ",z_neutral
 write(*,*)"Flexural Ridigity, D: ",D
END
-----------------------------------------------------------------------------------------------------------
!       INDEX OF VARIABLES USED
!
!        ARR() = Array (dimensions), arrays are double precision
!        DP  = Double Precision
!        INT = Integer
!
!       a               DP, Side-length of the membrane
!       c               DP, Inertial constant term
!       cen             INT, Index for the center node of the membrane
!       ci              INT, center coordinate in the x-direction
```

```
!       cj              INT, center coordinate in the y-direction
!       clim    DP, Convergence limit
!       compatr         DP, Function that gives the value obtained for the b-vector for the
!                               psi matrix
!       concrt  DP, Convergence check variable
!       counti  INT, Counts the number of iterations to converge
!       ct              DP, Time for current solution
!       D               DP, Flexural ridigity
!       drs             DP, dimensional residual stress
!       dx              DP, nodal spacing (1/(n-1))
!       E               DP, Modulus of Elasticity
!       ftm             DP, Final time, or the total time for model
!       h               DP, Thickness
!       k               INT, indexing variable for time stepping
!       lamb            DP, Multiplicative factor for iterative convergence
!       md              INT, Matrix dimensions
!       mu              DP, 12(1-nu^2)
!       n               INT, number of inclusive interior nodes
!       nu              DP, Poison's ratio
!       p               DP, Pressure variable used within subroutines,
!                               either dynamic or static depends on the subr.
!       pd              DP, Pressure for the dynamic analysis
!       ps              DP, Pressure for the static analysis
!       ps              ARR(md,md), matrix for compatibility matrix
!       psb             ARR(md), b-vector for compatibility matrix
!       psc             ARR(md,md), psi-matrix used within the compatibility sub
!       psd             ARR(md,md), psi-matrix used within the u/v displacment sub
!       pse             ARR(md,md), psi-matrix used within the strainbc sub
!       pss             ARR(md), Airy stress solution for current k
!       pst             ARR(md), Airy stress for the static case, it is passed to the
!                               dynamik subroutine.
!       r               INT, represents the position in a matrix from [i+1+2+(j+1)*(n+2)]
!       rho             DP, Density
!       rs              DP, non-dimensional residual stress
!       timef   INT, calls routine that counts the seconds between calls of the routine
!       timefin         INT, variable used to keep track of time to solve
!       ts              DP, Time step
!       tts             DP, Total time steps
!       u0              DP, Initial velocity
!       w               ARR(md,md), matrix for the equilibrium eqn.
!       wbd             ARR(md,md), w-matrix variable used within the boundary
!                               condition subroutine
!       wbend ARR(md,md), w-matrix variable used within the bending subroutine
!       wsk             ARR(md), w-deflection for current k
!       wsm             ARR(md), w-deflection for k minus 1
```

```
!       wsp             ARR(md), w-deflection for k plus 1
!       wspi    ARR(md), w-deflection for past nonlinear iteration (used with lamb)
!       wr              ARR(md), b-vector for eql. eqn. matrix
!       wres    ARR(md,md), w-matrix variable used within the residual stress sub
!       ws              ARR(md), w-deflection solution for iterative subroutines.
!       wstrt   ARR(md,md), w-matrix variable used within the membrane subroutine
!       wst             ARR(md), w-deflection for the static case it is passed to the
!                       dynamik subroutine.
```

References

[1] Hoppensteadt, F. C., Nonlinear Oscillations in Biology, American Mathematical Society, Providence, Rhode Island, 1979

[2] Wang, C., "Nonlinear Large-Deflection Boundary-Value problems of Rectangular Plates", NACA TN 1425, 1948

[3] Vallabhan, G.C.V., "Nonlinear Dynamic Response of Window Glass Plates Using the Finite Difference Method", Dynamic Response of Structures, ASCE, Proceedings of the Third Conference, 1986

[4] Yang, X., Grosjean, C., Tai, Y., Ho, C., "A MEMS Thermopneumatic Silicone Membrane Valve", Sensors and Actuators, A: Physical, Vol. 64(1), pp. 101-108, 1998

[5] Williams, C. B. , Shearwood, C., Harradine, M. A., Mellor, P. H., Birch, T. S., Yates, R. B., "Development of an electromagnetic micro-generator", IEE Proceedings: Circuits, Devices and Systems, Vol. 148(6), pp. 337-342, 2001

[6] Sullivan, T. M., Development of a Novel Method for Measuring the Transverse Piezoelectric Coefficients of Thin Piezoelectric Films, Masters Thesis, Washington State University, August 2004

[7] Benamar, Rhali, Nonlinear Dynamic Behaviour of Fully Clamped Beams and Rectangular Isotropic and Laminated Plates, PhD Diss. , University of Southampton, April 1990

[8] Szilard, R., Theory and Analysis of Plates: Classical and Numerical Methods, Prentice-Hall, Inc., New Jersey, 1974

[9] Cook, R. D., Malkus, D. S., Plesha, M. E., Concepts and Applications of Finite Element Analysis, John Wiley & Sons, New York, 1989

[10] Leissa, A. W., "Vibration of Plates", SP 160, 1969

[11] Timoshenko, S., Woinowsky-Krieger, S., Theory of Plates and Shells, McGraw-Hill Book Company, New York, 1959

[12] Leissa, A. W., "The Free Vibration of Rectangular Plates", Journal of Sound and Vibration, Vol. 31(3), pp. 257-293, 1973

[13] Voigt, W., "Bemerkungen zu dem problem der transversalen Schwingungen rechteckiger Platten", Nachr. Ges. Wiss. (Gottingen), no. 6, p. 225-230, 1893

[14] Inman, D. J., Engineering Vibration, Prentice Hall, Inc., New Jersey, 2001

[15] Warburton, G. B., "Vibration of Rectangular Plates", Proc. Inst. Mech. Eng. Ser. A, Vol. 168(12), pp. 371-384, 1954

[16] Houmat, A., "Hierarchical Finite Element Analysis of the Vibration of Membranes", Journal of Sound and Vibration, Vol. 201(4), pp. 465-472, 1997

[17] Kharab, A., "Technical Note: A Finite-Difference Solution to a Two-Dimensional Vibratin Membrane Problem Using a Spreadsheet Program", Advances in Engineering Software, Vol. 23, pp. 115-120, 1995

[18] Han & Petyt, "Linear Vibration Analysis of Laminated Rectangular Plates Using the Hierarchical Finite Element Method - I. Free Vibration Analysis", Computers and Structures, Vol. 61(4), pp. 705-712, 1996

[19] Han & Petyt, "Linear Vibration Analysis of Laminated Rectangular Plates Using the Hierarchical Finite Element Method - II. Force Vibration Analysis", Computers and Structures, Vol. 61(4), pp. 713-724, 1996

[20] Kirchhoff, G., Vorlesungen uber mathematishce Physik, B. G. Teubner, Leipzig, 1876

[21] von Karman, Theodore, "Festigkeitshprobleme im Machinenbau", Encyklopadie der Mathematishen Wissenchaften, Vol. IV, pp. 349, 1910

[22] Herrmann, G., "Influence of large Amplitudes on Flexural Motions of Elastic Plates", NACA TR 3578, 1955

[23] Lee, J., "Comparison of two formulations of the w-u-v and w-F in nonlinear plate analysis", AIAA 1477, 2001

[24] Chia, C. Y., Nonlinear Analysis of Plates, McGraw-Hill International Book Company, New York, 1980

[25] Washizu, K., Variational Methods in Elasticity and Plasticity, Pergamon Press, Oxford, 1975

[26] Reismann, H., Elastic Plates: Theory and Application, John Wiley & Sons, New York, 1988

[27] Way, S., “Bending of Circular Plates with Large Deflections”, Transactions of the ASME, Vol. 56, pp. 627-636, 1934

[28] Berger, H. M., "A New Approach to the Analysis of Large Deflections of Plates", Journal of Applied Mechanics, Vol. 22, pp. 465-472, 1955

[29] Levy, S., "Bending of Rectangular Plates with Large Deflections", NACA TR 737, 1942

[30] Mazumdar, J., Jones, R., "A simplified approach to the large amplitude vibration of plates and membranes", Journal of Sound and Vibration, Vol. 50(3), pp. 389-397, 1976

[31] Sathyamoorthy, M., "Non-linear Vibration of Rectangular Plates", Journal of Sound and Vibration, Vol. 58(2), pp. 301-304, 1978

[32] Meirovitch, L., Elements of Vibration Analysis, McGraw Hill, Inc., 1975

[33] Han, W., Petyt, M., "Geometrically Nonlinear Vibrations of Thin, Rectangular Plates Using the Hierarchical Finite Element Method - I: The Fundamental Mode of Isotropic Plates", Computers and Structures, Vol. 63(2), pp. 295-308, 1997

[34] Han, W., Petyt, M., "Geometrically Nonlinear Vibration Analysis of Thin, Rectangular Plates Using the Hierarchical Finite Element Method - II: 1st Mode of Isotropic and Laminated Plates", Computers and Structures, Vol. 63(2), pp. 309-318, 1997

[35] Seide, P., "Large Deflections of Rectangular membranes Under Uniform Pressure", International Journal of Non-Linear Mechanics, Vol. 12, pp. 397-406, 1977

[36] Maier-Schneider, D., "New analytical solution for the load-deflection of square membranes", Journal of Microelectromechanical Systems, Vol. 4(4), pp. 238-241, 1995

[37] Teng, T., Cheng, F., "The Realization of Boundary Conditions in the Vibration Analysis of Plates", J. Franklin Inst., Vol. 335B(5), pp. 799-812, 1998

[38] Teng, T. L., Liang, C. C., Liao, C. C., "Nonlinear forced vibration analysis of the rectangular plates by the Fourier series method", Computational Mechanics, Vol. 23, pp. 1-7, 1999

[39] Chu, H. N., Herrmann, G., "Mechanics, Influence of large Amplitudes on Free Flexural Vibrations of Rectangular Elastic Plates", Journal of Applied Mechanics, Vol. 23-24, pp. 532-540, 1956-57

[40] Nayfeh, A. H., Mook, D. T., Nonlinear Oscillations, John Wiley & Sons, New York, 1979

[41] Yasuda, K., Torii, T., "Multi-Mode Response of a Square Membrane", JSME International Journal, Vol. 30(264), pp. 963-969, 1987

[42] Lau, S. L, Cheung, Y. K., Wu, S. Y., "Nonlinear Vibration of Thin Elastic Plates, Part 2: Internal Resonance by Amplitude-Incremental Finite Element", Journal of Applied Mechanics, Vol. 51, pp. 845-851, 1984

[43] Harras, B., Benamar, R., "Geometrically Non-Linear Free Vibration of Fully Clamped Symmetrically Laminated Rectangular Composite Plates", Journal of Sound and Vibration, Vol. 251(4), pp. 579-619, 2002

[44] Bikri, K., "Geometrically non-lineaer free vibrations of clamped simply supported rectangular plates. Part I: The effects of large vibration amplitudes on the fundamental mode shape", Computers and Structures, Vol. 81, pp. 2029-2043, 2003

[45] Pica, A., Wood, R. D., Hinton, E., "Finite Element Analysis of Geometrically Nonlinear Plate Behaviour Using a Mindling Formulation", Computers and Structures, Vol. 11(3), pp. 203-215, 1980

[46] Lau, S. L., Cheung, Y. K., Wu, S. Y., "Nonlinear Vibrations of Thin Elastic Plates. Part 1: Generalized and incremental Hamilton's Principle and Element Formulation", Journal of Applied Mechanics, Vol. 51, pp. 837-844, 1984

[47] Aalami, B., "Large Deflection of Plates Under Hydrostatic Pressure", Journal of Ship Research, Vol. 16(4), pp. 261-270, 1972

[48] Newmark, N. M., "A Method of Computation for Structural Dynamics", Jour. Eng. Mech. Div., Proceedings of the American Society of Civil Engineers, EM3, pp. 67-94, July 1959

[49] Malvern, L. E., Introduction to the Mechanics of a Continuous Medium, Prentice-Hall, Inc., New Jersey, 1969

[50] W. F. Riley, L. D. Sturges, D. H. Morris, Mechanics of Materials, John Wiley & Sons, Inc., New York, 1999

[51] Nye, J. F., Physical Properties of Crystals: Their Representation by Tensors and matric, Oxford University Press, New York, 1987

[52] Chapra, S. C. , Raymond, P. C., Numerical Methods for Engineers: With Programming and Software Application, WCB McGraw-Hill, Boston, 1998

[53] Wilson, E. L., Clough, R. W., "Dynamic Response by Step-By-Step Matrix Analysis", Proceedings, Symposium On The Use of Computers in Civil Engineering, Laboratorio Nacional de Engenharia Civil, Lisbon – Portugal, pp. 45.1-45.14, Oct. 1-5, 1962

[54] Skinner, J., Piezoelectric Membrane Generator Characterization and Optimization, Masters Thesis, Washington State University, December 2002

[55] Cho, J., Electro-Mechanical Characterization of Piezoelectrics for MEMS Power, Masters Thesis, Washington State University, December 2004

[56] Kennedy, M. S., Mechanical Property Determination of Thin Films for PZT MEMS Applications, Masters Thesis, Washington State University, December 2003

[57] Whalen, S., Thompson, M., Bahr, D., Richards, C., Richards, R.,"Design, fabrication and testing of the P3 micro heat engine", Sensors and Actuators, A: Physical, Vol. 104, pp. 290-298, 2003